Development and application of methods for spatio-temporal perturbation and analysis of protein interactions via intracellular protein microarrays

Technische Universität Dortmund
Fakultät für Chemie und Chemische Biologie

PhD Dissertation

Zur Erlangung des akademischen Grades eines
Doktors der Naturwissenschaften
(Dr. rer. Nat.)

vorlegt von
Master of Technology

Muthukumaran Venkatachalapathy

aus Villupuram, Tamil nadu (India.)

Dekan: Prof. Dr. Insa Melle
1.Gutachter: Priv. Doz. Dr. Leif Dehmelt
2.Gutachter: Prof. Dr. med. Jan G. Hengstler

"This work is dedicated to my father, for his infinite and unconditional love towards my mother and our family."

"தந்தை மகற்காற்றும் நன்றி அவையத்து
முந்தி இருப்பச் செயல்"

--- திருவள்ளுவர் (குறள் 67)

"Sire greatest boon on son confers, who makes him meet,
In councils of the wise to fill the highest seat"

--- Thiruvalluvar (Couplet 67)

Ich versichere hiermit, dass ich die vorliegende Dissertation selbständig und ohne unzulässige fremde Hilfe erbracht habe. Ich habe keine anderen als die angegeben Quellen und Hilfsmittel benutzt, sowie wörtliche und sinngemäße Zitate kenntlich gemacht.

....

Ort, Datum Unterschrift

Eidesstattliche Versicherung (Affidavit)

Name, Vorname
(Surname, first name)

Matrikel-Nr.
(Enrolment number)

Belehrung:

Wer vorsätzlich gegen eine die Täuschung über Prüfungsleistungen betreffende Regelung einer Hochschulprüfungsordnung verstößt, handelt ordnungswidrig. Die Ordnungswidrigkeit kann mit einer Geldbuße von bis zu 50.000,00 € geahndet werden. Zuständige Verwaltungsbehörde für die Verfolgung und Ahndung von Ordnungswidrigkeiten ist der Kanzler/die Kanzlerin der Technischen Universität Dortmund. Im Falle eines mehrfachen oder sonstigen schwerwiegenden Täuschungsversuches kann der Prüfling zudem exmatrikuliert werden, § 63 Abs. 5 Hochschulgesetz NRW.

Die Abgabe einer falschen Versicherung an Eides statt ist strafbar.

Wer vorsätzlich eine falsche Versicherung an Eides statt abgibt, kann mit einer Freiheitsstrafe bis zu drei Jahren oder mit Geldstrafe bestraft werden, § 156 StGB. Die fahrlässige Abgabe einer falschen Versicherung an Eides statt kann mit einer Freiheitsstrafe bis zu einem Jahr oder Geldstrafe bestraft werden, § 161 StGB.

Die oben stehende Belehrung habe ich zur Kenntnis genommen:

Official notification:

Any person who intentionally breaches any regulation of university examination regulations relating to deception in examination performance is acting improperly. This offence can be punished with a fine of up to EUR 50,000.00. The competent administrative authority for the pursuit and prosecution of offences of this type is the chancellor of the TU Dortmund University. In the case of multiple or other serious attempts at deception, the candidate can also be unenrolled, Section 63, paragraph 5 of the Universities Act of North Rhine-Westphalia.

The submission of a false affidavit is punishable.

Any person who intentionally submits a false affidavit can be punished with a prison sentence of up to three years or a fine, Section 156 of the Criminal Code. The negligent submission of a false affidavit can be punished with a prison sentence of up to one year or a fine, Section 161 of the Criminal Code.

I have taken note of the above official notification.

Ort, Datum
(Place, date)

Unterschrift
(Signature)

Titel der Dissertation:
(Title of the thesis):

Ich versichere hiermit an Eides statt, dass ich die vorliegende Dissertation mit dem Titel selbstständig und ohne unzulässige fremde Hilfe angefertigt habe. Ich habe keine anderen als die angegebenen Quellen und Hilfsmittel benutzt sowie wörtliche und sinngemäße Zitate kenntlich gemacht.
Die Arbeit hat in gegenwärtiger oder in einer anderen Fassung weder der TU Dortmund noch einer anderen Hochschule im Zusammenhang mit einer staatlichen oder akademischen Prüfung vorgelegen.

I hereby swear that I have completed the present dissertation independently and without inadmissible external support. I have not used any sources or tools other than those indicated and have identified literal and analogous quotations.

The thesis in its current version or another version has not been presented to the TU Dortmund University or another university in connection with a state or academic examination.*

*Please be aware that solely the German version of the affidavit ("Eidesstattliche Versicherung") for the PhD thesis is the official and legally binding version.

Ort, Datum
(Place, date)

Unterschrift
(Signature)

ZUSAMMENFASSUNG

Zahlreiche zelluläre Prozesse, wie zum Beispiel die Adhäsion and Migration, benötigen dynamische Änderungen spezialisierter Filamente, welche zusammen als Zytoskelett bezeichnet werden. Diese dynamischen Änderungen werden durch Signalproteine, wie zum Beispiel die Rho Familie von kleinen GTPasen in Raum und Zeit kontrolliert. In dieser Arbeit wird die Entwicklung und Anwendung von Techniken präsentiert, um die Aktivität von Rho GTPasen in Raum und Zeit zu stören und zu messen. Zunächst wird die Entwicklung von miniaturisierten, intrazellulären Protein Interaktions Arrays beschrieben. Mit dieser Technik konnten zwei unterschiedliche Protein Interaktionen simultan in individuellen, lebenden Zellen verfolgt werden, um Zell-Zell Varianz in der dynamischen Antwort auf akute pharmakologische Störungen aufzudecken. Um diese intrazellulären Interaktions Arrays zu generieren wurden bio-orthogonale, artifizielle Rezeptoren verwendet, welche die normale Zellfunktion nicht stören. Um die Prozessierung dieser Rezeptoren im sekretorischen Pathway zu optimieren, wurde deren Design durch systematische Deletions Analysen und Einfügen von Linkern und Glycosylierungs-Stellen optimiert. Diese Optimierung hat zu einer signifikanten Verbesserung der Plasma Membran Insertion der artifiziellen Rezeptoren geführt. Um Protein Aktivitäten in lebenden Zellen zu stören, wurde eine neue Klasse von artifiziellen Rezeptoren, sogenannte 'ActivatorPARCs', generiert, welche auf der subzellulären Re-lokalisation durch chemisch-induzierte Dimerisierung basieren. Die Rekrutierung dieser ActivatorPARCs in subzelluläre Bereiche der Plasma Membran erlaubte die Störung der Rho GTPase Aktivität in Raum und Zeit. Um die Geschwindigkeit dieser Störung zu beschleunigen, und um eine flexiblere Kontrolle der räumlichen Störungen zu ermöglichen, wurden ActivatorPARCs generiert, welche auf photochemisch-induzierter Dimerisierung basieren. Die laterale Diffusion des unaktivierten Photodimerizierungsmoleküls wurde durch kovalente Bindung an immobilisierte Rezeptoren eliminiert. Dies ermöglichte 'Molecular activity painting', eine neue Technik, durch welche akute und stabile Störungen direkt mit Licht in lebenden Zellen 'gemalt' werden können. Die Anwendung dieser Techniken zur direkten Analyse der räumlich-zeitlichen Signalausbreitung in zellulären Reaktionsnetzwerken wird diskutiert.

ABSTRACT

Many processes in mammalian cells, including adhesion and migration, require dynamic rearrangements of specialized filament structures, which are collectively called the cytoskeleton. Those dynamic rearrangements are controlled in space and time by signaling proteins, including the Rho family of small GTPases. In this thesis, the development and application of techniques to measure and perturb the activity of RhoGTPases in space and time is presented. First, a miniaturized, intracellular protein interaction array was developed to study multiple protein interactions inside an individual living cell. Using this technology, two distinct protein interactions were simultaneously monitored in individual cells to uncover cell-to-cell variance in their dynamic response to acute pharmacological perturbation. To generate those intracellular interaction arrays, bio-orthogonal artificial receptors were used that do not perturb normal cellular function. To optimize the processing of those receptors on the secretory pathway, their design was systematically improved by deletion analysis and insertion of linkers and glycosylation motifs. Those optimizations lead to a significant improvement of the plasma membrane targeting of artificial receptors. To perturb protein activities in living cells, a new class of optimized artificial receptors, termed ‘ActivatorPARCs’ was generated, that are based on subcellular targeting via chemically induced dimerization. Recruitment of ActivatorPARCs to subcellular regions in the plasma membrane enabled perturbation of RhoGTPase activity in space and time. To increase the speed of this perturbation and to enable more flexible control of spatial perturbations, ActivatorPARCs that are based on photo chemically induced dimerization were generated. Lateral diffusion of the uncaged photodimerizer was eliminated by covalent linkage on immobilized receptors. This enabled 'Molecular activity painting', a novel technique, in which rapid and stable perturbations can be directly “painted” with light inside individual living cells. The application of those tools to directly study spatio-temporal signal propagation in cellular reaction networks is discussed.

TABLE OF CONTENTS

LIST OF PUBLICATIONS

Methodologies and Results presented in this work has significantly contributed to the following peer reviewed articles:

- Chen Xi*, **Venkatachalapathy M***, Kamps D, Kapoor R, Weigel S, Orlich M, Hirtz M, Niemeyer CM, Yaowen Wu, Leif Dehmelt (2016) Molecular Activity Painting (MAP): Light-induced, Stable and Bio-orthogonal Targeting of Signal Proteins to the Plasma membrane (Manuscript in Preparation).

- Arrabito G, Schroeder H, Schröder K, Filips C, Marggraf U, Dopp C, **Venkatachalapathy M**, Dehmelt L, Bastiaens PI, Neyer A, Niemeyer CM (2014) Configurable Low-Cost Plotter Device for Fabrication of Multi-Color Sub-cellular Scale Microarrays Small Jul23; 10:2870-6.

- Gandor S, Reisewitz S, **Venkatachalapathy M**, Arrabito G, Reibner M, Schröder H, Ruf K, Niemeyer CM, Bastiaens PI, Dehmelt L (2013) A Protein Interaction Array Inside a Living Cell Angewandte Chemie Apr 26; 52(18): 4790– 4794.

  * - equal contribution.

LIST OF FIGURES

ABBREVIATIONS

°C: degree Celsius

Aa: aminoacids

APTS:3-amino propyl trimethy silicone

Arp: Actin related protein

ATP: Adenosine triphosphate

BFP: Blue fluorescent Protein

bp: Basepairs

BSA: Bovine Serum Albumin

cAMP: cyclic adenosine monophosphate

Cat α: Catalytic subunit of PKA

C:terminus: Carboxy terminus

CCL: Coiled Coiled linker

Cdc42: Cell division cycle 42

CFP: Cyan fluorescent protein

CID: Chemically induced dimerization

CMV: Cytomegalovirus

CRISPR: Clustered regulatory interspaced palindromic repeats

CNX: Calnexin

Cy7: Cyanin 7

ddH_20: dideionized water

DDI: DNA directed immobilization

delCMV: a truncated CMV promoter

DMEM: Dulbecco's modified Eagle's medium

DMSO: dimethylsulfoxide

DNA: deoxyribonucleic acid

DPN: Dip pen nanolithography

dNTPs: deoxyribonucleoside triphosphates

E: Relative enrichment

E.coli: Escherichia coli

e.g: exempli gratia

eDHFR: E.coli dihydrofolate reductase

EDTA: ethylenediaminetetracetic acid

EGFP: Enhanced green fluorescent protein

ER: Endoplasmic reticulum

EtOH: Ethyl alcohol

et al: and others

FBS: Foetal bovine serum

Fig: Figure

FKBP': F36V mutant of FKBP

FKBP: FK506:binding protein

fM: femtomolar

For: Forward

FRET: Fluorescence resonance energy transfer

g: gram(s)

GAP: GTPase activating protein

GBD: GTPase binding domain

GDI: Guanine dissociation inhibitor

GDP: Guanosine diphosphate

GEF: Guanine nucleotide exchange factor

GPCR: G-Protein coupled receptor

GTP: Guanosine triphosphate

HA: Haemagglutinin

KRC: K Ras C terminus

Ig: Immunoglobulin

L : Liter(s)

LB: Luria:Bertani

MEM: minimum essential medium

min: minutes

mL: milliliter(s)

mm: millimeter(s)

mM: millimolar

mN: milli newton

mTFP: Monomeric teal fluorescent protein

mTOR: Mechanistic targeting of Rapamycin

μL: microliter(s)

N term amino terminus

N2a: Neuro-2a

NA: Numerical aperture

NEAA: Non essential aminoacids

NES: Nuclear export sequence

ng: nanograms

nM: nanomolar

nm: nanometer

NVOC: Nitro vera triloxy

OST: Oligosaccharyl transferase

PA: Photoactivation

PARC: Presenting artificial receptor construct

PLL: Poly-L-Lysine

PBS: Phosphate buffered saline

pCID: Photochemically induced dimerization

PCA: Protein complementation assay

PCR: Polymerase chain reaction

PDB: Protein Data Bank

PDGFR: Platelet derived growth factor receptor

PDMS: Polydimethoxy silane

PEG: Polyethylene glycol

PKA: Protein kinase A

pH: Potentium hydrogen

PM: Plasma membrane

POI: Protein of interest

Rac1: ras related C3 botulinum toxin substrate 1

Rev: reverse

RBD: Rhotekin GTPase binding domain (aa 8:89)

RFP: Red fluorescent protein

r:GBD: Rhotekin GTPase binding domain (aa 7:89)

RhoA: ras homolog family member A

RhoGDI: Rho Guanine nucleotide Dissociation Inhibition

Rpm: Rotations per minute

RIα: Regulatory subunit I of PKA

RII β: Regulatory subunit II of PKA

RT: Room temperature

Sec: Seconds

SRP: Signal receptor particle

ss: Single stranded

SV40: Simian virus 40

T: temperature

TAE: tris acetic acid EDTA

TALEN: Transcriptional activator like effector nucleases

TIR: total internal reflection

TIRF: total internal reflection fluorescence

TMP: Trimethoprim

Tris: tris[hydroxymethyl] aminomethane

U: unit(s) of enzyme

UV: ultraviolet

VSVG: Vesicular stomatitis virus glycoprotein

WASP: Wiskott:Aldrich Syndrome Protein

INTRODUCTION

One of the most important challenges of modern biomedical research is to understand how dynamic cellular processes such as cell migration, morphology and adhesion are controlled by protein interactions. Protein interactions can either form the basis of structural assemblies, such as cytoskeletal filaments, or they can form network motifs, that include positive or negative feedback regulation. Individual protein interactions are interconnected to form a higher order network that controls overall cell behavior**.** One example for highly interconnected protein interactions are RhoGTPases and their signal networks. RhoGTPase signal networks regulate actin and microtubule polymerization, leading to cell protrusion and retraction, thereby controlling cell migration and cell morphology [**Figure 1.1]**. RhoGTPase signal networks also play an important role in disease related processes, such as cancer cell metastasis. This thesis presents novel perturbation approaches to unravel protein interaction networks in dynamic cellular processes.

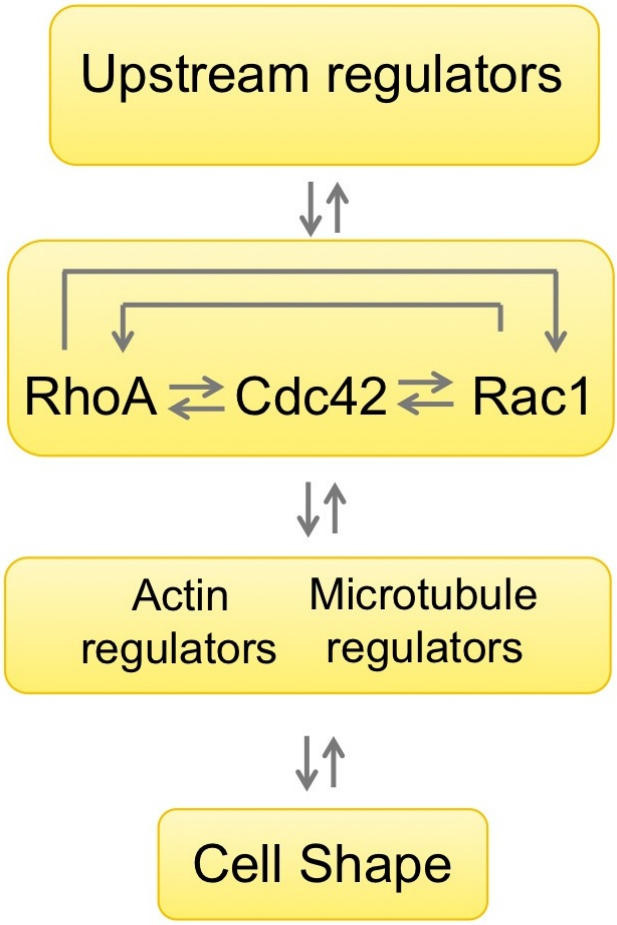

Figure 1.1: RhoGTPase signal networks control cell shape. Rac1, Cdc42 and RhoA are the best characterized RhoGTPase family members and are known to regulate cytoskeletal dynamics. These proteins interact with many other proteins to perform their function: they are modulated by upstream regulators, including growth factor receptors, they can influence each other via crosstalk and they can activate actin and microtubule regulators that control cytoskeletal dynamics and thereby alter the shape of cells.

1.1 Control of cell shape by the cytoskeleton

The cytoskeleton is a complex dynamic network of filaments and tubules that are formed throughout the cell. Cytoskeletal filaments are composed of actin, microtubules and intermediate filaments. These dynamic cytoskeletal filaments are organized into structures that can span the entire cell; yet, the individual proteins are

just a few nanometers in size. Those large, relatively stable cytoskeletal structures are thus built by the repetitive self-assembly of smaller, diffusible subunits within cells.

1.2 Polymerization of actin filaments

Actin filaments have the ability to polymerize rapidly at the leading edge of the protruding cell and they depolymerize preferentially near the trailing rear edge. Nucleation of actin filaments predominantly takes place in the plasma membrane and is frequently regulated by external signals. Polymerization of actin filaments leads to cell protrusion during migration. Two main types of nucleators control the rate-limiting step of this process. a) Formins b) Arp2/3 (**TD Pollard et al 2007**). Formin nucleators like mDia2 and mDia3 possess two actin-binding sites, which undergo conformational changes to promote actin growth in a linear fashion. Arp2/3 is highly concentrated on the leading edge. Binding of Arp2/3 complex to the sides of already formed actin filaments promote extension of new actin filament from its pointed end at a 70° angle, thereby forming a highly cross-linked dendritic actin filament network. The nucleation promoting factors WAVE/Scar, WASP and N-WASP activate the Arp2/3 mediated actin polymerization. By controlling the nucleation, polymerization and interaction between actin filaments, those regulators control the formation of different kinds of cell surface projections, including spiky bundles called filopodia **[Allan Hall et al, 1998] [Figure 1.3d]** and flat protrusive sheet-like structures called lamellopodia **[Figure 1.3c]**

1.3 Protrusion-retraction cycles in cell migration

Cell protrusion formed due to actin polymerization is responsible for cell migration and formation of new focal adhesions in the leading edge **[Figure 1.2a-b]**. However, cell translocation also requires disassembly of adhesions at the rear end for cell retraction **[Figure 1.2d]**. This process is driven by the activity of myosin motors that shift anti-parallel actin filaments against each other, leading to cell contraction. This so-called actomyosin activity is found near the leading edge of cells, where it alters actin flow and plays a role in modulating the direction of migration, near the trailing edge, where it generates stress fibres that drive cell retraction **[Mattila et al., 2008]**.

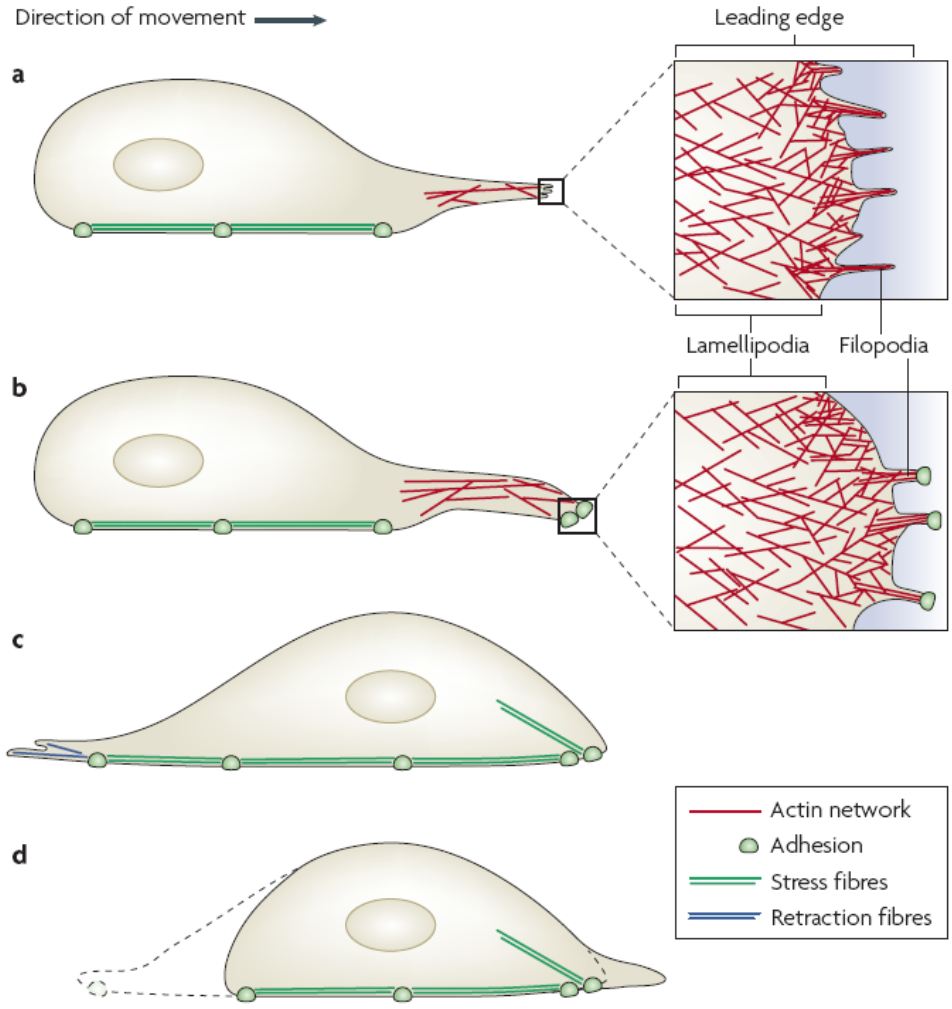

Figure 1.2: Cell protrusion and retraction cycle a. Actin dependent cell protrusion is driven by lamellopodia and filopodia formation at the leading edge. These dynamic structures are generated as a result of elongated barbed actin ends pushing towards the plasma membrane **b.** Cellular extensions create new adhesions under the leading edge **c.** Actomyosin contraction forces and focal adhesion linked stress fibers translocate the nucleus and cell body forward and mediate substrate attachment **d.** Trailing edge of the cell retracts after the disassembly of adhesions at the rear end and pulling of retraction fibres to move the cell forward. **Picture Source: Mattila et al., 2008**

1.4 Control of cytoskeletal dynamics by RhoGTPases

Rho GTPases are best known for their ability to control regulators that modulate the assembly, disassembly and spatio-temporal arrangement of actin filaments **[M Raftopoulou et al., 2004].** In a seminal study in Swiss 3T3 fibroblasts, it was found

that activation of Rho resulted in the formation of contractile actomyosin filaments in the cell center, which are called stress fibers **[Alan Hall, 1998]**. Conversely, activation of Rac and Cdc42, the other two major members of the Rho GTPase family, gave rise to a meshwork of actin filaments in the cell periphery, including lamellopodia **[Figure 1.3c]**, membrane ruffles and actin-rich, finger-like extensions called filopodia **[Figure 1.3d]**. These findings provided strong evidence for a key regulatory role of Rho GTPases in controlling the organization of the actin cytoskeleton **[L Van Aelst., 1997 & Alan Hall 2000].**

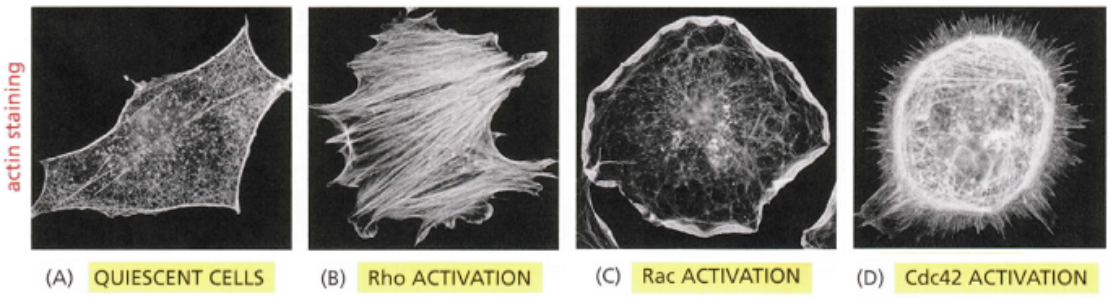

Figure 1.3: Activation of individual RhoGTPases in Neuro-2A cells. Phenotypic responses due to the activation of Rho, Rac and Cdc42: stress fibers, lamellopodia and filopodia formation. **Picture source: Alan Hall et al, 1998**

Rho GTPases exist in two forms: An active, GTP-bound or inactive GDP-bound state. Switching between those states is mainly controlled by *Guanine nucleotide exchange factors* (GEFs) and *GTPase-activating proteins* (GAPs). *Guanine nucleotide dissociation inhibitors* (GDIs) extract Rho proteins from the membranes and solubilize them in cytosol **[Jaffe AB et al, 2005] [Figure 1.4].** In order to activate GTPases, GEF proteins promote nucleotide exchange by removing the bound GDP nucleotide, thus allowing the binding of the more abundant GTP **[Jaffe AB et al, 2005]**. To inactivate Rho GTPases, GAPs provide a catalytic arginine to enable GTP

hydrolyzing activity, which results in the GDP-bound state GDIs interact only with the prenylated Rho GTPases and inhibit GTP hydrolyzing activity and nucleotide exchange activities of Rho Proteins [**Dovas et al., 2005**].

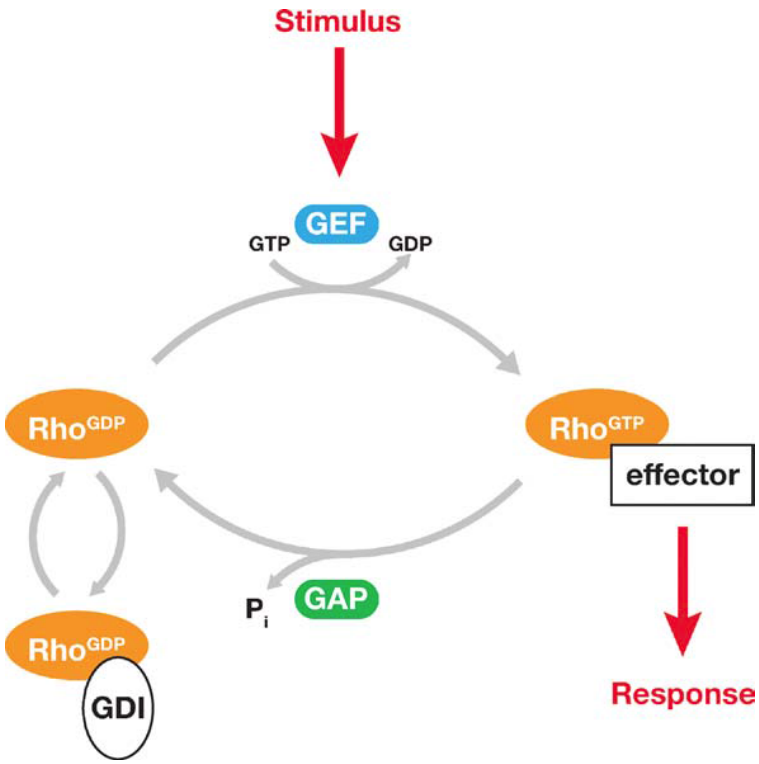

Figure 1.4: Schematic representation of a RhoGTPase signal module. The inactive GDP bound RhoGTPase is switched into the active form if a corresponding GEF is activated by an input stimulus. The GTP bound RhoGTPase activates effector proteins that lead to a response. Conversely, GAPs inactivate RhoGTPases to close the regulatory cycle. The inactive RhoGTPase associates preferentially with RhoGDI to solubilize the RhoGTPase in the cytosol. **Picture source: Jaffe AB et al., 2005**

Interestingly, the activity of RhoGTPases is dynamically regulated in subcellular regions, but unfortunately most of the information available in the literature was obtained from bulk measurements using techniques that do not consider those spatial and temporal dimensions. **[O Pertz, 2010].** In order to overcome these limitations, fluorescent biosensors and acute perturbation methods were developed to monitor

and modulate Rho GTPase signaling with high spatio-temporal resolution **[Nalbant et al., 2004, Pertz et al., 2006, Machacek et al., 2009, Wu et al., 2009, Peng Liu et al., 2014**].

1.5 Crosstalk between RhoGTPases

To coordinate their activity in space and time, it is thought that Rho GTPases influence each other via complex cross-talk mechanisms. This crosstalk can occur at different levels **[Guilluy et al, 2009].** For example, activation of one Rho GTPase could turn off another Rho GTPase via specific GEF inactivation**.** Alternatively, activation of a GAP by one Rho GTPase could also lead to inactivation of another RhoGTPase. Conversely, the activation of a GEF or the inactivation of a GAP can activate another Rho GTPase. Finally, one RhoGTPase can interfere with the downstream signaling of another RhoGTPase by inactivating or activating a shared target or effector protein**.**

Several studies proposed specific GAPs, GEFs and downstream effectors in the regulation of the crosstalk among RhoGTPases. For example, crosstalk mechanisms that are thought to regulate Rac1 and RhoA are summarized in **[Guilluy et al, 2009] [Figure 1.5].** However, the crosstalk may vary depending on the subcellular location and could also vary depending on the functional context or between specific cell types **[Pertz O et al, 2010]**. Thus, studying how RhoGTPases communicate with each other in space and time is important to understand how dynamic cytoskeletal filaments are organized in dynamic cell behaviors, such as cell migration **[Figure 1.5].**

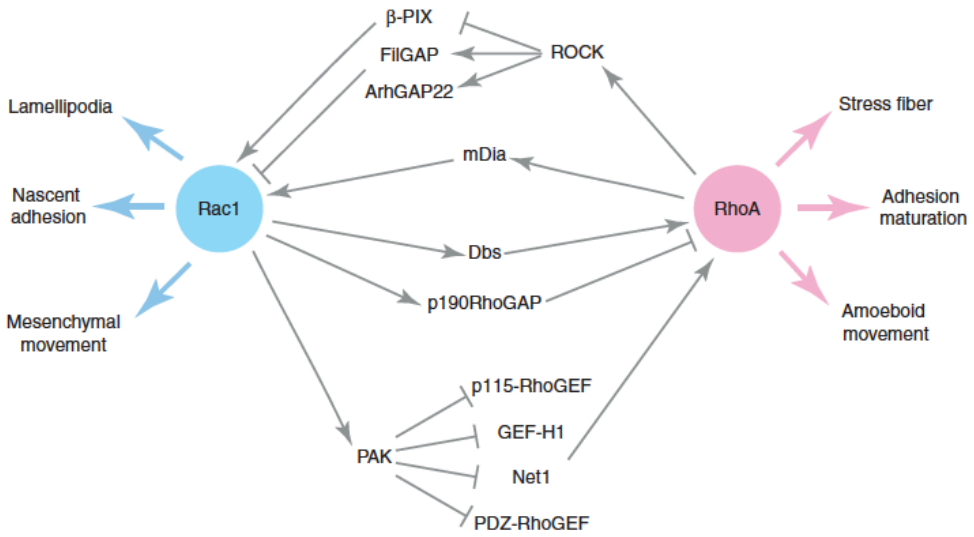

Figure 1.5: Crosstalk between Rac1 and RhoA: Schematic representation of proposed crosstalk mechanisms between Rac1 and RhoA GTPases. **Picture Source: Guilluy et al, 2009.**

1.6 Current state of techniques for the analysis of protein interactions

The yeast two-hybrid system (Y2H) is a very efficient classical method to study protein interactions. It was used to screen large libraries to build proteome interaction networks (**Brückner A et al., 2009**) via the complementation of a transcriptional activator. However, this feature limited the yeast two-hybrid system to study protein interactions that can take place in nucleus of yeast cells. Another variant of this technique, called the protein fragment complementation assay (PCA) (**Piehler et al., 2005**), overcame this limitation by probing interactions at the plasma membrane, a subcellular region that harbors about 30% of the interactions expected to occur in the mammalian proteome. Both Y2H and PCA confer high false positive hit rates, which stimulated new ideas to study protein interactions. More recently, mass spectrometry methods were developed for high-throughput analysis of protein interactions in cell extracts (**Aebersold R et al, 2003**). However, dynamic networks of protein

interactions that are organized in space and time determine cell phenotype and behavior. Therefore, such techniques that are based on large numbers of cells from extracts only offer a very limited view of dynamic protein interaction networks. In contrast, fluorescent resonance energy transfer (FRET) can be used to directly monitor and measure static and dynamic protein interactions inside living cells (**Socher E et al., 2013**). However, FRET is limited by the spectral properties of the fluorescent proteins, therefore only one or few protein interactions can be measured. To directly analyze interconnected protein activities in dynamic signal networks, multiple protein interactions need to be analyzed simultaneously in individual cells. Hence, there is a demand for novel methods that overcome those limitations. An example for interconnected proteins in dynamic signal networks is the RhoGTPases and their interactions with each other and downstream effectors **[Hanna et al 2013]**.

1.7 Current state of techniques for the perturbation of protein interactions in living cells

One of the classical ways to determine the function of a gene is by altering its activity and monitoring the phenotypic response. Genes and their products were manipulated at different organizational levels using specialized perturbation approaches. Each method has advantages and limitations. For example, Zinc finger nucleases, transcription activator like effector nucleases (TALENs) and clustered repeats of interspaced palindromic repeats (CRISPR) were used to edit genes on the genomic level via site-specific homologous recombination (**Gaj et al., 2013**). Even though these genetic manipulation methods are specific and robust, they are difficult to implement, time consuming, irreversible and they have very slow effects on phenotype based on the turnover of the associated gene products. Transcript level

gene silencing with siRNA treatment is easier to implement compared to genetic manipulation but still restricted by the relatively slow turnover of most proteins. Furthermore, siRNA methods are often restricted due to low efficiency of knockdown and non-specific target effects [**Aagard et al 2007**]. On the other hand, direct targeting of proteins via small molecules can be acute and is usually simple to perform, but can be limited due to specificity and associated off-target effects [**Milstein et al., 2013**]. An optimal manipulation strategy should offer the following attributes i) robustness ii) rapid onset iii) specificity iv) tunability v) reversibility vi) easy to implement vii) cheap viii) spatially controlled [**Rakhit et al., 2014**].

Combining chemical and genetic perturbation strategies provides the advantage of small molecules to perturb protein activity rapidly and reversibly with the advantage of molecular biology to specifically address a selected protein of interest. Rapamycin induced FKBP and FRB dimerization is the classical implementation of this "chemically induced dimerization" strategy and was used in various contexts to study cellular processes (**Brown, E. J et al., 1994, Derose R et al., 2013**). However, unspecific binding of Rapamycin to mTOR kinase lead our group to develop a novel bio-orthogonal chemically induced dimerization (CID) system together with Dr. Yaowen Wu, that enabled rapid dimerization of eDHFR-FKBP' fused proteins upon addition of the small molecule SLF-TMP' **[Peng Liu et al, 2014] [Figure 1.6]**. The reversibility of this system, with fast reaction times, low cytotoxicity, minimal perturbation of endogenous proteins and the possibility to integrate with other chemically induced dimerization strategies made it an interesting tool to perturb protein activities in living cells [**Peng Liu et al, 2014**].

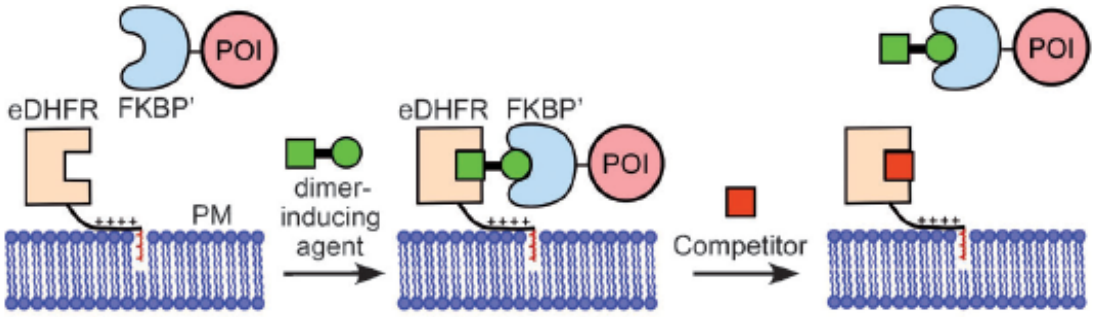

Figure 1.6: Schematic representation of a novel, reversible chemical inducible dimerization system. Two proteins (eDHFR and FKBP') are brought together in order to localize a protein of interest to a desired subcellular localization. Addition of competitor dissociates this interaction, thereby causing the proteins to dissociate. **Picture source: Peng Liu et al., 2014**

As light can be confined to a small spot, light inducible dimerization systems offer the possibility to manipulate proteins both in space and time (**Levskaya et al., 2009, Kennedy et al., 2010, Karginov et al., 2011, Ballister et al., 2014, Zimmermann et al., 2014, Gautier et al., 2014, van Bergeijk et al, 2015**). However, current approaches for light inducible dimerization are limited by diffusion of photoactivated molecules, in particular if photoactivation is performed on soluble molecules in the cytosol or on mobile proteins within the plasma membrane.

Novel methods were required to induce stable perturbation and analyze RhoGTPase activity in spatio temporal resolution. Combining protein arrays with photochemically induced dimerization strategies can address our objective. This thesis discuss about the advanced perturbation methods and analysis that can be applied to discover the crosstalk mechanisms between RhoGTPases that can be used to build RhoGTPase signal network.

2.1 Materials

2.1.1 Chemicals and Reagents for Molecular cloning

Reagents	Trademark
Absolute ethanol	AnalaR Normapur
Acetic acid	Sigma Aldrich
Acetone	Sigma Aldrich
Adenosine-5'-Phosphate	Sigma Aldrich
Agarose	Carl Roth GmbH
Ampicillin sodium salt	Carl Roth GmbH
Antartic Phosphatase	New England Biolabs
Atto 740 Biotin	ATTO-Tec-GmbH
3-aminopropyltriethoxy-silane	Sigma Aldrich
BSA	Serva
Dimethyl sulfoxide	Carl Roth GmbH
Disodium hydrogen phosphate	Sigma Aldrich
dNTP mix	Fermentas
Doxycycline	Clontech
DPBS	PAN Biotech GmbH
EGF-Biotin	MPI-Dortmund
Ethidium bromide	Carl Roth GmbH
Ethylenediaminetetra-acetic acid	Sigma Aldrich
Formaldehyde	Carl Roth GmbH
Forskolin	Sigma Aldrich
Glycerol	Sigma Aldrich
Hoechst 33342	Sigma Aldrich
IBMX	Thermo-fischer Scientific
Isopropanol	Carl Roth GmbH
Isoproterenol	Sigma Aldrich
Kanamycin sulfate	Carl Roth GmbH
Nuclease free water	Ambion
PBAG	Sigma Aldrich
PEG 1000	Sigma Alrich
Potassium chloride	Sigma Aldrich
Propranolol	Sigma Aldrich
Sodium Chloride	Sigma Aldrich
Sodium hydroxide	Sigma Aldrich
Sodium acetate	J.T.Baker
Tris base	Sigma Aldrich
Tris HCl	Sigma Aldrich
Triton-X-100	SERVA Electrophoresis GmBH
Tween-20	Merck

2.1.2 Enzymes and Antibodies

Enzymes and Antibodies	Trademark
Accuprime Pfx DNA polymerase	Thermofischer
AgeI	New England Biolabs
Alexa Fluor 488 goat-anti mouse Antibody	Molecular Probes
Alexa Fluor 488 goat-anti rabbit Antibody	Molecular Probes
Alexa Fluor 568 goat-anti mouse Antibody	Molecular Probes
Alexa Fluor 568 goat-anti rabbit Antibody	Molecular Probes
ApaI	New England Biolabs
BamH1	New England Biolabs
BsrE1	New England Biolabs
Calf intestinal phosphatase	Thermofischer
DNA ligase	New England Biolabs
EcoRI	New England Biolabs
EcoRV	New England Biolabs
Goat polyclonal Anti-[HA] antibody (Biotinylated)	Abcam
HindIII	New England Biolabs
NheI	New England Biolabs
NotI	New England Biolabs
Phusion High fidelity DNA polymerase	New England Biolabs
PmlI	New England Biolabs
PvuI	New England Biolabs
Rabbit polyclonal Anti-[VSVG] antibody (Biotinylated)	Abcam
SacI	New England Biolabs
SacII	New England Biolabs
XbaI	New England Biolabs
XhoI	New England Biolabs
XmaI	New England Biolabs

2.1.3 Primers

Oligos	Type	Sequence
NotI DA-KRC Forward	Forward (494)	TA*GCGGCCGC*CAATGATCAGTCTGATTGCGGCG TTAG
XhoI DA-KRC Reverse	Reverse (495)	AC*CTCGAG*TTACCGCCGCTCCAGAATCTCAAAGCA ATA
NheI DA KRC BFP forward	Forward (496)	CCACT*GCTAGC*ATGAGCGAGCTGATTAAGGAGAA
NotI DA KRC BFP Reverse	Reverse (497)	TA*CGCGGCCG*CTTAACCGGAACCGCCGGAT
NheI mcitrine Forward	Forward (498)	AA*GCTAGC*ATGGTGAGCAAGGGCGAGGAGC
mcitrine Reverse AccI	Reverse (499)	AA*TCCGGA*TGTACAGCTCGTCCATGCCGAG
NheI CCL mcitrine CCL Forward	Forward (500)	AA*GCTAGC*CTGGCCGCCGCCTATAGCAG
AccI CCL mcitrine CCL Reverse	Reverse (501)	AA*TCCGGA*GCTGCTCAGAATGCTGCTATAC
AccI SNAPf pDisplay Forward	Forward (502)	TA*TCCGGA*CTCAGATCTCGAGCTATGGACAAAGACTGC GAAATGAAG
Not_SNAPf pDisplay Reverse	Reverse (503)	GCACGCGCT*GCGGCCGC*TCATTAATTAACCT

Forward AccIII Halotag	Forward (504)	CT*TCCGGA*ATGGCAGAAATCGGTACTGGCTTT
Reverse BamH1 Halotag	Reverse (505)	AT*GGATCC*GGTGGCTACGTAACCGGAAAT
Forward AccIII_Halotag	Forward (506)	CT*TCCGGA*ATGGCAGAAATCGGTACTGGCTTT
Reverse SacII baitPARC	Reverse (507)	CA*CCGCGG*TTAGGCTACGTAACCGGAAATCTC
Strongsignal adapter Forward-Pho	Forward (508)	ATCATGAACTTTATCCCAGTCGACATTCCACTCTTGATG ATCTTCCTTGTGACAACTGGGGGCTCAGCGGG
Strongsignal adapter Reverse-Pho	Reverse (509)	GGCCCCCGCTGAGCCCCCAGTTGTCACAAGGAAGATCA TCAAGAGTGGAATGTCGACTGGGATAAAGTTCATGAT
EcoRV Strong signal seq Forward	Forward (510)	GGAA*GATATC*GAGGTGTGGCAGGCTTG
ApaI Strong signal seq Reverse	Reverse (511)	TA*GGGCCC*CCGCTGAGCCCCCAGTTGTCA
NheI DA KRC BFP Forward	Forward (512)	TCGCCACCGCTAGCATGAGCGAGCTGATTAAGGAGAA
NheI DA KRC BFP Reverse	Reverse (513)	GGGGGGGCTAGCATGAGCGAGCTGATTAAGGAGAA
XbaI Ephrin CCL mcitrine CCL Forward	Forward (514)	AA*TCTAGA*TTGGCGGTGATTGGCGGCGTGG

NheI Ephrin CCL mcitrine CCL Reverse	Reverse (515)	AA*GCTAGC*GCTGCTCAGAATGCTGCTATAC
NheI Adapter Forward delBFP	Forward (516)	*CTAGC*GGCGGTACCGGTGGTACCGGT*T*
AccII Adapter Reverse delBFP	Reverse (517)	*CCGGA*ACCGGTACCACCGGTACCGCC*G*
NheI Adapter AccII Forward delBFP delD1	Forward (518)	*CTAGC*AAGGC*GC*
NheI Adapter AccII Reverse delBFP delD1	Reverse (519)	*GGCCGC*GCCTT*GCTAG*
AccI Adapter NotI Forward delD1	Forward (520)	*CCGGA*AGAGC*GC*
AccI Adapter NotI Reverse delD1	Reverse (521)	*GGCCGC*GCTCT*T*
PvuI BFP Forward	Forward (522)	*CGATCG*ATGAGCGAGCTGATTAAGGAGAA
PvuI BFP Reverse	Reverse (523)	*CGATCG*ATTAAGCTTGTGCCCCAGTTTG
eDHFR sitedirected	Forward (524)	CCGGCCTGGAG*TCTAGG*ATCAGTCTGATTG

Forward		
eDHFR sitedirected Reverse	Reverse (525)	CAGACTGATCCTAGACTCCAGGCCGGC
ApaI mcherry eDHFR Forward	Forward (526)	ATGGGCCCATGGTGAGCAAGGGCGAG
BamH1 Halotag CAAX Reverse	Reverse (527)	ATGGATCCGAGATTTCCGGTTACGTAGCC
SNAPf GSGS Annealing Forward	Forward (528)	AAACTCGAGGTTAATGCTTCTGGCGGTTCAGGGGGACCCGGGTAAGC
SNAPf GSGS Annealing Reverse	Reverse (529)	GGCCGCTTACCCGGGTCCCCCTGAACCGCCAGAAGCATTAACCTCGAGTTT
6xKGP Linker Forward	Forward (530)	GTGGCCCCGGCGGCAAGAAGAAGAAGAAGAAGCCCGGCG
6xKGP Linker Reverse	Reverse (531)	CTAGCGCCGGGCTTCTTCTTCTTCTTCTTGCCGCCGGGGCCAC
6xKGS Linker Forward	Forward (532)	GTGGCAGCGGCGGCAAGAAGAAGAAGAAGAAGAGCGGCG
6xKGS Linker Reverse	Reverse (533)	CTAGCGCCGCTCTTCTTCTTCTTCTTCTTGCCGCCGCTGCCAC
XmaI 2*SNAPf Forward	Forward (534)	AGCCCGGGATGGACAAAGACTGCGAAATGAAGCGC
NotI 2*SNAPf Reverse	Reverse (535)	TTCACCGCGGCCGCTTACCC

2.1.4 Plasmids

Plasmids	Description of the construct	Source/Creator
pDisplay	Hemagglutinin displayed on the surface with multiple cloning sites in the intracellular part	Invitrogen **[pDisplay Invitrogen manual,2010, Chestnut JD, 1996]**
pCMV-Tet3G	Regulator plasmid of Tet-On®3G system	Clontech
pTRE3G	Response plasmid of Tet-On®3G system	Clontech
pTRE3G [mcherry] [cat-α]	Response plasmid of Tet-On®3G system fused with catalytic subunit of cAMP dependent protein kinase A.	This thesis
HA Titin bait [GFP][RI-α]	To the pDisplay vector, a Titin linker is added over the extracellular part and the intracellular part is fused with green fluorescent protein and Regulatory subunit of Protein Kinase I	baitPARC 1.0 **[Gandor et al,2013]**
VSVG Titin bait [TFP][RII-β]	To the pDisplay vector, a Titin linker is added over the extracellular part and the intracellular part is fused with green fluorescent protein and Regulatory subunit of Protein Kinase II	baitPARC 2.0 **[Gandor et al,2013]**
VSVG bait [empty]	Titin, mTFP and RII-b] is removed from baitPARC 2.0	Micheal Orlich
VSVG bait [TFP]	Titin and RII-b is removed from baitPARC 2.0	Micheal Orlich
VSVG bait [RII-β]	Titin and mTFP is removed from baitPARC 2.0	Micheal Orlich
VSVG Titin bait [TFP]	RII-b is removed from baitPARC 2.0	Micheal Orlich
VSVG Titin bait [RII–β]	mTFP is removed from baitPARC 2.0	Micheal Orlich

VSVG Titin [empty]	RII-b and mTFP is removed from baitPARC 2.0	Micheal Orlich
VSVG bait [TFP] [RII–β]	Titin is removed from baitPARC 2.0	Micheal Orlich
VSVG Titin GSGS bait [TFP][RII-β]	Glycine based 'small' linker is added between the transmembrane domain and mTFP sequence to baitPARC 2.0	Martin Kares
VSVG Titin GSGS-L bait [TFP][RII-β]	Glycine based 'long' linker is added between the transmembrane domain and mTFP sequence to baitPARC 2.0	Martin Kares
VSVG –glyco-Titin bait [TFP][RII–β]	Glycosylation signal added in front of the titin linker to baitPARC 2.0	Darius Kaszta
VSVG Titin–glyco- bait [TFP][RII-β]	Glycosylation signal added at the back of titin linker to baitPARC 2.0	Darius Kaszta
VSVG –glyco-Titin–glyco- bait [TFP][RII-β]	Glycosylation signal added in front and back of the titin linker to baitPARC 2.0	Darius Kaszta
VSVG Titin activator [TagBFP][eDHFR]	RII-b bait protein from the baitPARC 2.0 is replaced with eDHFR	This thesis (activatorPARC 1.0)
VSVG Titin GSGS activator [TagBFP][eDHFR]	Glycine linker is added to the activatorPARC 1.0	Martin Kares (activatorPARC1.1)
VSVG Titin GSGS activator [mCitrine][eDHFR]	BFP fluorescent protein is replaced with monomeric citrine in Activator 1.1	This thesis (activatorPARC 1.2)
VSVG Titin GSGS activator [ccl Citrine][eDHFR]	BFP fluorescent protein is replaced with coiled coiled linker citrine in Activator 1.1	This thesis (activatorPARC1.3)
VSVG –glycol-Titin–GSGS activator [TagBFP][eDHFR]	Glycosylation signal sequence is added to Activator 1.1	This thesis (activatorPARC1.4)

VSVG –glyco-Titin–GSGS activator [ccl Citrine] [eDHFR]	Glycosylation signal sequence is added to activatorPARC 1.3	This thesis (activatorPARC1.5)
VSVG –glyco-Titin–GSGS activator [TagBFP] [eDHFR]	KPS positively charged linker is added to activatorPARC 1.4	This thesis (activatorPARC 1.6)
VSVG -glyco-Titin–GSGS activator [ccl-Citrine-ccl] [eDHFR]	KPS positively charged linker is added to activatorPARC 1.5	This thesis (activatorPARC 1.7)
VSVG - glyco-Titin–GSGS activator [ccl-Citrine-ccl] [SNAPf]	E.coli Dihydrofolate reductase is replaced with SNAPf protein in activatorPARC 1.7	This thesis (activatorPARC 2.0)
VSVG -glyco-Titin–GSGS activator [ccl-Citrine-ccl] [Halotag]	E.coli Dihydrofolate reductase is replaced with Halotag protein in activatorPARC 1.7	This thesis (activatorPARC 3.0)
VSVG -glyco-Titin–GSGS activator [TagBFP] [Halotag]	E.coli Dihydrofolate reductase is replaced with Halotag protein in activatorPARC 1.6	This thesis (activatorPARC 3.1)
TagBFP-2xeDHFR-CAAX	TagBFP linked to 2 copies of E.coli Dihydrofolate reductase and C-terminus of K-Ras (-CAAX)	Abram Calderon
mTurquoise2-NES-2xFKBP-Rac1Q61LΔCAAX	mTurquoise2 linked with nuclear export signal to 2 copies of FK506 binding protein and constitutively active mutant of Rac	Abram Calderon
mTurquoise2-NES-2xFKBP-Cdc42Q61LΔCAAX	mTurquoise2 linked with nuclear export signal to 2 copies of FK506 binding protein and constitutively active mutant of Cdc42	Abram Calderon
delCMV-mCherry-RBD	mCherry linked to GTPase binding domain (GBD) of Rhotekin	Abram Calderon
delCMV-mCherry-p67phox (aa1-203)	mCherry linked to the Rac1 GTPase binding domain (GBD) of $p67^{phox}$	Abram Calderon
delCMV-mCherry-WASP-GBD	mCherry linked to the Cdc42 GTPase binding domain (GBD) of WASP	Abram Calderon
pmCitrine-N1	mCitrine	MPI Dortmund
Ubiquitin-Actin-Cherry	mCherry labeled actin	Melanie Graßl

EGFP-CAAX	Green fluorescent protein is fused with C-terminus of K-Ras (-CAAX)	MPI Dortmund
TagBFP-Halotag-CAAX	TagBFP linked to a copy of Halotag sequence and C-terminus of K-Ras (-CAAX)	This thesis
mCitrine-eDHFR	Citrine fluorescent protein fused with a single copy of E.coli Dihydrofolate reductase	Dr. Yaowen Wu, CGC Dortmund
mCitrine-eDHFR-RacQ61LΔCAAX	mCitrine linked with a single copy of eDHFR is fused with constitute mutant of Rac	This thesis
mCitrine-eDHFR-NES-RacQ61LΔCAAX	mCitrine linked with a single copy of eDHFR is fused with nuclear export signal and a constitute mutant of Rac	This thesis
mCitrine-FKBP'-NES-RacQ61LΔCAAX	mCitrine linked with a single copy of FKBP is fused with nuclear export signal and a constitute mutant of Rac	This thesis
mCitrine-eDHFR-NES-GEFH1C53	mCitrine linked with a single copy of eDHFR and GEF-H1 mutant	This thesis
mTurquoise2-2xFKBP-GEFH1C53	mTurquoise2 linked with two copies of FKBP and GEFH1 mutant	Wiebke Obermann
mCherry-eDHFR-NES-RacQ61LΔCAAX	mCherry linked with a single copy of eDHFR is fused with nuclear export signal and a constitute mutant of Rac	This thesis
EGFR-mTFP	EGFR fused with turquoise fluorescent protein	MPI Dortmund
EphA2 ccl-mCitrine-ccl	Ephrin fused with citrine fluorescent protein via coiled coiled linker	Ola Sabet
Halotag GFP mito mCherry eDHFR	Bicistronic expression of halotag fused with green fluorescent protein and fused with cherry eDHFR	pERB217 Addgene (#61500)

Plasmid	Source of backbone	Insert
TagBFP Halotag CAAX	Double digestion of (BspE1 and BamH1) TagBFP-2xeDHFR-CAAX	PCR amplification of Halotag-mito-eDHFR-mcherry (504 and 505)
baitPARC TagBFP Halotag	Double digestion of (BspE1 and SacII) baitPARC-glycotag-KPS-TagBFP-2xeDHFR.	PCR amplification of Halotag-mito-eDHFR-mcherry (506 and 507)
mCitrine eDHFR Rac1Q61LΔCAAX	Double digestion of (MfeI and XbaI) mCitrine-eDHFR.	Double digestion of (MfeI and XbaI) mTurquoise2-NES-2xFKBP-Rac1Q61LDCAAX
mCitrine NES 2xFKBP Rac1Q61LΔCAAX	Double digestion of (NheI and XhoI) mCitrine-eDHFR.	Double digestion of (NheI and XhoI) mTurquoise2-NES-2xFKBP-Rac1Q61LDCAAX
mCitrine NES eDHFR Rac1Q61LΔCAAX	Double digestion of (XhoI and BamH1) mCitrine-NES-2xFKBP-Rac1Q61LDCAAX	Double digestion of (XhoI and BamH1) mCitrine-eDHFR-Rac1Q61LDCAAX
baitPARC CCL citrine Halotag	Double digestion of (BspE1 and SacII) baitPARC-CCL-citrine-2xeDHFR	Double digestion of (BspE1 and SacII) baitPARC-TagBFP-Halotag
Cherry NES eDHFR Rac1Q61LΔCAAX	Double digestion of (NheI and BsrGI) mCitrine-NES-eDHFR-Rac1Q61LDCitr	Double digestion of (NheI and BsrGI) delCMV-RBD-mcherry
mCitrine eDHFR GEF-H1	Double digestion of (XbaI and MfeI) mCitrine-eDHFR	Double digestion of (XbaI and MfeI) mTurquoise-NES-eDHFR-GEFH1

2.1.5 Buffers

Buffers & Kits	Trademark
Accuprime Pfx Reaction Mix	New England Biolabs
Antartic Phosphatase buffer	New England Biolabs
Big dye terminator	New England Biolabs
6x DNA loading buffer	Thermo Scientific
Gene ruler 1kb	Fermentas
LB agar plates	MPI Dortmund
LB medium	MPI Dortmund
Ligation buffer	New England Biolabs
NucleoBond Xtra Midiprep Kit	Macherey-Nagel
QIAprep ®Spin Miniprep Kit	Qiagen
QIAprep ®Spin PCR Purification Kit	Qiagen
QIAprep ®Gel Extraction Kit	Qiagen
Restriction buffers (1-4)	New England Biolabs

1xPBS Buffer	137 mM NaCl 2,68 mM KCl 8,10 mM $Na_2HPO_4 \cdot 7$ H2O 1,47 mM KH_2PO_4 pH = 7,4
1x TAE Buffer	40 mM Tris-Acetate 1 mM EDTA pH = 8,3
6x DNA loading Buffer	50 % Glycerol 0,25 % Bromophenolblue
Cos7 Culture Media	440 mL DMEM Phenolred 10 % (v/v) FBS 1 % (v/v) L-Glutamine 1 % (v/v) Penicillin/Streptomycin
Hela Culture Media	435 mL DMEM Phenolred 10 % (v/v) FBS 1 % (v/v) L-Glutamine 1 % (v/v) Penicillin/Streptomycin 1 % (v/v) Non essential aminoacids
Imaging Media	90 % (v/v) DMEM 10 % (v/v) FBS
LB Media	dH2O 10 g/L Tryptone 10 g/L NaCl

	5 g/L Beef extract pH = 7,4
LB Agar Plate – (Ampicillin)	LB-Sterile medium 1,5 % Agar 100 mg/L Ampicillin
LB Agar Plate – (Kanamycin)	LB-Sterile medium 1,5 % Agar 100 mg/L Kanamycin
MESTBS Buffer	20mM Tris 150mM NaCl 4.5% (w/v) milk powder 5mM EDTA 1 mg/ml herrings sperm DNA 0.2% (w/v) NaN_3 pH 7.35
N2a Culture Media	435 mL DMEM Phenolred 10 % (v/v) FBS 1 % (v/v) Sodium Pyruvate 1 % (v/v) L-Glutamine 1 % (v/v) Penicillin/Streptamycin
DPBS-EDTA	200 mg/L KCl 200 mg/L KH_2PO_4 8 g/L NaCl 1,15 g/L Na_2HPO_4 10 mM EDTA
Trypsin-EDTA	0,02 % EDTA 0,05 % Trypsin
TETBS Buffer	20mM Tris-HCl 5mM EDTA 150mM NaCl 0.05% Tween pH 7.5
U2OS Culture Media	435 mL DMEM Phenolred 10 % (v/v) FBS 1 % (v/v) L-Glutamine 1 % (v/v) Penicillin/Streptomycin 1 % (v/v) Non essential aminoacids

2.1.6 Cell culture reagents

Cell Culture	Trademark
Bovine Insulin	Sigma aldrich
Collagen	Sigma aldrich
DMEM	PAN Biotech GmbH
DNA MB (fish sperm)	Roche
DPBS	PAN Biotech GmbH
Fetal Bovine Serum	PAN Biotech GmbH
Fugene	Pro-mega
L-Glutamine	PAN Biotech GmbH
Lipofectamine	Invitrogen
MEM Eagle	PAN Biotech GmbH
NEAA	Carl Roth GmbH
Trypsin EDTA	PAN Biotech GmbH
Xtremegene TM 9	Roche Diagnostics GmbH

2.1.7 Cell lines

Cos-7	African monkey kidney cells	ATCC
HEK-293	Human embryonic kidney cells	ATCC
Hela	Human cervical cancer cells	ATCC
MCF-7-EGFR	Human breast cancer cells	ATCC
SOC	*Escherichia coli*	ATCC
Top 10	*Escherichia coli*	Invitrogen
U2OS	Human osteosarcoma	ATCC
XL Gold	*Escherichia coli*	Stratagene

2.1.8. Materials and Equipment

Materials and Equipments	Trademark
0.45 μm Filter	Millipore
10cm petridishes	Sarstedt
1cm holed mattek	TU Dortmund, Workshop
8 well labtek	Thermo fischer scientific
Burner	WLD-TEC GmBH
Butane	Campingaz
Gel Camera	Samsung
Cell scraper	Sarstedt

Centrifuge machine	Eppendorf
Electrophoresis unit	Bio-RAD
Freezer (-152°C)	Sanyo
Vials (500ul, 1500ul, 2000ul)	Sarstedt
Falcon tubes	Thermo-scientific
Gel imaging device	Biostep GmbH
Gloves	Blossom Europe
Haemocytometer	Brand GmbH
Heating DRI block	Techne
Humidity chamber	Prof Niemeyer lab
Lens cleaning tissue	Whatman
Immersion Oil Type-F	Olympus
Mattek	MatTek Corporation
Micro-pippettes (1ml,100ul, 10ul and 2.5ul	Eppendorf
Micro-pippette tips	Star lab
Microscope coverslip & Slides	Roth GmbH
Nano-drop	Thermo-scientific
Parafilm	Carl Roth GmbH
PCR cycle	Eppendorf
pH meter	Mettler Toledo
Rotor (Swing-bucket)	Eppendorf
Scalpels	Braun
Serological pipettes (5,10,25ml)	Sarstedt
Shaking mixer	Eppendorf
Short spin centrifuge	VWR
Silicone MED RTV	ASC Applied Science Corporation
Microscope (Cell culture)	Nikon
Sterile Syringe	Braun
Insulation tape	Tesla
Tough tags/Spots	Microtube
UV lamp	Biostep GmbH
Vortex device	Scientific instruments
Water bath	Koettermann

2.1.9. Softwares

Softwares	**Inventor**
Adobe Photoshop	Adobe systems
ApE	Wayne Davis

Cell Profiler	Broad Institute
Cell R	Olympus
Graphpad Prism	GraphPad Software Inc.
ImageJ	Wayne Rasband
Labview	National Instruments
Office	Microsoft

2.1.10 Microscopes

Microscopes	Configuration	Trademark
wide-field Microscope (MPI-Dortmund)	Filters: BFP/GFP/RFP. Camera: Hamamatsu ER Objective: UPlans APO 60x NA Software: Scan^R	Olympus
wide-field/TIRF Microscope (TU-Dortmund)	Filters: BFP/GFP/RFP, TBFP/TGFP/TRFP (Triple TIRF), TBFP/TCFP/TYFP/TRFP (QuadTIRF) Camera: Hamamatsu Image EM CCD Objective: PlanApo 60xOil TIRF (NA-1.45) Software: Cell^R	Olympus

2.2 Methods

2.2.1 DNA Recombinant Technology

To generate new plasmid constructs, the following steps were followed: An aliquot of frozen E. Coli cells in the glycerol stock was inoculated overnight to isolate a fresh batch of plasmid constructs. Two plasmid DNAs with common restriction recognition sites were cut using respective restriction enzymes to create compatible sticky ends. When the plasmids lacked common restriction sites, primers were designed with respective restriction sites and a PCR reaction was performed. In some cases, commercially available single stranded short oligonucleotides were annealed to form double stranded linkers/adapters, which were used instead of PCR products. Phosphatases were used to de-phosphorylate the 5' end of one of the DNA fragments. Short single stranded oligonucleotides without a phosphate group were also used for linker sequence cloning; In that case, the de-phosphorylation step was

neglected. Via the ligation reaction compatible sticky ends were assembled into the desired plasmid of interest. Ligated plasmids were subjected to heat transformation and were plated onto selective antibiotic LB agar plates overnight. The following day, Plasmid DNA was recovered through the Qiagen Miniprep Kit procedure. Finally, the DNA concentration was measured using the Nanodrop device and a restriction digestion was performed followed by DNA sequencing for construct validation.

Polymerase chain reaction

For PCR, Primers were designed which were around 18-30 nucleotides long. Melting temperatures of complementary regions of forward and reverse primers were 55-65°C and within 5°C of each other with a GC content of around 40-60%. Recognition sequences for restriction enzymes and 2-4 additional nucleotides were added to the 5' end for efficient restriction enzyme digestion. Primer sequences were chosen to avoid secondary structure formation and intra/inter primer homology to would lead to primer dimers. DNA vector sequences were viewed, edited and annotated using the open source software ApE **(Paradis E et al 2004).** PCR reactions comprised three steps which include denaturation of the template DNA at 98°C, annealing of primers to the template at 55-60°C followed by extension of the primer at 72°C.

PCR	Volume	Final Concentration
Template DNA	1.0µl	0.2ng/µl
Forward Primer	1.0µl	0.5µM
Reverse Primer	1.0µl	0.5µM
Accuprime polymerase	0.5µl	0.0125U/µl
Accuprime buffer	10µl	1X

Nuclease water	86.5µl	
Total	100µl	

PCR Cycle

Repetitions	T° [C]	Time
5	98°	3 min
25	98°	15 sec
	68°	30 sec
	72°	15 sec
1	72°	8 min
1	4	∞

Once the PCR reaction finished, PCR products were purified using the Qiagen PCR Purification Kit protocol as described in the manual.

Restriction digestion

Type II restriction enzymes can recognize specific DNA sequences. In general, restriction digestion was carried out at 37°C for 3 hours. The table below shows an example of a double digestion reaction.

Contents	Volume	Final Concentration
Vector	3.5 µl	3 µg
Restriction enzyme 1	1.0µl	10 units
Restriction enzyme 2	1.0µl	10 units
Buffer	2.0µl	1X
Nuclease free H_2O	12.5µl	
Total	20µl	

In a de-phosphorylation step, the phosphate groups were removed from the 5' ends of the vector DNA to prevent self-annealing during ligation. 10 units of Calf intestinal or alkaline phosphatase were added for the de-phosphorylation. Before this, the restriction enzymes were deactivated in a heat block at 65°/80°C based on the restriction enzyme used.

Gel electrophoresis

1g of agarose dissolved in 100ml of TAE buffer was placed inside a microwave for 2 minutes. Later, 2-3 drops of Ethidium bromide was added to this solution. Once the gel was casted, DNA samples were mixed with loading dye and were loaded onto the gel. 1kb gene ruler DNA was loaded in a similar fashion in the gel for size reference. The voltage in the electrophoresis unit was set to be around 85V. In this method, DNA was segregated based on the size. Once the sample dye markers reached half way, the electrophoresis was stopped and the gel was carefully carried to the dark room for gel extraction using a UV lamp. DNA was extracted from the gel using the long wavelength UV lamp (366 nm) and was subjected to QIAGEN gel extraction for DNA isolation and purification.

Ligation

DNA Ligase was used to ligate two distinct DNA segments that were restricted with the same set of restriction enzymes at 16°C overnight. To calculate the amount of vector and insert DNA for the ligation, we used the formula below.

$$X\ (ng\ of\ insert) = 3\times (ng\ of\ vector\ DNA)\times \frac{Size\ of\ insert}{Size\ of\ vector}$$

Transformation

Heat competent XL Gold or TOP 10 E. coli cells were thawed on ice and 5ul of the control and ligated sample were added in separate vials and gently mixed with a pipette tip. After 5 minutes on ice, the tubes were subjected to a heat shock at 42°C for 2 minutes, followed by incubation on ice for 2 minutes. Then, 1 ml of fresh LB medium was added under sterile conditions and incubated in a shaker at 37°C. After an hour, an aliquot of the culture was spread using a Drigalski-spatula onto agar plates containing selective antibiotics and incubated at 37°C overnight.

Overnight culture

Single bacterial colonies were transferred to a culture tube containing 6ml of LB media supplemented with the matching antibiotic (Ampicillin or Kanamycin) and incubated at 120rpm at 37°C overnight.

Preparation of glycerol stocks

Under sterile conditions, 500ul of exponentially growing bacteria (~0.5 OD) or overnight culture were mixed with 500ul of 50% glycerol, and frozen at -80°C for long-term storage.

Plasmid DNA isolation

Plasmid was isolated using the Qiagen Miniprep kit following the manufacturers instructions starting from 6 ml overnight cultures. Elution was performed with 30ul of EB buffer. Concentration of the plasmid DNA was measured using the Nano drop device.

Mammalian cell culture and transfection

Cos7 cells, Hela, N2a and U2OS cells were used for live cell experiments. When the cells reached 70-80% confluency, they were split using trypsin-EDTA and were incubated at 37°C for 7-10 minutes.

For DNA transfection, we used lipofectamine 2000 (N2a and U2OS cells) and Xtremegene 9 (Cos7 and Hela cells). Transfection was performed according to the manufacturers protocol using a ratio of 1:3 (DNA: transfection reagent).

2.2.2 Preparation of Functionalized arrays

The collaborating groups of Prof Christof M.Niemeyer and Dr. Michael Hirz at the Karlsruhe Institute of Technology (KIT) mostly performed the following procedures. Those methods were previously published **[Reisewitz et al 2010, Gandor et al, 2013, Arrabito et al 2013].**

Silanization procedure

The microscope coverslips were cleaned with absolute EtOH, and incubated with 3-aminopropyltriethoxy-silane (APTS, Sigma-Aldrich) solution containing 93% EtOH, 5% ddH_2O and 2% APTS for 4hours. Once the aminosilylation was complete, the coverslips were washed with EtOH and acetone for 10mins. This was followed by a drying step for 15 mins at 110°C and finally the coverslips were stored at -20°C over night. Using the sandwich method, the activated coverslips were coated with PBAG overnight, washed with acetone and dried under nitrogen.

Preparation of DNA array culture dishes

Molecular ink containing reactive 5' amino modified single stranded oligonucleotide was mixed with glycerol, Tween 20 and TE buffer and passed through the microfluidics chamber. Aligned cantilevers or PDMS pens were used to transfer the DNA from the microfluidic chamber onto the microscopic coverslips using dip-pen nanolithography (DPN) or polymer-pen nanolithography (PPN). Forces during printing

ranged between 50-150mN. After overnight incubation at room temperature, the samples were stored at -20°C.

DNA directed immobilization

Process A: A brown eppendorf tube containing 1μl of 10uM aF10 DNA conjugated streptavidin was mixed with 9 μl of diluted anti-VSVG antibodies (1:5) and kept under shaker for 15 minutes. To the same tube, 15 μl of Biotin-Cy7 fluorescent dye was added and kept under shaker for 15 minutes. This is followed by the addition of 20 ml of TETBS-Biotin buffer (20mM TrisHCl, 5mM EDTA, 150mM NaCl, 0.05% Tween, 800 μM Biotin, pH 7.5) was incubated in the shaker for 30 minutes.

Process B: Amino modified F10 oligonucleotides printed on the coverslip (KIT sample) was taken from the freezer and stored at room temperature for 10 minutes. The coverslip was glued to the 1 cm holed mattek using tissue grade RTV silicone adhesive. Once the glue has dried, the mattek was washed with TETBS buffer. (20mM Tris-HCl, 5mM EDTA, 150mM NaCl, 0.05% Tween, pH 7.5). 50 μl of MESTBS buffer (20mM Tris, 150mM NaCl, 4.5% (w/v) milk powder, 5mM EDTA, 1 mg/ml herrings sperm DNA, 0.2% (w/v) NaN3, pH 7.35) was added to the center of the mattek for blocking. The mattek was placed with the wetted tissue paper humidity chamber and was subjected to shaking (150rpm). After 30 minutes, the mattek was subjected to three-time wash off with DPBS. 45 μl of the ssDNA-Streptavidin-Biotinylated-Antibody complex mixture from Process A was added on to the center of the mattek for efficient DNA hybridization and placed in the shaker for 60 – 90

minutes. This is followed by gentle wash offs with DPBS. After this step, the array sample was ready to get incubated with living cells.

2.2.3 PBS-EDTA treatment to detach cells

Cos7 Culture and Imaging Medium were warmed at 37°C. DPBS-EDTA was equilibrated to room temperature. Old Cos7 growth medium was removed from the 10cm petridish gently without perturbing the adherent transfected cells. First, the cells were washed with 5 ml PBS-EDTA. Later, fresh 5 ml PBS-EDTA was added to the cells and the dish was incubated for 7-10 min at 37°C. After this, cells were gently detached from the plate with a small cell scraper. 10 ml Cos7 growth medium was added to the cell plate in the presence of 5 ml PBS– EDTA. The resulting liquid solution was pipetted up and down few times to reduce cell aggregation and was added to a 50 ml Falcon tube. This tube was led to centrifugation at 1000 rpm for 10 minutes. Supernatant was carefully removed and 10 ml of Cos7 growth medium was added to the falcon tube again to dilute the EDTA content in the tube. Centrifugation of the same tube was performed at 1000 rpm, 10 minutes. Supernatant was carefully removed and the pellets were suspended in 200-500 μl of imaging Medium. Cell number was calculated using Haemo-cytometer and Cell counter. 50-100 μl of these living cells were carefully added in the middle of the prepared dish containing the array. Cells were allowed to settle for 1-2 hours. Further, 2 ml of fresh Cos7 growth medium was added and the sample was kept over night at 26°C. A day later, imaging was performed after the replacement of old Cos7 growth medium with imaging media.

2.2.4 Immunofluorescence

Cells were fixed by incubating with warm 4% formaldehyde solution and incubated at 37°C for 20 minutes. This was followed by three-time wash out with PBS without triton detergent. Blocking the unspecific binding was carried out with 125 ml of 2% warm BSA for 30 minutes. BSA was replaced with 125 ml (1 primary antibody: 1000 PBS) of anti VSVG antibody from the rabbit. After 60 minutes incubation, three time PBS wash out was carried out followed by incubation with appropriate fluorophore labeled (488/565nm) secondary antibody for 90 minutes. Final step involves washing out with PBS thrice and storing the sample at 4°C for further imaging.

2.2.5 Microscopy

The configuration of the Olympus TIRF set up is summarized in section (2.1.10). Imaging was performed either at 26°C or 37°C with imaging media containing 10% serum. The critical angle was set to match the maximum fluorescence signal of a test sample. Images were processed using ImageJ and assembled using Photoshop. Images of antibody patterns were always acquired using widefield microscopy. Expect if noted otherwise, all other images were obtained using TIRF Microscopy.

3. RESULTS

3.1 Development of intracellular protein interaction arrays and artificial receptor constructs

To generate intracellular protein interaction arrays, we developed artificial receptors that can transfer a pattern of surface linked antibodies into a corresponding array of bait proteins in the plasma membrane **[Figure 3.1a].** These artificial receptors were referred to as BaitPARCs (bait Presenting Artificial Receptor Constructs). The extracellular domain of BaitPARCs contains an antibody epitope, which interacts with surface-immobilized antibodies. This interaction enriches BaitPARCs to a pattern of antibodies. The identity of distinct BaitPARCs was encoded by their position within the array. BaitPARCs were co-expressed with a cytosolic prey protein, which was fused to a fluorescent protein. The interaction between immobilized BaitPARCs and this prey protein was monitored using TIRF (Total Internal Reflection Fluorescence) microscopy**.** This is possible, as the exponentially decaying evanescent field in this microscope selectively excites only those fluorophores that are in close proximity to the plasma membrane within 50-200nm **[D Axelrod 2001] [Figure 3.1a].** Thus, proteins that directly interact with BaitPARCs in the plasma membrane are excited efficiently and cytosolic proteins only contribute a weaker background fluorescent signal. It is therefore possible to detect the interaction between the cytosolic prey protein and the BaitPARC with a high signal to noise ratio.

Footnote: Results shown from 3.1 till 3.1.4 were published in Gandor et al, 2013

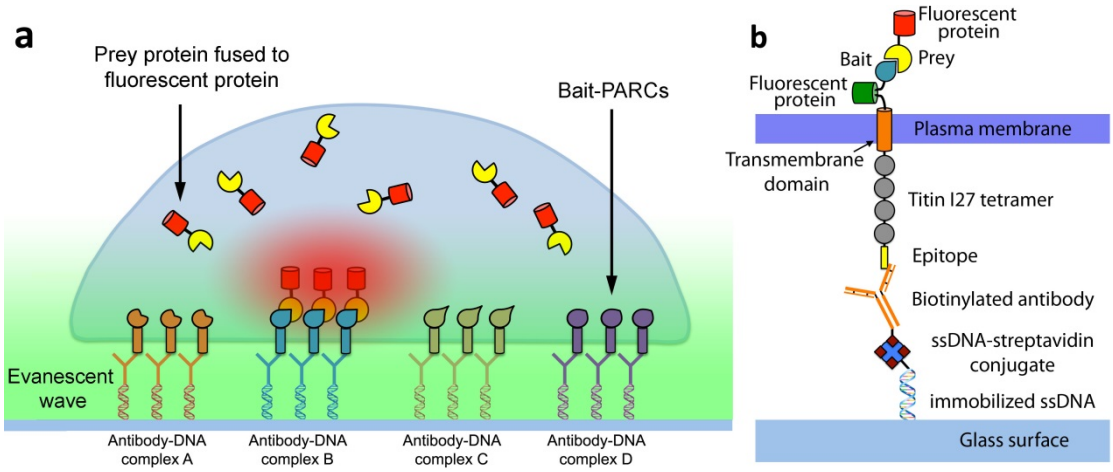

Figure 3.1: Protein interaction arrays inside living cells. **a.** Schematic Representation of a living cell expressing Bait-Presenting Artificial Receptor Constructs (baitPARCs) growing on an array of distinct antibodies (Antibody-DNA complexes A-D). These antibodies immobilize and enrich corresponding baitPARCs in the plasma membrane. Prey fused with a fluorescent protein is expressed in the cytosol. Bait-prey interactions are monitored via Total Internal Reflection Fluorescence Microscopy (TIRFM). The evanescent field generated in this microscope excites only the fluorophores that are in close proximity to the cell surface. **b.** BaitPARCs were designed with an extracellular region that displays a viral epitope on the cell surface, and an intracellular domain that displays a bait protein to the cytosol. **Figure source: Gandor et al, 2013**

3.1.1 Design of BaitPARCs

As represented in **Figure 3.1b,** Bait PARCs are composed of an intracellular domain with an arbitrary bait fused to a fluorescent protein, a transmembrane domain derived from PDGFR **(Gronwald et al, 1987)** (Platelet Derived Growth Factor Receptor), and an extracellular domain that displays an epitope that directs the enrichment of the artificial receptors to the immobilized antibody microstructures. In addition, four repeats of the Titin Ig domain I27 were added between the transmembrane domain and the epitope to act as a spacer to minimize steric hindrance between the cell periphery and the surface during epitope-antibody interaction. BaitPARCs were specifically designed to minimally perturb endogenous cellular processes and function. The extracellular I27 linker is derived from the intracellular protein Titin and

was therefore expected not to interact with any extracellular surface proteins. The PDGFR transmembrane domain is only known to interact with the bovine pappilomavirus E5 protein, which is not present in uninfected cells. Importantly, the viral epitopes (VSVG from Vesicular Stomatitis Virus G protein and HA from Haemagglutinin) are also not expressed in uninfected cells. Therefore, neither the epitope-antibody interaction nor the transmembrane domain or the viral epitopes are expected to exert perturbations that alter normal biological processes inside cells. Known interactions of baitPARCs with the cellular machinery are limited to those that are essential for plasma membrane targeting of baitPARCs, i.e. interactions of the cleaved signal peptide sequence with signal receptor particle (SRP) and the transmembrane domain with the lipid bilayer to direct baitPARCs into the secretory pathway.

3.1.2 BaitPARC patterning via immobilized Antibody arrays

DNA directed immobilization (DDI) offers the possibility to generate distinct micrometer sized antibody array patterns. First, amino modified single stranded oligonucleotides were immobilized on a glass surface via DPN (Dip Pen Nanolithography) **(Reisewitz S et al 2010, Arrabito G et al 2013).** Our collaborators in the Niemeyer group at the Karlsruhe Institute of Technology (KIT) performed the DPN step and the generation of DDI reagents, and detailed descriptions of those methods are presented elsewhere (**Niemeyer et al., 1999, Arrabito G et al., 2013, Stephanie Reisewitz 2013)**. Here, DPN was used to print oligonucleotides onto a glass surface using an AFM tip via capillary force, in order to create patterns in sub-micrometer dimensions. Complementary oligonucleotides conjugated with streptavidin were incubated with biotinylated antibodies and this functional complex

was allowed to hybridize with the immobilized oligonucleotide strand **[Figure 3.2a].** Micrometer-sized patterns with two distinct antibodies were immobilized using distinct DNA streptavidin conjugates coupled with respective biotinylated antibodies and fluorophores **[Figure 3.2b].** In previous experiments of Silke Gandor, another PhD student from our group, arrays of single immobilized antibody type were generated that had an average feature diameter of 4.5±0.5μm and an average feature distance of 11.4±1.4 μm from neighboring spots (Silke Gandor, unpublished and Stefanie Reisewitz, 2013). The recruitment of Bait PARCs to antibody arrays was measured by calculating the relative enrichment according to the following equation:

$$Relative\ Enrichment\ of\ bait\ (in\ \%) = \frac{I_{bait,spot} - I_{bait,bg}}{I_{bait,cell} - I_{bait,bg}} \times 100$$

This relative enrichment represents the local enrichment of BaitPARCs in microarray structures. E=100% means no enrichment, while E=200% represents a 2-fold enrichment in spots compared to the surrounding regions. Living cells expressing BaitPARCs that displayed the VSVG epitope on the cell surface showed a relative enrichment of 265±55% when cultured with anti-VSVG microstructures. In the context of this thesis, we extended those previous studies and generated multifunctional arrays by targeting two distinct streptavidin conjugates to two distinct, immobilized oligonucleotides via their corresponding capture oligonucleotides. To reduce the number of distinct fluorophores that need to be distinguished via microscopy, the antibody identity was encoded with a single fluorophore (Cy7) via fluorophore intensity as shown in **Figure 3.2c** (Anti HA – low intensity Cy7 and Anti-VSVG – high

intensity Cy7). Two distinct bait PARCs were enriched in corresponding anti-VSVG and anti-HA microstructures with a factor of 289±125% and 322±127% respectively.

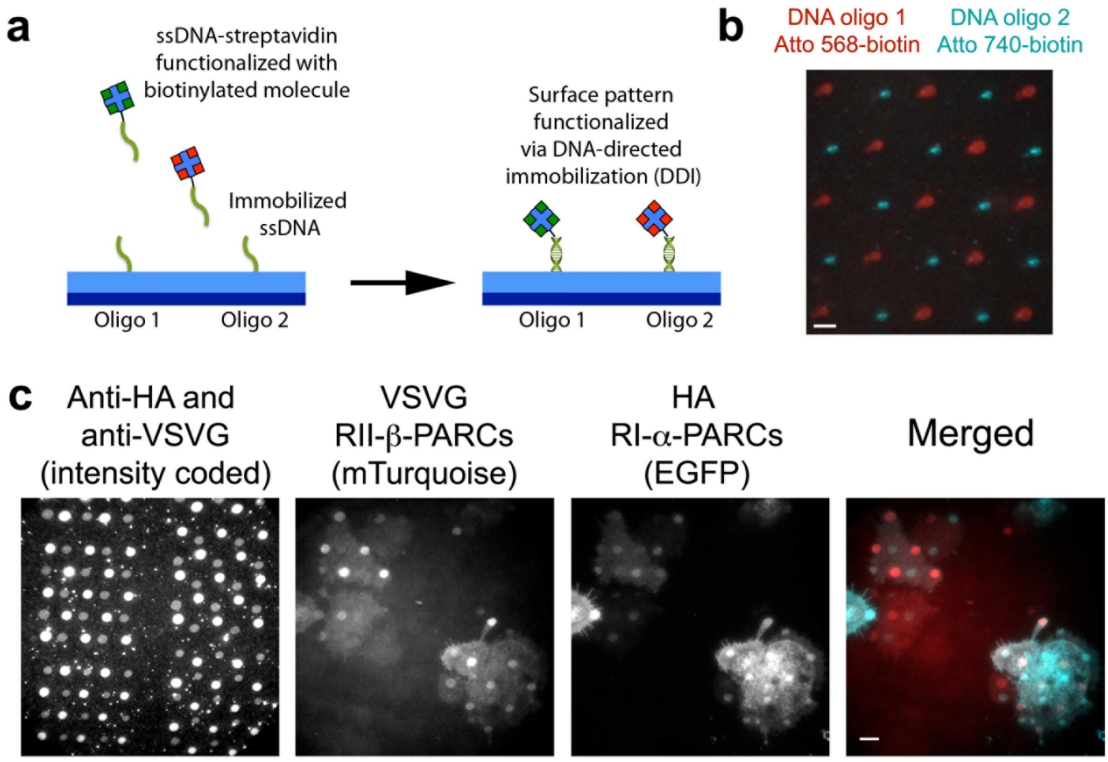

Figure 3.2: DNA directed immobilization. **a**. Schematic representation illustrating the concept of DNA directed immobilization. Distinct single stranded DNA oligos (Oligo 1 & Oligo 2) are printed on a glass surface via DPN. To this surface, respective complementary oligonucleotides conjugated with functional antibody complexes are added to create antibody-functionalized arrays. **b.** Immobilization of two distinct oligonucleotide microstructures labeled with Atto 568 and Atto 740 fluorophores **c**. Anti-HA and Anti-VSVG arrays were distinguished based on Atto 740 fluorescence intensity. Living cells cultured on top of these antibody arrays shows enrichment of individual baitPARCs (RI-α & RII-β). **Figure source: Gandor et al, 2013**

3.1.3 Monitoring multiple protein interactions inside living cells via baitPARC arrays

As a proof of concept to study multiple protein interactions using baitPARCs, the well-established signal transduction pathway via the second messenger cAMP was employed. In cells, cAMP levels are increased by activation of adenylyl cyclase

following agonist-mediated activation of G-Protein coupled receptors (GPCR). Alternatively, direct activation of adenylate cyclase via forskolin and/or inhibition of phosphodiesterases via IBMX can also stimulate cellular cAMP levels **[C Guirland et al., 2003]**. Binding of cAMP to regulatory subunits of the cAMP dependent Protein Kinase A (PKA) disrupts the interaction with the associated catalytic subunit [**Wong et al., 2003**]. Here, two distinct regulatory subunits, RI-α and RII-β, of the cAMP dependent Protein Kinase A were fused to distinct bait PARCs, which displayed HA and VSVG epitopes on the extracellular domain. The catalytic subunit cat-α was expressed in the cytosol and was used as a prey protein. RI-α, RII-β containing baitPARCs and cat-α were fused with the spectrally separable fluorophores EGFP, mTurquoise and mCherry respectively. The two distinct baitPARCs were named HA RI-α-PARC [EGFP] and VSVG RII-β PARC [mTurquoise]. The prey fusion protein is referred to as cat-α [mCherry]. First attempts to express all three proteins in cells were not successful, presumably due to superfluous, unregulated catalytic subunit. This problem was overcome by controlling catalytic subunit expression using a Tet-inducible system **(Gossen M et al 1992).** Furthermore, the cell incubation temperature had to be reduced to 26°C to facilitate plasma membrane targeting of baitPARCs (see also section 3.15). Together, these optimizations enabled co-expression of both baitPARCs and the prey protein. To quantify the interaction of the bait with the prey, we calculated the bait-prey recruitment via the following formula:

$$\boldsymbol{Bait-prey\ recruitmemt\ (R)} = \frac{(I_{prey,spot} - I_{prey,cell})}{E_{bait}}$$

$$E_{bait} = \frac{(I_{bait,spot} - I_{bait,bg}) - (I_{bait,cell} - I_{bait,bg})}{(I_{bait,spot} - I_{bait,bg})} = \frac{(I_{bait,spot} - I_{bait,cell})}{(I_{bait,spot} - I_{bait,bg})}$$

Here, the enrichment factor E_{bait} is used as a normalization factor to account for differences in the primary recruitment of bait proteins to spots. E_{bait} is 1 if all receptors are recruited to spots and 0 if they are all distributed evenly. First, we observed the interaction of the prey with both the regulatory subunits of cAMP dependent Protein Kinase A **[Figure 3.3a]**. This interaction between the bait and prey was lost upon β-adrenergic receptor stimulation via isoproterenol. This shows, that the activation of G-protein coupled receptors increases intracellular cAMP levels, thereby disrupting the bait-prey interaction. Interestingly, the bait-prey dissociation displayed an adaptive response, possibly due to receptor desensitization and cAMP hydrolysis by phosphodiesterases **[Vandamme et al., 2012]**. Further pharmacological treatments with Forskoline/IBMX elevated the total cellular cAMP concentration, which lead to strong and persistent dissociation of the catalytic and regulatory subunits **[Figure 3.3b]**. After repeated drug washout, the bait-prey interaction was restored. This reversible and maximal stimulation can be used to determine the dynamic range of this cAMP sensor system.

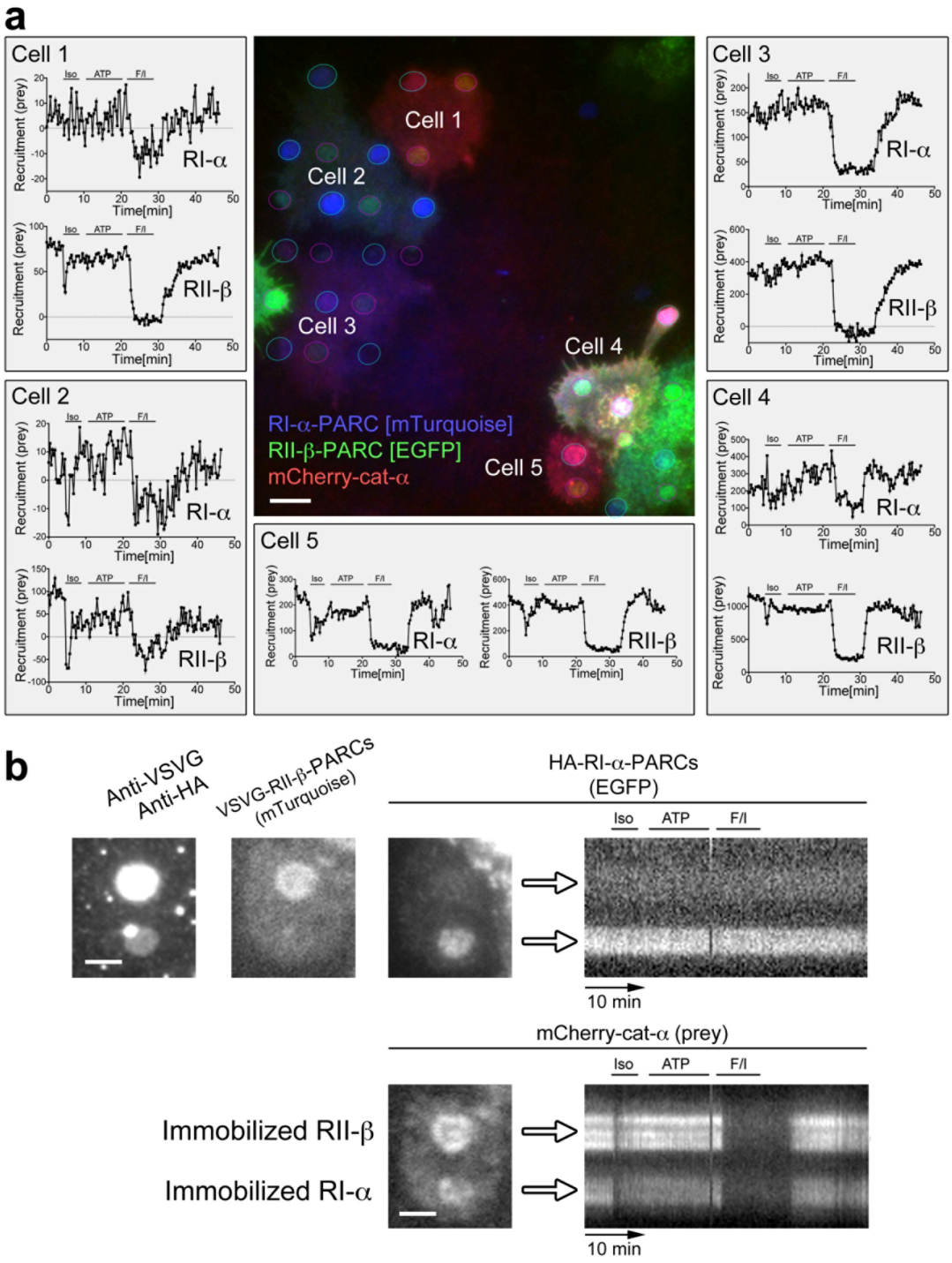

Figure 3.3: Kinetics of bait-prey interaction during pharmacological stimulation a. Merged false color image in the center, showing cells 1-5 with patterned RI and RII baitPARCs. Association and dissociation kinetics of the cat-α-RI-α/RII-β interactions were plotted during pharmacological treatment for each individual cell **b.** Left: Microscopic images showing successful immobilization of anti-HA and anti-VSVG antibodies and enrichment of the corresponding RI-α and RII-β baitPARCs to this immobilized antibody array. Right: Kymograph analysis showing no change in the signal corresponding to immobilized RI-α baitPARC during pharmacological stimulation, while prey fluorescence was modulated during pharmacological stimulation. **Figure source: Gandor et al, 2013.**

3.1.4 Correlative analysis of multiple bait-prey interaction dynamics

To directly compare the interaction between the two distinct regulatory subunits and the catalytic subunit in distinct cells, we normalized the bait-prey recruitment R also to the total intensity of the prey protein. This normalization was based on the following formula:

$$Normalized\ bait-prey\ recruitment = \frac{R}{I_{prey,cells}}$$

This measurement of the normalized recruitment showed preferred association of cat-α with RII-β over RI-α in resting cells (**Figure 3.4a**). This preference cannot be explained by differences in affinity of the prey with these two bait proteins, as in *vitro* studies show a slightly higher affinity of RI-α over RII-β in the absence of cAMP (Kd for RI-α: 0.19nM; RII-β: 0.6nM) [**Herberg et al., 1996**]. However, the effective cAMP concentration to dissociate the regulatory subunit is lower for RI-α vs RII-β (EC_{50} for RI-α: 101nM; RII-β: 610nM) [**Herberg et al., 1996**]. This suggests that the cellular resting concentration of cAMP is sufficiently high to disrupt the association of cat-a with RI-α, while the interaction with RII-β is less affected. Furthermore, reassociation of cat-α and RI-α after isoproterenol treatment was also slower compared to the reassociation of cat-α and RII-β (RI-α: $t_{1/2}$=2.45±0.85 min; RII-β: 1.23±0.46 min), suggesting that the lower effective concentrations of cAMP for reassociation of the cat-α/RI-α interaction is reached later than the higher effective concentrations to dissociate the cat-α/RII-β interaction. Thus, these kinetic

measurements provide a reasonable explanation for the differential normalized recruitment of the catalytic subunit to the two regulatory subunits.

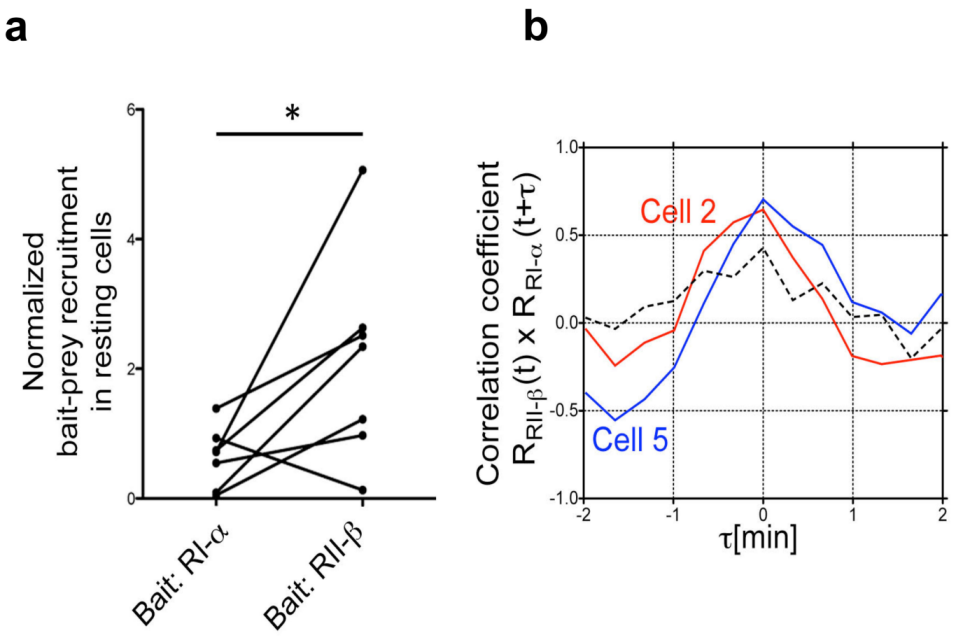

Figure 3.4: Correlation of multiple bait-prey interactions a. Normalized bait prey recruitment in resting cells suggests that catalytic subunit interacts with RII-β preferentially when compared to RI-α **b.** Correlation analysis shows positive temporal cross-correlation of the interaction of the catalytic subunit with the two distinct regulatory subunits after stimulation of β-adrenergic receptors with isoproterenol. **Figure source: Gandor et al, 2013**

Additionally, we observed significant cell-to-cell variance **[Figure 3.4a]** in response to β-adrenergic receptor stimulation, which was presumed to be due to varying strength of adaptive mechanisms in underlying signal networks **[Vandamme et al., 2012].** Protein interaction studies that are based on ensemble measurements fail to extract this variance information thereby losing the opportunity to study differences between individual cells with respect to the dynamic relationship among the distinct regulatory subunits. In addition, in cell ensemble interaction studies, this dynamic relationship among regulators is averaged over many cells, which blurs temporal response

profiles to perturbations. Here, by studying protein interactions inside individual cells, our array technology can offer a more focused view on relations that exist among different signal network components. Indeed, cross-correlation analysis **[Figure 3.4b]** of the interaction of the catalytic subunit with the two distinct regulatory subunits after stimulation of β-adrenergic receptors shows higher temporal cross-correlation in two individual cells (cell 2 and cell 5) as compared to the average of 7 cells (dotted line). This highlights that single cell analyses can overcome the blurring of temporal response profiles due to cell-to-cell variance.

3.1.5 Optimization of baitPARC plasma membrane localization

In the experiments above, plasma membrane targeting of RI-α and RII-β baitPARCs was improved by culturing the cells at low temperature (26°C). At the optimal growth temperature of COS7 cells (37°C), a large fraction of baitPARCs was present in intracellular membranes, presumably due to inefficient folding during processing in the secretory pathway. Even at low temperatures, plasma membrane localization of artificial receptors was low compared to naturally occurring receptors, such as EGFR or Ephrin receptors. Extending the application of baitPARCs to perturb and study signal networks therefore required optimization of plasma membrane targeting.

3.1.5.1 Deletion analysis to characterize the initial baitPARC design

Three segments of baitPARCs might contribute to the inefficient plasma membrane localization and were therefore investigated via deletion mutant analysis. These three segments of interest are the 4xtitin spacer, the fluorescent tag and the bait protein. Under my supervision, a Bachelor student generated and characterized a set of deletion constructs by removing single and multiple segments of the parental

construct RII-β baitPARCs as shown in the list below (**Michael Örlich, 2013**) [**Figure 3.4a**]. In order to quantify the plasma membrane fraction of each construct, the VSVG epitope that exist in all those constructs was used for immunofluorescence staining. The plasma membrane fraction was calculated by dividing the average, background-corrected fluorescence intensity of the individual construct in a cell region that only contained the plasma membrane by the average background-corrected fluorescence intensity of the entire cell (**Figure 5**).

$$Plasma\ membrane\ fraction = \frac{(Average\ Intensity\ in\ the\ PM - Background\ intensity)}{(Average\ Intensity\ of\ the\ entire\ cell - Background\ intensity)} \times 100$$

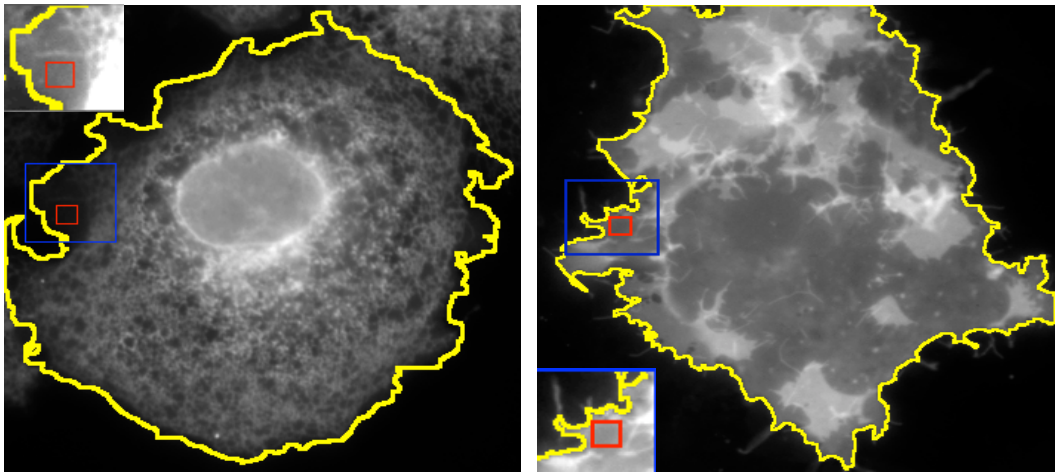

Figure 3.5: Calculation of the plasma membrane fraction. Widefield microscopy image of fixed Cos7 cell that expressed unoptimized baitPARC (left) and the control pDisplay vector (Right). The entire cell was selected using the threshold function of ImageJ (yellow outline). The plasma membrane region of the cell was selected based on uniform plasma membrane and background signals. The average fluorescence intensity of the plasma membrane region (red square region highlighted with an orange arrow) was divided by the average fluorescence intensity of the entire cell to measure the plasma membrane fraction. Enlarged regions show the expression of the receptor in the plasma membrane.

To increase the dynamic range in our optimization procedure, we cultured cells at (37°C), which resulted in only minimal (5-10%) plasma membrane targeting of the original parental baitPARC construct. This analysis revealed that the empty VSVG

bait-PARC lacking all three non-essential segments localized very effectively to the plasma membrane with an average fraction of >50% **[Figure 3.6b]**.

Re-addition of the Titin-linker reduced the plasma membrane fraction only minimally (Empty vs +Titin) **[Figure 3.6b].** Conversely, a construct lacking only the Titin-linker from the original parental construct showed no improvement in plasma membrane fraction (Control vs +mTFP/RII-β) **[Figure 3.6b]**. Interestingly, re-addition of the RII-β or mTFP segments reduced plasma membrane localization. This effect was even stronger, if both segments were present. It was not surprising that linking a cytosolic signaling protein such as RII-β to a transmembrane receptor might affect its transport to the plasma membrane, as endogenous interactions with RII-β binding proteins might perturb processing in the secretory pathway. We were however surprised that the presence of a fluorescent protein, that does not have any known interactions with endogenous proteins, interferes with processing in the secretory pathway. We reasoned that this effect might be due to a relatively short linker sequence between the transmembrane domain and the fluorescent protein tag.

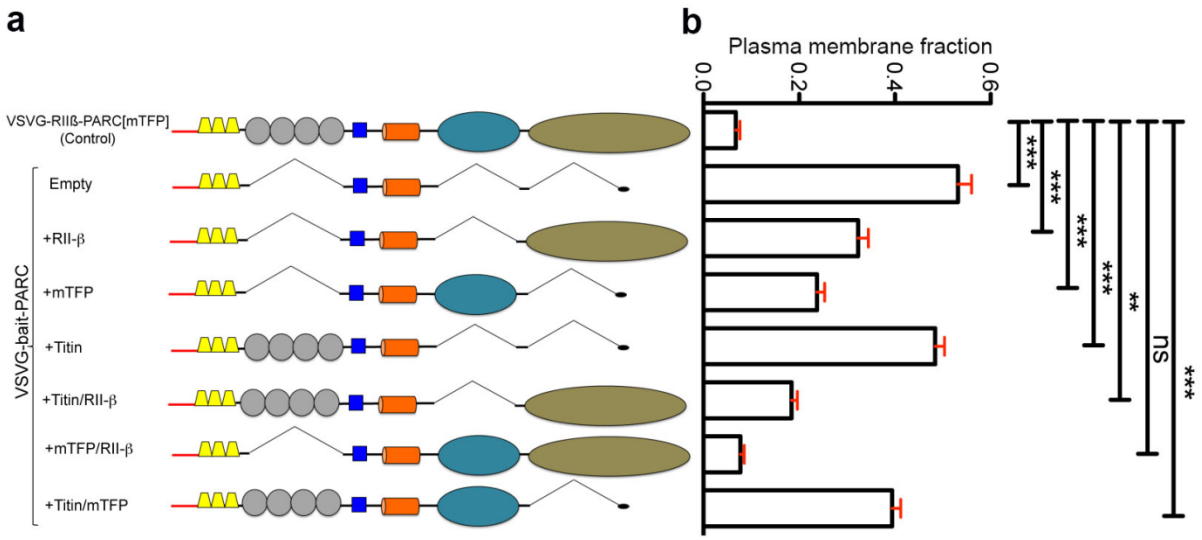

Figure 3.6: Optimization of baitPARC plasma membrane localization a. Graphical representation of the VSVG-bait-PARC based deletion mutants derived from the original baitPARC **b.** Quantitative analysis of plasma membrane fraction calculated for each corresponding construct (**: p<0.001; ***: p<0.0001; ns: not significant; one-way ANOVA and Tukey's Multiple Comparison Test; n>=26 cells from 3 independent experiments). **Figure source: Michael Orlich, 2013**

3.1.5.2 Introduction of additional linker sequences

We therefore decided to add a longer linker sequence at this position. Flexible glycine-rich linkers are recommended to facilitate efficient folding of adjacent regions due to its small side chain and high degree of flexibility (**X Chen et al., 2012**). Under my supervision, another bachelor student inserted a glycine linker sequence between the transmembrane domain and the fluorescent protein of VSVG RII-β PARC (mTurquoise) (**Martin Kares, 2014**). This new construct showed a small but significant improvement in the plasma membrane fraction **[Figure 3.7c-d]**

3.1.5.3 Introduction of Glycosylation motifs

Glycosylation is an important posttranslational modification that is employed in the endoplasmic reticulum to target transmembrane proteins either to the plasma

membrane or degradation in lysosomes. Specifically, N-glycans (Glc3Man9GlcNAc2) are attached on Asn-X-Ser/Thr motifs by the enzyme Oligosacchryl transferase (OST) during translocation of the nascent translated protein in the ER (**Khalkhall et al., 1975**). During glycosylation, monoglycosylated proteins are produced by glucosyltransferase (UGGT). CNX and CPT chaperones interact with these glysosylated proteins to prevent protein aggregation by retaining them in the ER and thereby promote folding (**Anelli et al., 2008**). Under my supervision, another Bachelor student added glycosylation motifs to the construct VSVG-RII-β PARC (mTurquoise) and tested if their addition improved the plasma membrane fraction of baitPARCs (**Darius Kazeska, 2014**). This analysis revealed that addition of the glycosylation group after the titin linker showed significant improvement in the plasma membrane fraction compared to the construct without any glycosylation signal sequence **[Figure 3.7a-b]**. Interestingly there was no improvement in localization when the glycosylation signal sequence was placed before the titin linker.

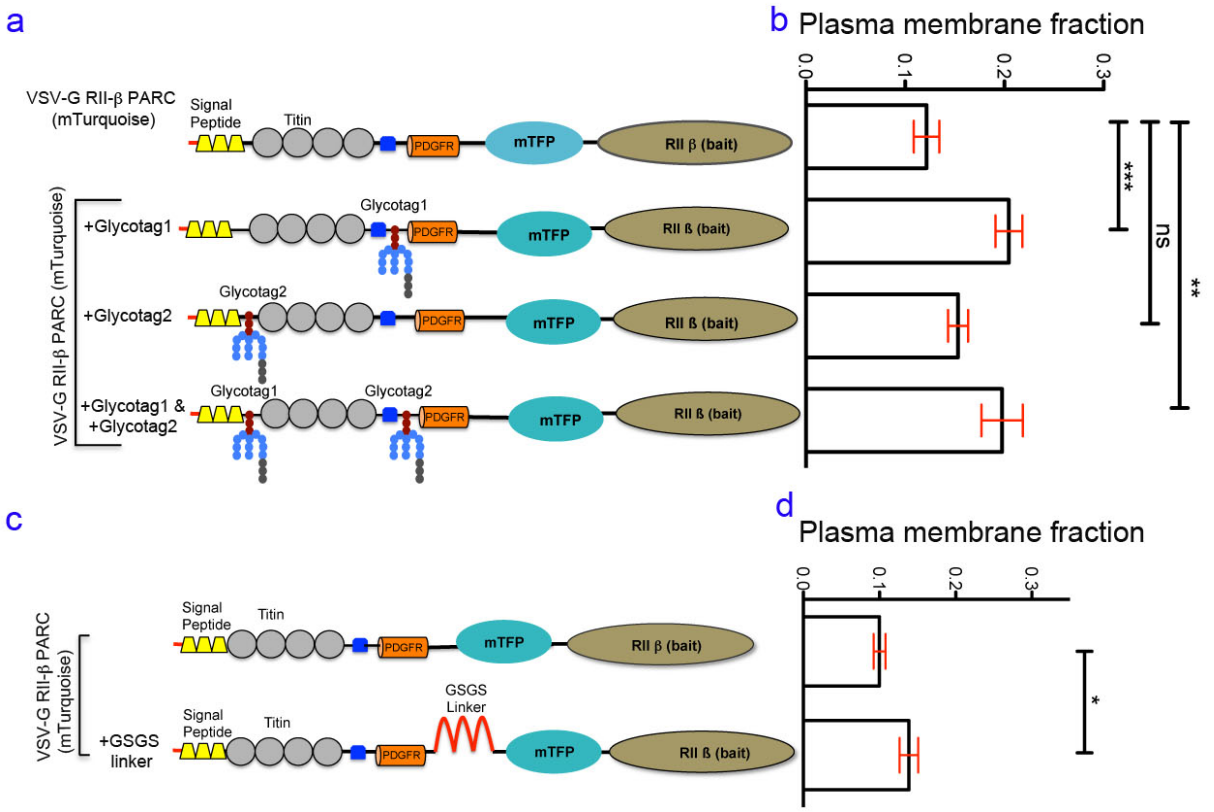

Figure 3.7: Optimization of plasma membrane fraction of baitPARCs a-b. Graphical representation of baitPARC constructs with a glycine linker and their respective plasma membrane fraction values **c-d.** Graphical representation of baitPARCs constructs with one or multiple glycosylation motifs and their corresponding plasma membrane fractions calculated for each corresponding construct (**: p<0.001; ***: p<0.0001; ns: not significant; one-way ANOVA and Tukey's Multiple Comparison Test; n>=30 cells from 3 independent experiments). **Figure source: (Martin Lucas, 2014) (Darius Kazeska, 2014)**

3.1.6 Development of activatorPARCs

In order to extend the applications of our artificial receptor design, we developed constructs to acutely target proteins to subcellular regions in the plasma membrane. Acute plasma membrane targeting of signal molecules increases their local concentration and this can be used to modulate the activity of their effector proteins **[Figure 3.8]** In analogy to baitPARCs described above, we named those constructs activator Presenting Artifical Receptor Constructs (activator PARCs).

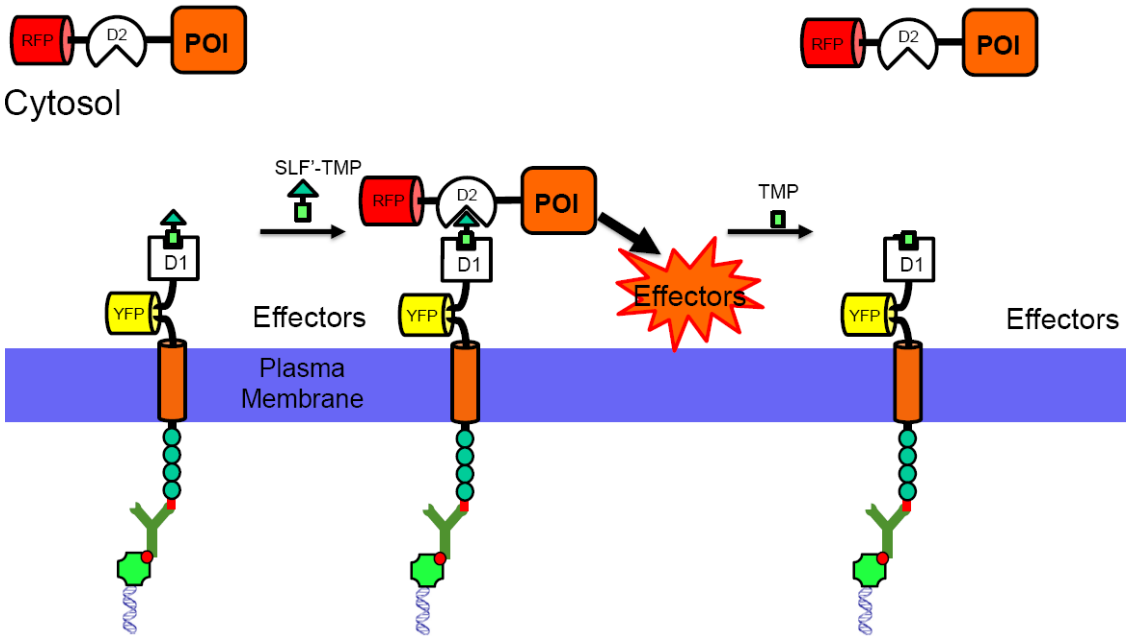

Figure 3.8: Concept of heterodimerization between a cytosolic and plasma membrane targeted protein.

These constructs were derived from VSVG-RII-β PARC (mTurquoise) by exchanging the bait RII-β with the heterodimerization domains eDHFR (E.coli Dihydrofolate reductase), SNAP-Tag (**Figure 3.10c**) or Halo-Tag (**Figure 3.10d**) Optimal plasma membrane localization of activatorPARCs was especially important, as acute targeting to activatorPARCs to internal membranes that can get very close to the plasma membrane might induce activation in undesired regions. Fortunately, just replacing the mTFP and RII-β segments with TagBFP and eDHFR increased plasma membrane targeting more than 3-fold (compare 5-10% for VSVG RII-β PARC (mTurquoise) in **Figures 7a-d** with ~30% for VSVG eDHFR PARC (TagBFP) in **Figure 8a**. This might be due to the bio-orthogonal nature of eDHFR **(Peng Liu et al, 2014)**. In contrast to RII-β, eDHFR is not thought to interact with endogenous proteins in mammalian cells and might therefore be less affected by processing in the secretory pathway. Based on our previous optimization of baitPARCs and earlier

studies on transmembrane translocation efficiency (**Heijne et al., 1988, Lerch-Bader, M et al., 2008**), and fluorescent protein folding (**Schröder M et al., 2005, Prydzk et al., 2013**), variants of the initial activatorPARC design were generated (**Figure 8a**). As expected, addition of linker sequences next to the transmembrane domain and a glycosylation motif significantly improved the plasma membrane fraction. Unexpectedly, exchanging the TagBFP with monomeric Citrine, we observed a significant decline in plasma membrane fraction. Previous studies showed that folding of citrine fluorescent protein can be a problem if expressed at 37°C (**Griesbeck et al., 2001**). It was previously shown that coiled-coil linkers can promote folding of recombinant proteins (**Yoshizumi et al., 2011**). Therefore, we introduced such a linker to connect the mCitrine fluorescent protein to activatorPARCs. This significantly improved the plasma membrane fraction to a similar extent as the corresponding TagBFP-based construct. Another study showed that positively charged residues at the cytoplasmic side of the transmembrane domain could promote membrane insertion of transmembrane domains (**ML Bader et al., 2008**). Addition of such a positively charged linker indeed increased the plasma membrane fraction of activatorPARCs to reach an average of ~60-70% [**Figure 3.9b].**

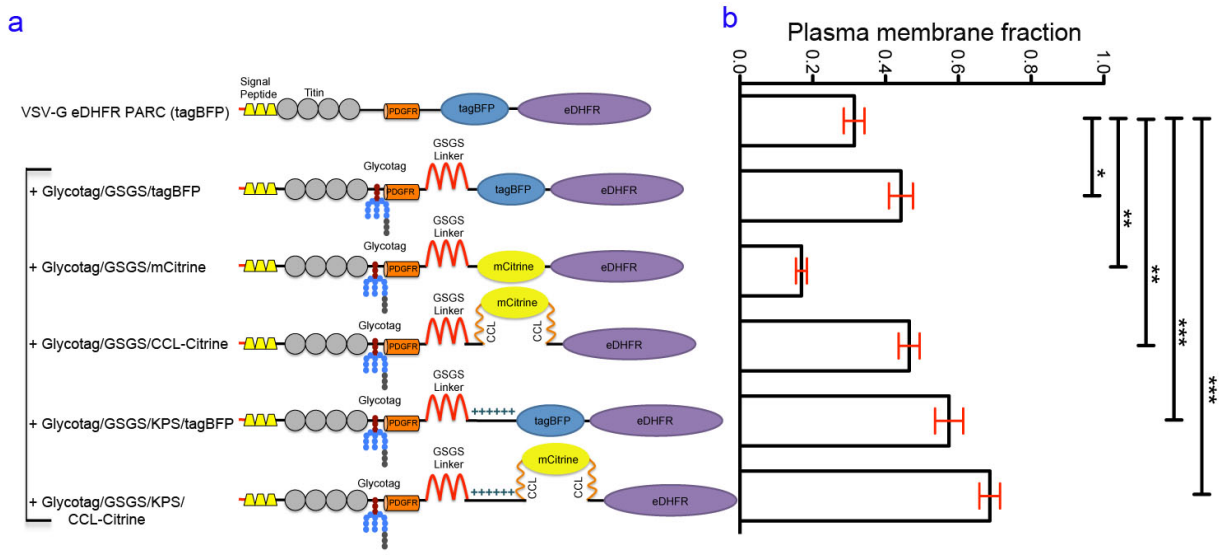

Figure 3.9: Optimization of plasma membrane fraction in activatorPARCs a. Graphical representation of activator PARC constructs with additional linkers and different fluorescent proteins **b.** Corresponding plasma membrane fraction calculated for each corresponding construct (**: p<0.001; ***: p<0.0001; ns: not significant; one-way ANOVA and Tukey's Multiple Comparison Test; n>=24 cells from 3 independent experiments)

We then used this optimized activatorPARC design (second generation) to generate variants that contain the SNAPf and Halotag hetero-dimerization domains. All those variants showed very efficient plasma membrane targeting [**Figure 3.10 b-d**].

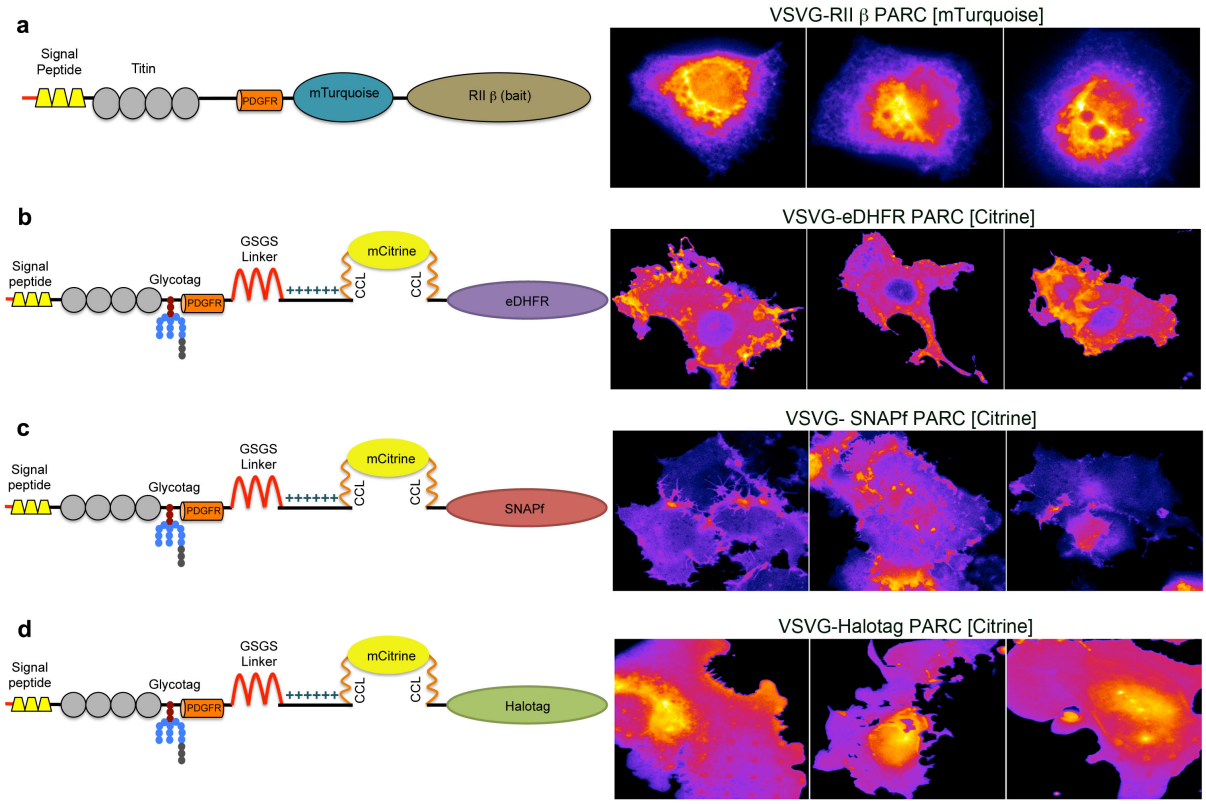

Figure 3.10: Optimization of bait/activator PARCs for plasma membrane localization. The original RII-β presenting baitPARCs design shows only poor plasma membrane targeting if expressed at 37°C. ActivatorPARCs presenting eDHFR, SNAPf or Halotag heterodimerization domains, which were based on an improved design containing a glycosylation motif and an optimized linker, are efficiently targeted to the plasma membrane.

3.2 Application of artificial receptor constructs: Analysis of Rho GTPase signal processing in living cells

Rho GTPases are thought to regulate their spatio-temporal activity by mutual crosstalk (**Guilluy et al, 2009**). To better understand, how activity patterns arise from such crosstalk, we aimed to directly investigate how Rho GTPases influence each other. To reach this goal, Abram Calderon, a PhD student in our lab, developed biosensors to monitor the activity of the major Rho GTPases Rac1, RhoA and Cdc42 (**Abram Calderon 2014**). Each of these biosensors were based on a GTPase binding domain (GBD) from an effector protein that was specific for one of those Rho GTPases **(Pertz O et al, 2010).** The GBD was fused with the mCherry fluorescent protein and expression was controlled by the weak delCMV promotor. The effector proteins in the biosensors were $p67^{phox}$ (aa 1-203) for Rac1, WASP (aa 201-231) for Cdc42 and Rhotekin (aa 8-89) for RhoA. Abram Calderon also developed a novel chemically induced dimerization system in colloboration with Dr. Yaowen Wu (Chemical Genomic Centre, Dortmund) (**Abram Calderon 2014**, **Liu P et al, 2014**). In this method, addition of the small molecule (SLF'-TMP) enabled dimerization between the two proteins eDHFR (*E.coli* dihydrofolate reductase) and FKBP' (F36V mutant of FKBP). This system was used to globally perturb Rho GTPase activity by targeting constitutively active mutants that lack a membrane anchor to the plasma membrane. This lead to the formation of Rac1, Ccd42 and RhoA specific phenotypes, including actin-based cell protrusions and cell contraction in the neuronal cell line Neuro2a (**Abram Calderon 2014**, **Liu P et al 2014**).

Neuro2a cells are highly motile and only weakly adherent. Presumably due to these features, those cells were not compatible with surface modifications to pattern bait- or activatorPARCs. We therefore extended those studies by first applying Rho GTPase sensors and perturbation techniques in the COS7 cell line. We then used activatorPARCs to combine local perturbations of Rho GTPases with global Rho GTPase activity measurements.

3.2.1 Global RhoGTPase activity perturbation and activity measurements in COS7 cells

To study the crosstalk between Rho GTPases in COS7 cells, constitutively active mutants of Rac1 or Cdc42 lacking the membrane anchor (Q61L mutants of Rac1 or Cdc42 were targeted to the plasma membrane via chemically induced dimerization, and the corresponding activity was measured using Rac1 or Cdc42 biosensors. As expected, dimerizer addition induced targeting of constitutively active Rho GTPases to the plasma membrane, which was reversed upon competitor addition **(Figure 3.11a,d)**. We also observed an increase in Rac or Cdc42 sensor signals that mirrored the perturbation kinetics. (**Figure 3.11c,e).**

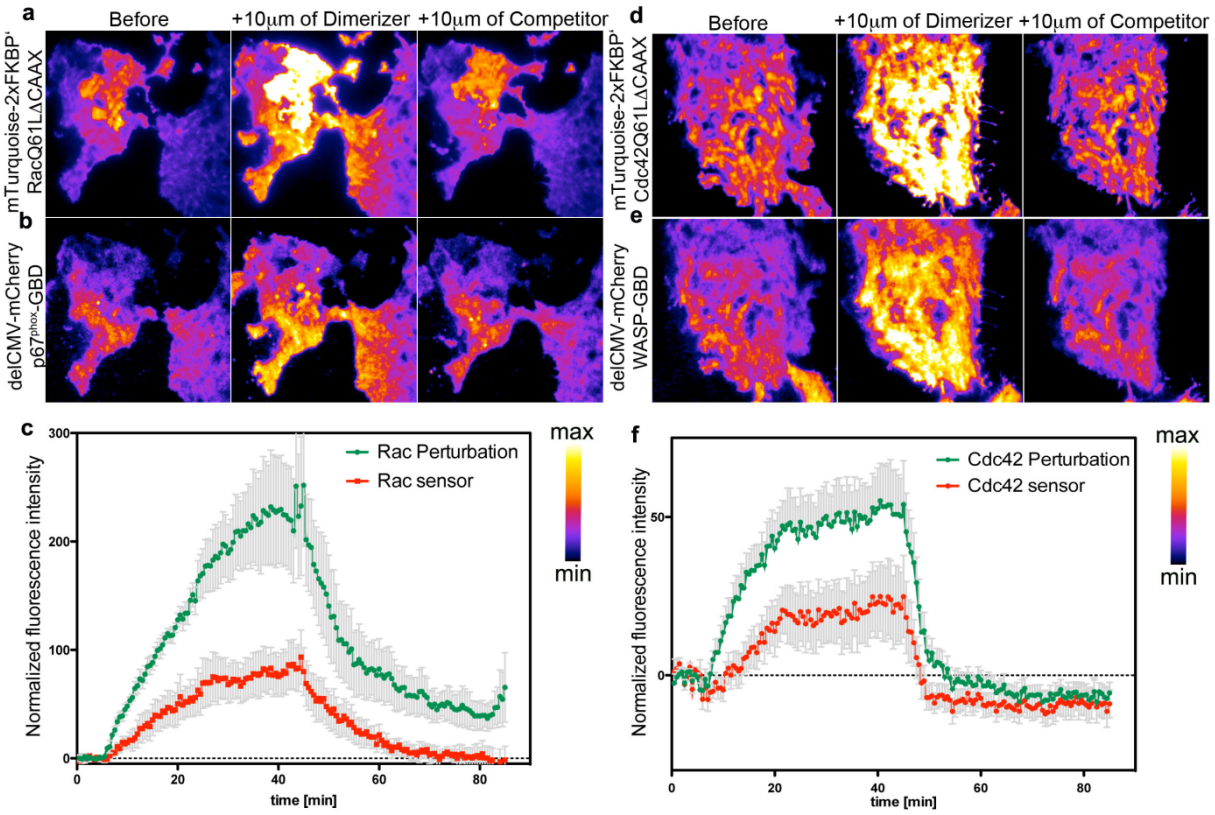

Figure 3.11: Global Rac1 and Cdc42 activity perturbation and activity measurements in COS7 cells. a,d. Observation of plasma membrane targeting of constitutively active RhoGTPases to the plasma membrane via TIRF microscopy. The targeting was reversed upon competitor treatment. b,e. The RhoGTPase activity sensor signal mirrored plasma membrane targeting of active RhoGTPase. C,f. Normalized RhoGTPase perturbation and corresponding sensor intensity measurements (n>=10 cells from 3 independent experiments).

From these experiments it became clear that global perturbation of RhoGTPases can also be performed in COS7 cells. Also, by combining these perturbation experiments with the corresponding Rho GTPase biosensors, we can investigate responses to those perturbations. Using different combinations of perturbation and biosensors (i.e Rac perturbation in combination a Cdc42 sensor), we can investigate the crosstalk between Rho GTPases.

We next investigated a RhoA-myosin based signal network that was identified in a collaborative project with Prof. Perihan Nalbant (University of Duisbürg-Essen). This

signal network is based on a positive feedback, in which RhoA activates its own activator GEF-H1, and a time-delayed negative feedback, in which RhoA activates its own inhibitor, myosin and associated RhoGAPs. This signal network leads to pulses, oscillations and propagating waves of Rho activity in U2OS (Osteosarcoma) cells (**Melanie Grässl, 2016**).

In order to directly study the role of GEF-H1 in Rho activity dynamics, a bachelor student under my supervision, targeted an active mutant of GEF-H1 (GEFH1C53R) to the plasma membrane via chemically induced dimerization (**Wiebke Obermann, 2015**). This GEF-H1 mutant interferes with the interaction with microtubules, which usually serves as a negative regulator of GEF-H1 activity **(Krendel M et al 2002).**

As expected, targeting of the Rho-specific GEF-H1 to the plasma membrane lead to increased Rho activity **(Figure 3.12a-b).** Interestingly, this response was only transient and even stronger pulses and propagating waves were observed after releasing GEF-H1 from the membrane following competitor addition (two sharp green peaks in **Figure 3.12d).** The observed response dynamics are expected from the underlying feedback loops: The transient Rho activity response could be due to the time-delayed activation of the Rho inhibitor myosin and the suppressed spontaneous Rho dynamics during GEF-H1 plasma membrane targeting could be due to the static GEF-H1 localization after chemically-induced dimerization that breaks the dynamics of the feedback cycles.

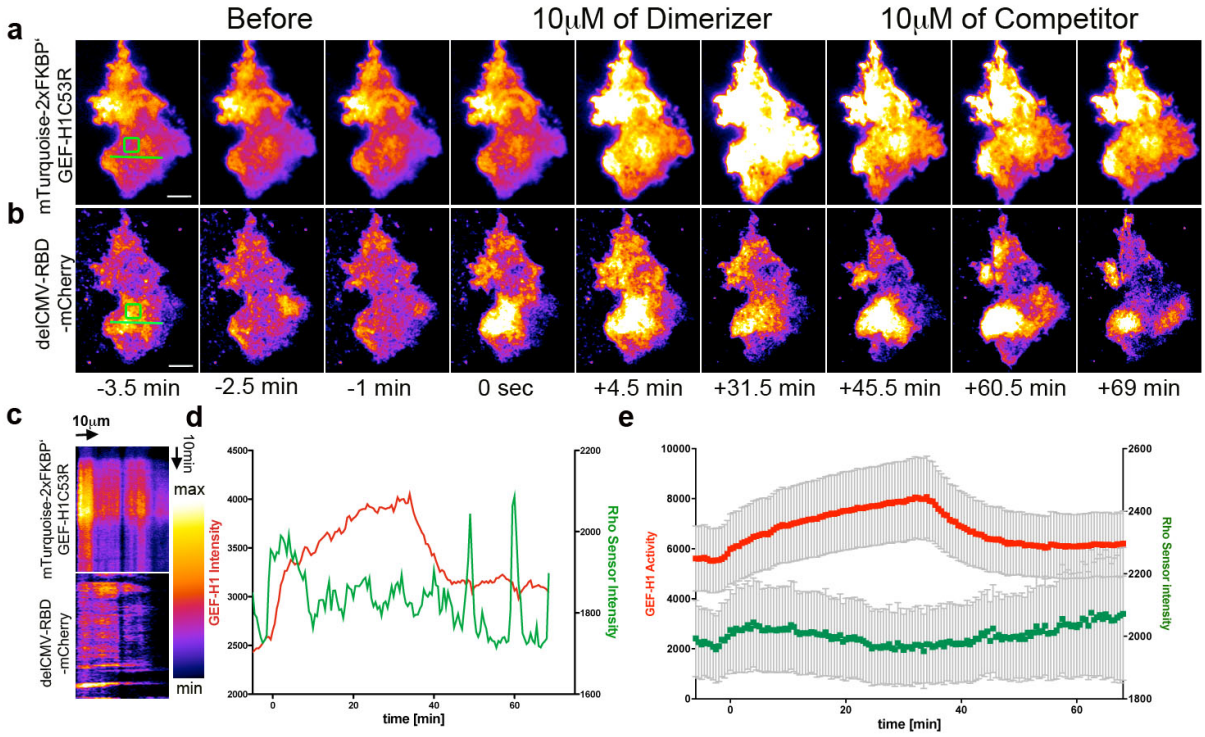

Figure 3.12: Modulation of spontaneous Rho dynamics by GEF-H1 plasma membrane targeting a-b. Microscopy images of U2OS cells showing recruitment of GEF-H1 to the plasma membrane and respective Rho sensor dynamics. Treatment with a competitor shows detachment of GEF-H1 and strong local Rho activity pulses **c.** Kymograph analysis of GEFH1 and Rho sensor dynamics. **d-e**. Intensity plot for GEF-H1 and Rho sensor activity over time from a single cell (d) and average measurements from 16 cells (e).

3.2.2 Local RhoGTPase activity perturbation via ActivatorPARCs in combination with activity measurements in COS7 cells

Next, we combined activatorPARCs (chapter 3.16) with chemically induced dimerization (chapter 3.2) to induce spatio-temporal perturbations of RhoGTPase activity. Such local perturbations can be combined with global activity measurements to directly investigate spatio-temporal signal propagation in living cells. For those experiments, we could capitalize on our optimized eDHFR-based activatorPARCs that were enriched by 900-1000% to spots containing VSVG antibodies (**Figure 3.13c, 3.14c**). This relative enrichment was ~3 times better compared to the un-optimized baitPARCs, which showed an enrichment of ~300%.

After addition of dimerizer, constitutively active RhoGTPases were targeted to optimized activatorPARCs (**Figure 3.13d, 3.14d**). As expected, addition of the competitor reversed this targeting and the corresponding activity sensors mirrored those kinetics (**Figure 3.13e, 3.14e**), similarly as in global perturbation experiments (**Figure 3.11 a-b, d-e**). This shows that local, reversible RhoGTPase activity perturbation and corresponding activity measurements can be achieved by combining activatorPARCs with chemically induced dimerization.

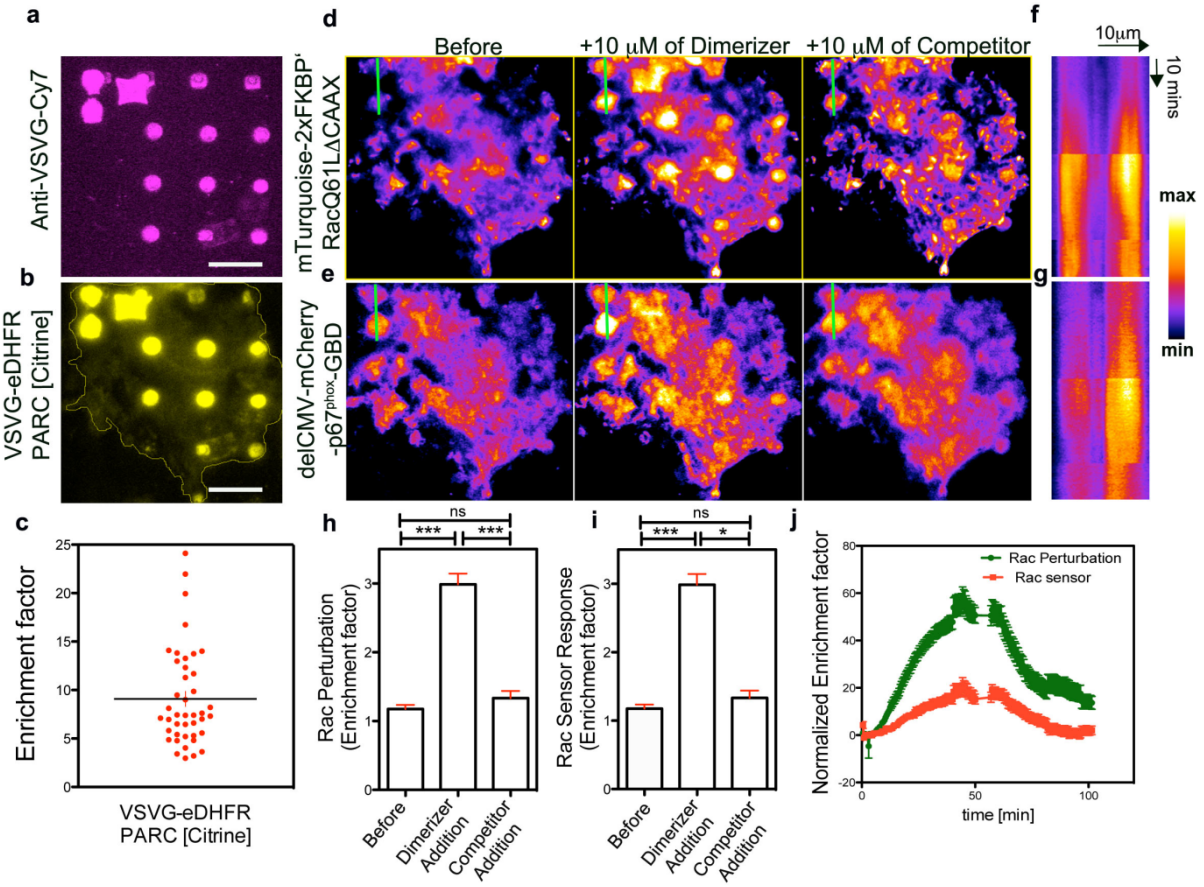

Figure 3.13. Localized Perturbation and Sensor response of constitutively active Rac. **a**. Immobilized Anti-VSVG-Cy7 arrays on a glass surface **b**. COS7 cells plated on top of antibody arrays showed enrichment of eDHFR activatorPARCs **c**. Quantification of the relative enrichment (n=10 cells from 3 independent experiments) **d**. Addition of the dimerizer induced recruitment of constitutively active Rac to activatorPARC patterns **e.** Rac sensor activity measurements mirrored recruitment of active Rac1 to spot patterns. **f,g**. Kymograph analysis of the perturbation and activity response kinetics, **h, i, j.** Quantitative analysis of plasma membrane fraction (*: p<0.01**: p<0.001; ***: p<0.0001; ns: not significant; one-way ANOVA and Tukey's Multiple Comparison Test; n>=10 cells from 3 independent experiments)

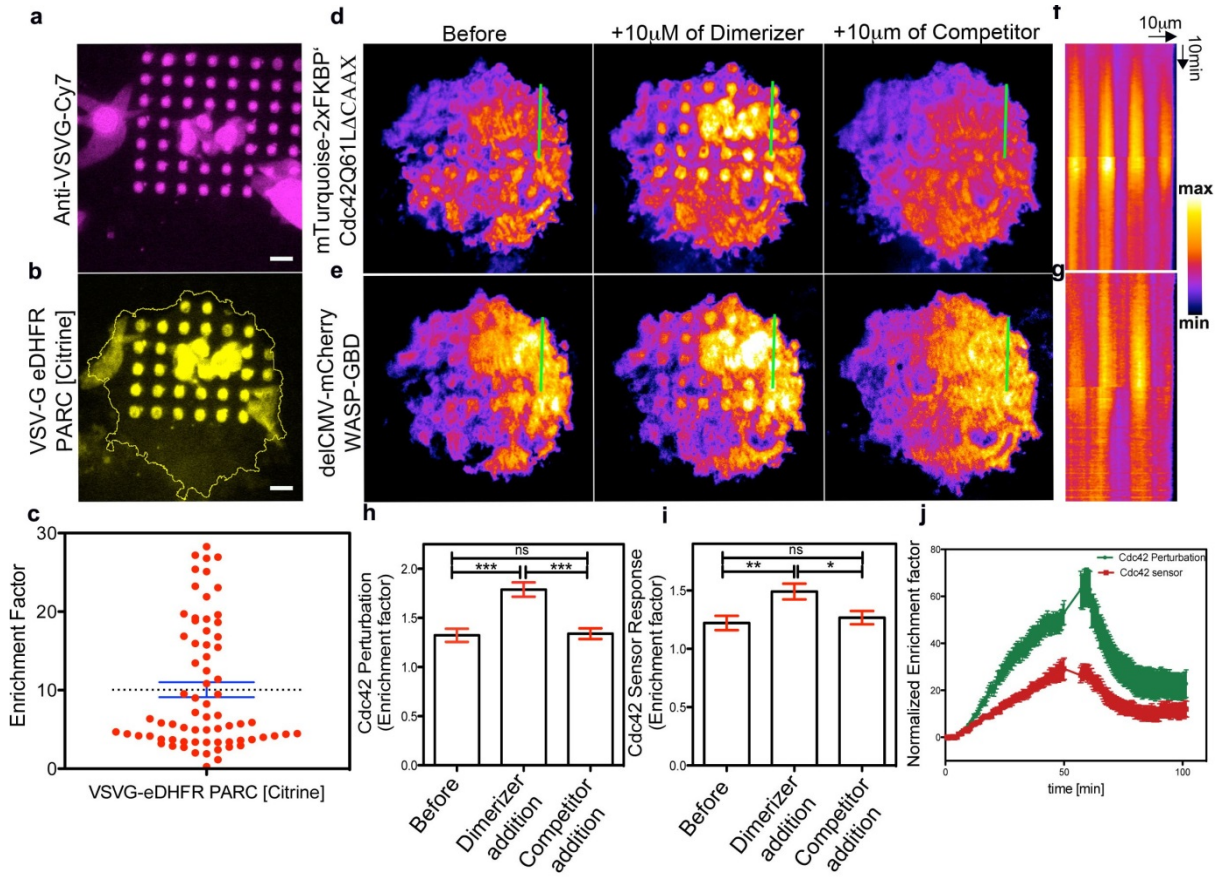

Figure 3.14: Local Perturbation and sensor measurement of constitutively active Cdc42. a. Immobilized Anti-VSVG-Cy7 arrays on a glass surface **b.** COS7 cells plated on top of antibody arrays showed enrichment of eDHFR activatorPARCs **c.** Quantification of the relative enrichment (n=10 cells from 3 independent experiments) **d.** Addition of the dimerizer induced recruitment of constitutively active Cdc42 to activatorPARC patterns **e.** Cdc42 sensor activity measurements mirrored recruitment of active Cdc42 to spot patterns **f,g**. Kymograph analysis of the perturbation and activity response kinetics **h. i. j.** Quantitative analysis of plasma membrane fraction (*: p<0.01**: p<0.001; ***: p<0.0001; ns: not significant;: not significant; one-way ANOVA and Tukey's Multiple Comparison Test; n>=10 cells from 3 independent experiments)

Interestingly, we observed differences between the kinetics of the perturbations vs the responses of Rac and Cdc42 at distinct spot positions **(Figure 3.15, 3.16).** In the case of the Rac perturbation, in some spots, the Rac sensor showed on average a more positive, on other spots it showed a more negative response. Those differences could either point to feedback mechanisms or differences in the saturation of the underlying cellular reactions.

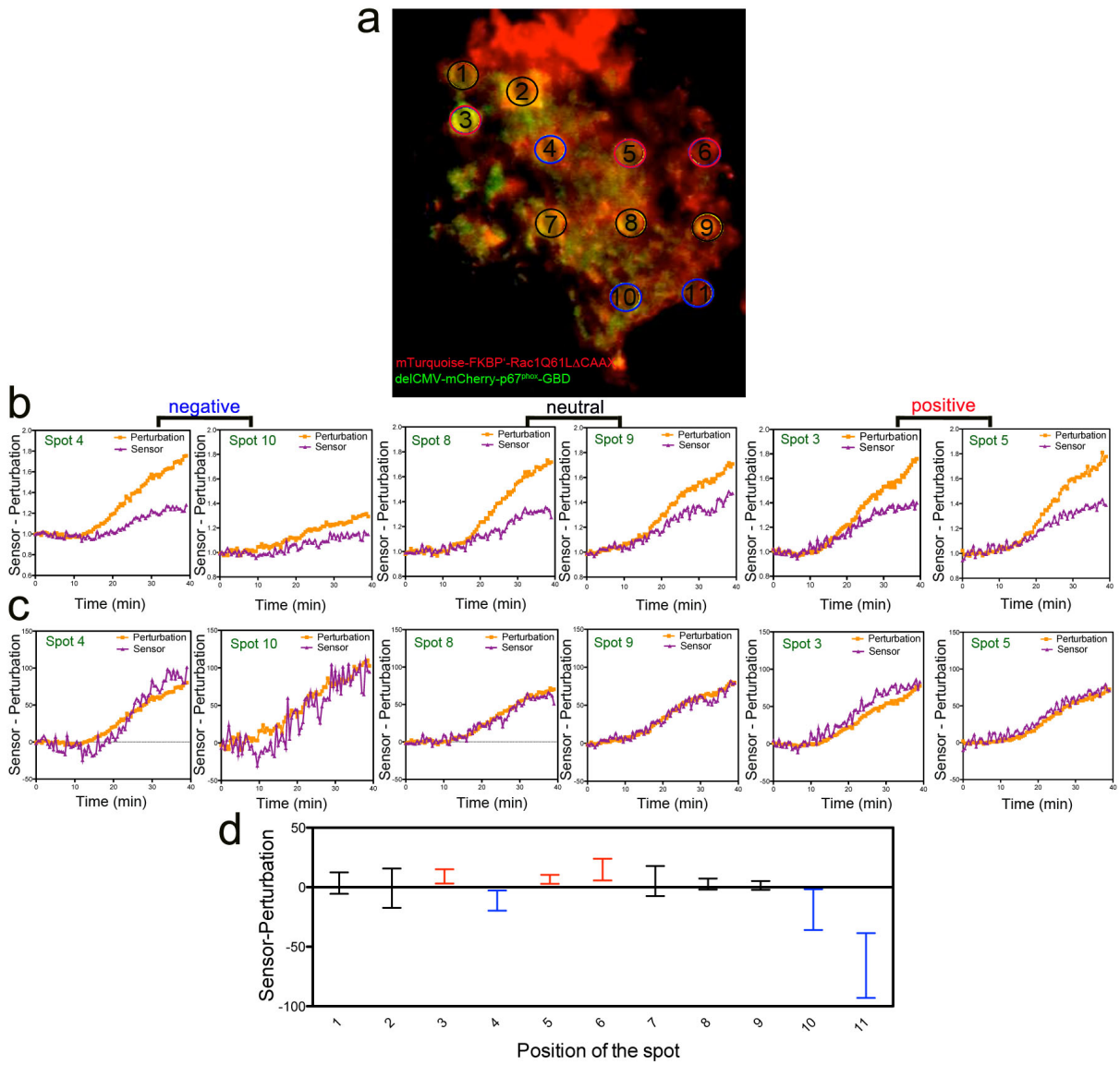

Figure 3.15: Position-dependent Rac1 activity responses to Rac1 perturbation a. Pseudo color image of a living cell showing the Rac perturbation (red) and corresponding sensor response (green). Circled spots are color-coded based on a more positive (red), neutral (black) or more negative (blue) sensor response during perturbation **b.** Normalization to the initial fluorescence intensities (t_0=0-5min) shows overall strength of the perturbation (orange) and response (purple) in distinct spots. **c.** Normalization to both the initial (t_0=0-5min) and the maximal fluorescence intensities (t=0-40min) shows relative differences in the kinetics. **d.** Curves are classified based on differences in the initial response: positive (red), neutral (black) and negative (blue). Mean values and standard deviation of the difference between sensor and perturbation in the initial phase of the perturbation (10 min).

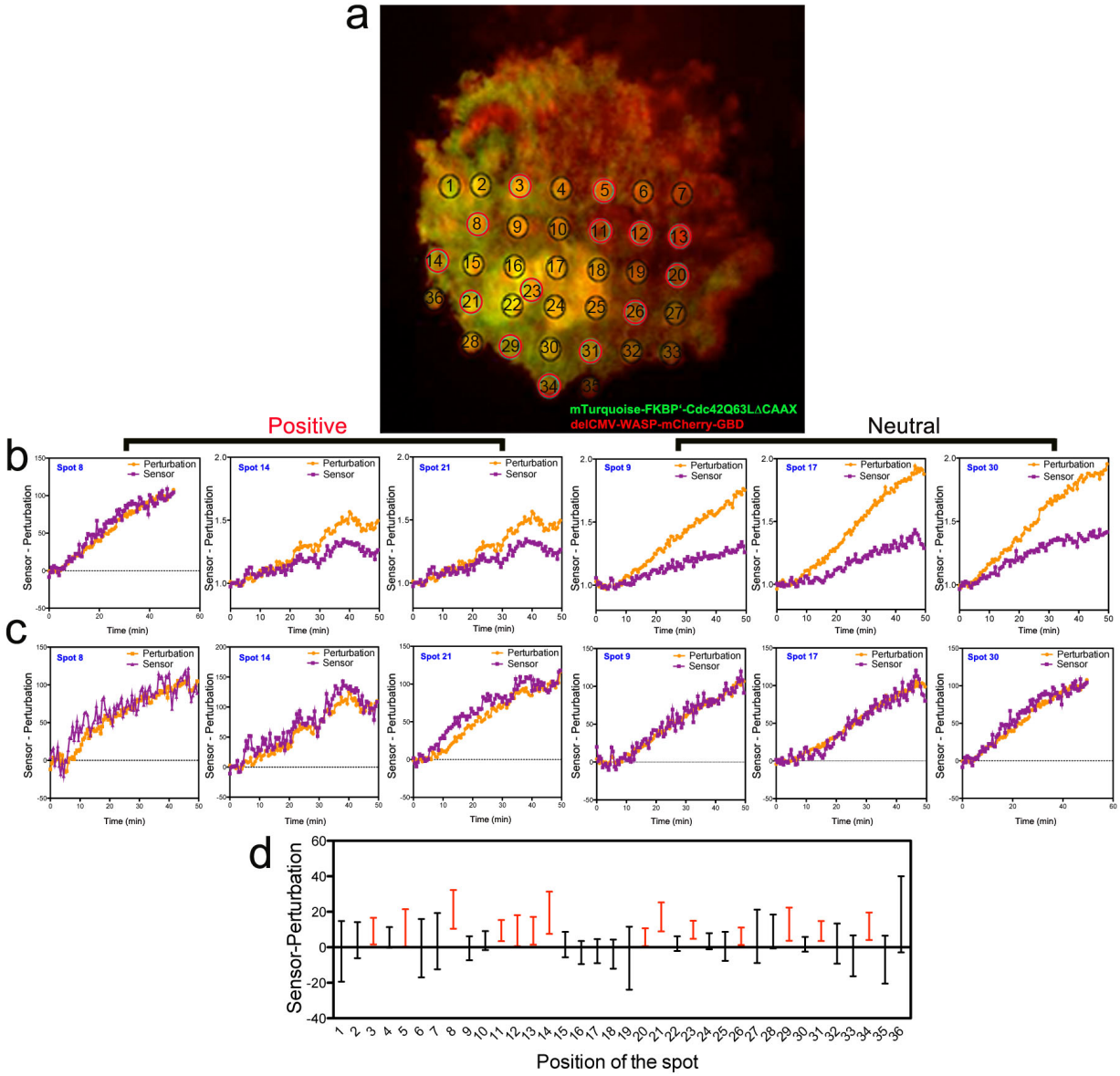

Figure 3.16: Position-dependent Cdc42 activity responses to Cdc42 perturbation a. Pseudo color image of a living cell showing the Cdc42 perturbation (red) and corresponding sensor response (green). Circled spots are color-coded based on a more positive (red) or neutral (black) sensor response during perturbation **b.** Normalization to the initial fluorescence intensities (t_0=0-5min) shows overall strength of the perturbation (orange) and response (purple) in distinct spots. **c.** Normalization to both the initial (t_0=0-5min) and the maximal fluorescence intensities (t=0-40min) shows relative differences in the kinetics. **d.** Curves are classified based on differences in the initial response: positive (red) and neutral (black). Mean values and standard deviation of the difference between Sensor and Perturbation in the initial phase of the perturbation (10 min).

3.2.3 Light controlled local RhoGTPase activity perturbation via photochemically induced dimerization

Together with the group of Dr.Yaowen Wu, we aimed to develop a light-inducable dimerization strategy that could allow faster subcellular targeting with increased spatial control. To reach this goal, a co-worker of Dr. Yaowen wu, Dr. Xi Chen developed a cell permeable and photoactivatable dimerizer called 'pTMP-Cl'. This dimerizer contains a trimethoprim (TMP) moiety that was caged by a photo labile 6-nitroveratroyloxycarbonyl (NVOC) group, linked to a chlorohexyl group via a Polyethylene glycol linker (PEG). First, the chlorohexyl moiety can form a covalent bond with a Halotag domain **(Los G et al 2008)**. Once the stable covalent bond is established, the NVOC group from the photodimerizer can be removed by illumination at a wavelength of 405nm **(Klán et al, 2013).** After photouncaging, the free TMP moiety can bind to eDHFR fused to a protein of interest. After initial characterization of this targeting system in the lab of Dr. Yaowen Wu, we decided to use it for local plasma membrane targeting of Rho GTPases.

Neuro-2a cells were transfected with the following constructs: 1) The Halotag fused to the plasma membrane targeting CAAX-Box derived from K-Ras (Halotag-TagBFP-CAAX), 2) dominant active Rac1 lacking its membrane anchor fused to eDHFR (eDHFR-mCitrine-NES-Rac1Q61LDac1Q). To reduce Rac localization to the nucleus, an additional nuclear export signal sequence (NES) was added to this construct **(Abram Calderon, 2014).** TIRF Microscopy was used to monitor the photo-induced recruitment of the eDHFR fusion protein to the plasma membrane (**Figure 3.17a**). Recruitment kinetics was determined both for an empty eDHFR-mCitrine construct ($t_{1/2}$=48ms, 30% increase) and for the fusion with the active Rac mutant, which was

considerably slower ($t_{1/2}$=780ms, 50% increase) (**Figure 3.17b**). This is expected, as the larger Rac containing fusion protein should diffuse slower to the site of activation. To our knowledge, this is the fastest targeting kinetics that was observed for any CID or pCID system (**Kennedy M et al., 2010**).

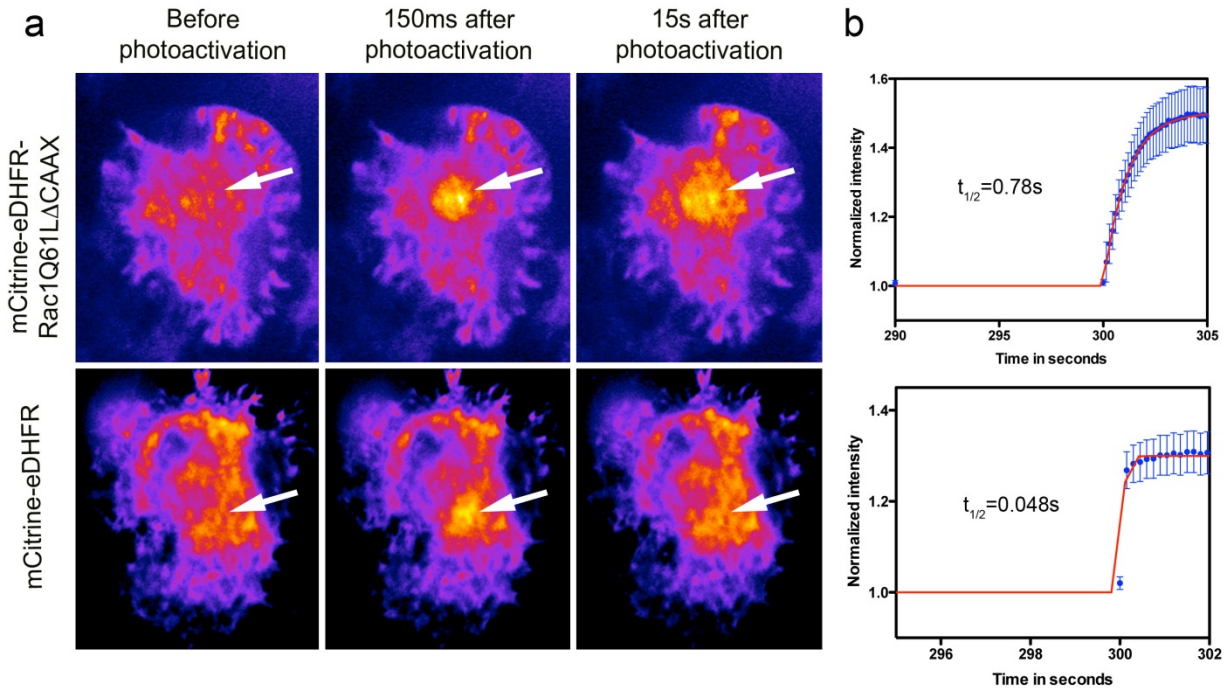

Figure 3.17: Recruitment kinetics of plasma membrane mediated targeting via pCID: a. Representative examples of Neuro-2a cells showing plasma membrane targeting of fluorescently labeled eDHFR alone and fused to constitutively active Rac (Rac1Q61LΔCAAX) (above) at the site of photo activation (white arrows). **b.** Recruitment kinetics of Rac and empty construct were used to calculate respective half times after exponential fitting.

We next tested, if plasma membrane targeting of constitutively active Rac leads to the expected phenotype: lamellopodium formation. To increase the local plasma membrane targeting, we uncaged the dimerizer in the same subcellular region repeatedly. Interestingly, targeting of active Rac induced localized lamellopodia formation and resulted in directed cell migration towards the region of Rac uncaging (**Figure 3.18c**). For every pulse, we observed a rapid decline in fluorescence signal, presumably due to lateral diffusion of CAAX-box based Halotag targeting domain

(**Figure 3.18d**). Kymograph analysis (**Figure 3.18e**) was used to measure cell protrusion and retraction velocity at the leading and trailing edge (**Figure 3.18f**).

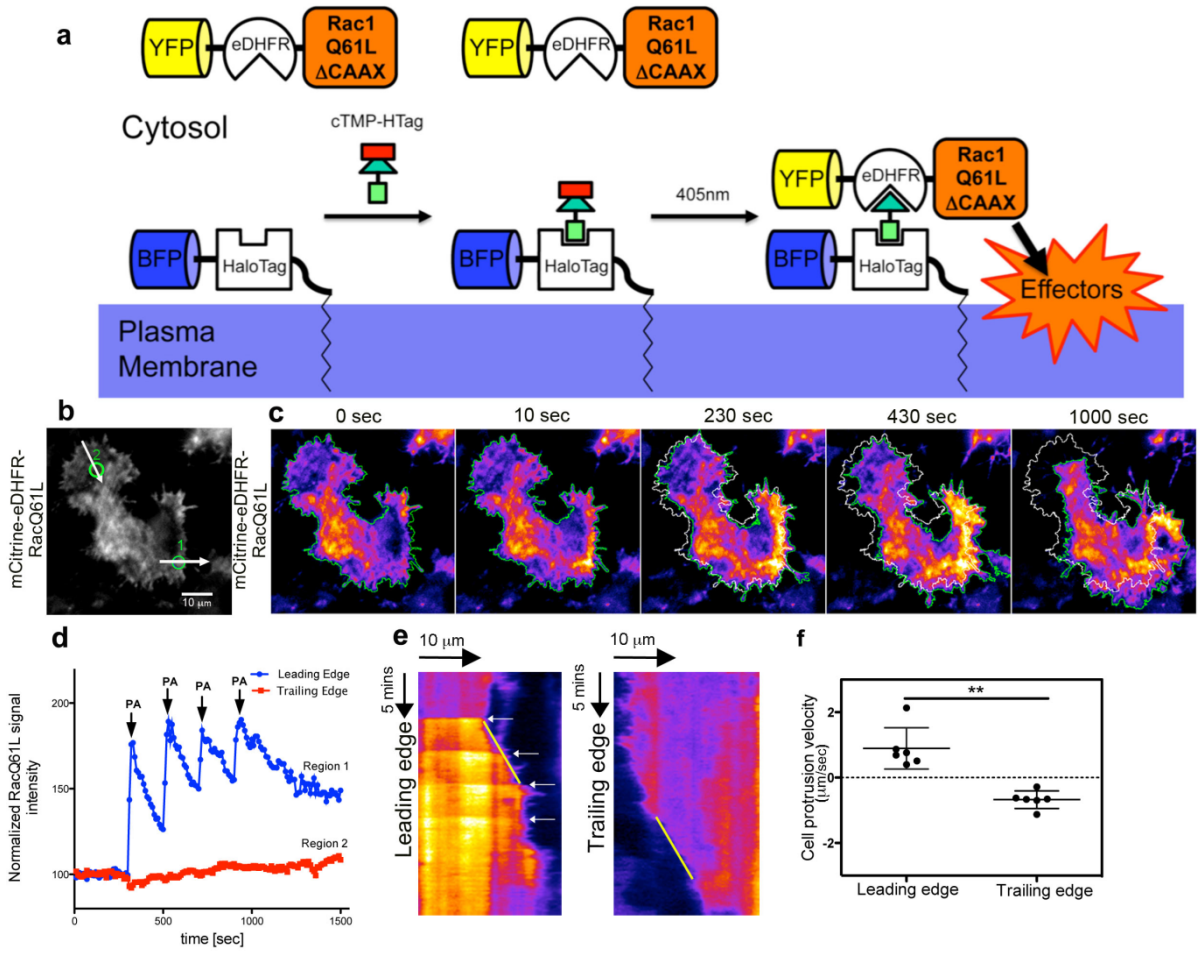

Figure 3.18: Directed cell migration controlled by photo-induced localized plasma membrane targeting of active Rac a. Concept of photochemically induced dimerization **b.** Representative TIRF image of a Neuro-2a cell expressing fluorescently labeled eDHFR-active Rac lacking the membrane anchor. The green circles mark regions 1 and 2 used for fluorescent intensity measurements. White arrows represent the regions used for kymograph analysis **c.** Sequential TIRF images showing local recruitment of eDHFR-mCitrine-NES-Rac1Q61LΔCAAX to the plasma membrane after individual laser photo activation pulses **d.** Quantitative analysis of plasma membrane recruitment in regions 1 and 2 labeled in a **e.** Kymograph analysis showing the cell protrusion and retraction in the leading and trailing edge **f.** Graph of Cell protrusion velocity at the leading edge and trailing edge of Neuro-2a cells (**:p<0.01; paired student's t-test; n=6 cells from 3 independent experiments).

We next studied how acute, global plasma membrane targeting of GEF-H1 by photo uncaging affects Rho signal activity. In order to achieve this, the active mutant of GEF-H1 described in chapter 3.2.1 was fused to eDHFR (mCitrine-eDHFR-

GEFH1C53R) and co-expressed in Hela cells with the Halotag fused to a plasma membrane anchor (Halotag-TagBFP-CAAX), and a Rho activity sensor (delCMV-Rhotekin-mCherry). Photo uncaging at two subsequent time points resulted in a moderate and minor increase in the targeted GEF-H1 signal, respectively (**Figure 3.19a**). This perturbation induced a strong and moderate increase in Rho activity at those two time points (**Figure 3.19b**). Interestingly, we also observed a delayed but very efficient adaptive response of Rho activity following those perturbations (**Figure 3.19e)**. A slower adaptive response was observed after slow GEF-H1 plasma membrane targeting via chemically induced dimerization (see chapter 3.2.1).

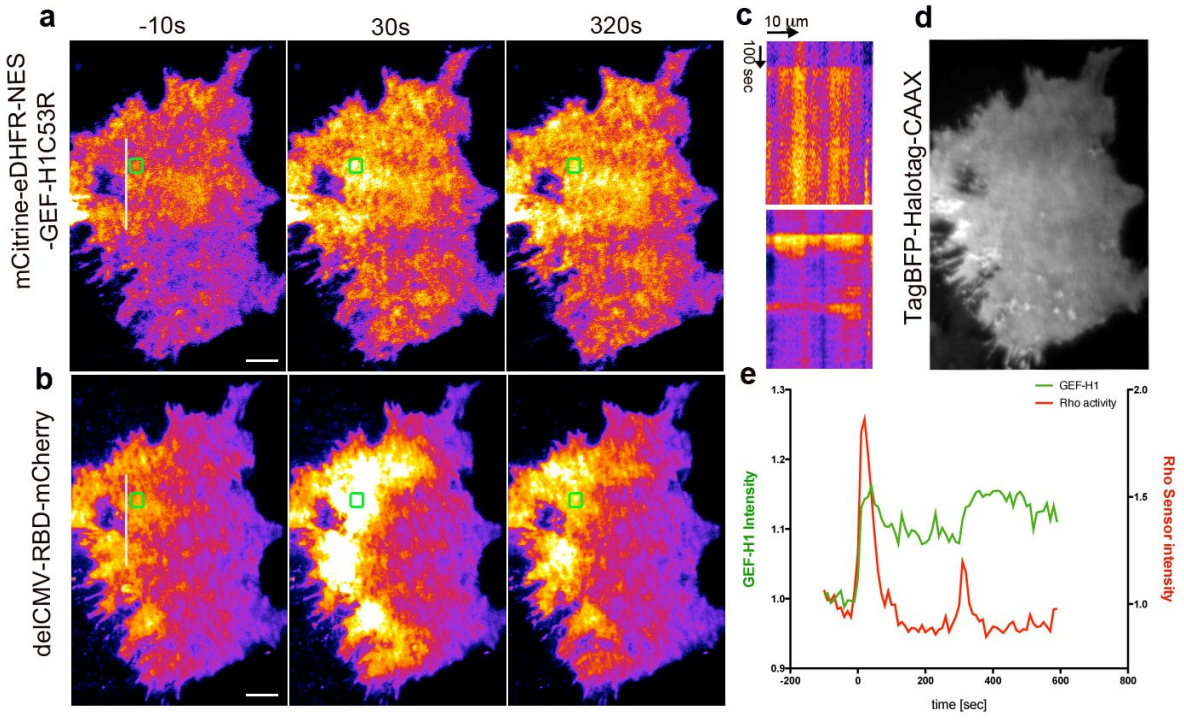

Figure 3.19: Adaptive Rho activity responses upon acute GEF-H1 plasma membrane recruitment via photochemically induced dimerization a-b. Global recruitment of GEF-H1 and Rho dynamics upon photouncaging in Hela cells **c.** Graph of the GEF-H1 andRho sensor signal intensity over time. d. Localization of the Halotag construct with a CAAX-box membrane anchor.

3.2.4 Stable, localized plasma membrane targeting via activatorPARCs

Even though active Rac was locally recruited to the plasma membrane, as shown in **Figure 3.18d**, fluorescence intensity decreased after each laser pulse presumably due to lateral diffusion of the CAAX box membrane anchor. Lateral diffusion was clearly observed in **Figure 3.17a.** In order to completely suppress lateral diffusion, we generated a HaloTag-containing activator PARC (VSVG-HaloTag PARC [mCitrine]) (See also **Figure 3.10**) to replace the CAAX box-based dimerization domain. We then transfected those receptors in Cos7 cells together with constitutively active Rac fused to eDHFR (mCherry-eDHFR-NES-Rac1Q61LDCher) and plated those cells on anti-VSVG-Cy7 arrays. We found that these receptors were enriched by up to ~400% (average ~250%) to spots containing the VSVG antibodies (**Figure 3.20f**). Blue light (405nm) illumination at the spot region leads to rapid and localized targeting of the eDHFR fusion protein (**Figure 3.20b**). Kymograph images revealed stable and sustained recruitment of this dimerization partner for more than 15 minutes (**Figure 3.20c**). Recruitment to artificial receptors neither showed detectable loss in fluorescence signal nor lateral diffusion after photo activation (**Figure 3.20d**). The stable recruitment was restricted to a narrow region and no recruitment was observed a few micrometers away from the site of photoactivation. We were also able to induce stable anchoring of the targeted protein to multiple distinct spots in a single living cell. Interestingly, while plasma membrane targeting of active Rac to a diffusible dimerization domain lead to lamellipodium formation and directed cell migration, targeting to immobile receptors did not induce a strong cellular phenotype. Presumably this is due to the inability of targeted Rac1 to reach the very leading edge of the cell, which might be necessary to induce lamellipodia.

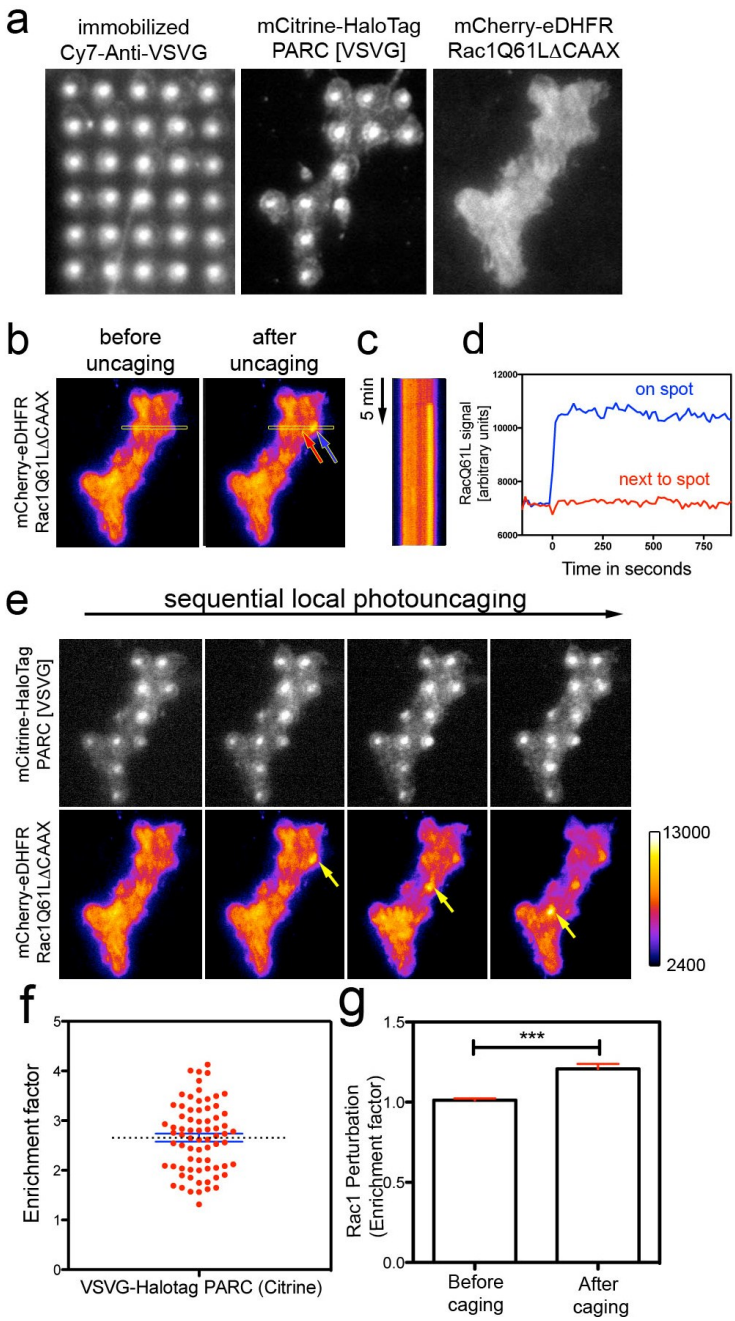

Figure 3.20: Stable, localized targeting of active Rac to the plasma membrane via activatorPARC a. Anti-VSVG-Cy7 arrays were able to enrich ActivatorPARCs inside living cells **b.** Representative TIRF images showing stable plasma membrane targeting of constitutively active Rac (mCherry-eDHFR-NES-Rac1Q61LΔCAAX) after photouncaging (blue arrow: site of photoactivation) **c.** Kymograph analysis of region marked in b showed stable and sustained plasma membrane targeting of constitutively active Rac **d.** Intensity profile shows sustained recruitment of active Rac to the illuminated spot region (blue arrow in b) and not in the region next to it (red arrow in b) **e.** Sequential uncaging of photo dimerizer in multiple spots leads to highly localized targeting of constitutively active Rac **g.** Average relative enrichment in Cos7 cells (n =24) **f.** Quantitative analysis of plasma membrane fraction calculated before and after uncaging (***: p<0.0001; one-way ANOVA and Tukey's Multiple Comparison Test; n>=24 cells from 3 independent experiments).

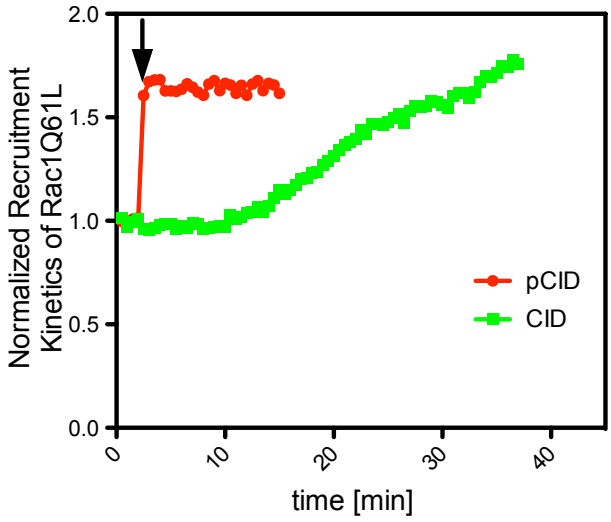

Figure 3.21: Graph showing slow and fast targeting of RacQ61L via CID and pCID, respectively.

In comparison to CID where the maximal perturbation of RhoGTPases takes place in tens of minutes, pCID can induce a much faster perturbation of RhoGTPases at the timescale of seconds (**Figure 3.21**).

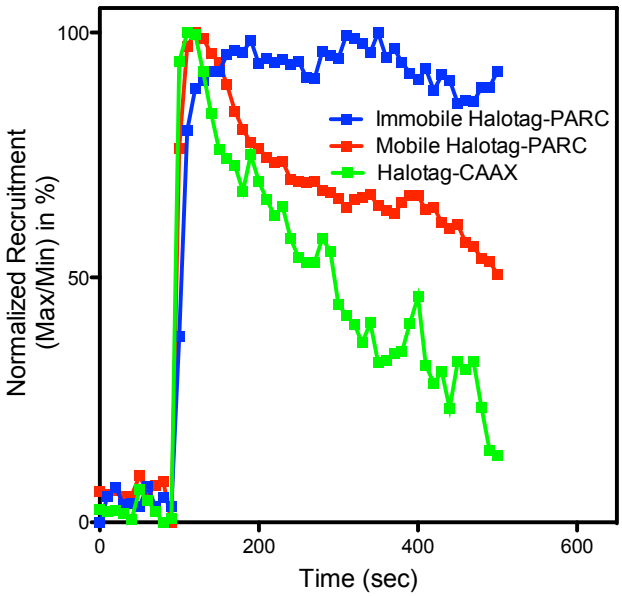

Figure 3.22: Recruitment kinetics of Halotag-CAAX, mobile Halotag-PARC and immobilized Halotag-PARC after photoactivation.

Halotag anchored to the plasma membrane with a CAAX box showed rapid loss of signal after photoactivation via uncaging (**Figure 3.22**). In comparison, immobilized Halotag PARC on arrays displayed stable perturbation (**Figure 3.22**), whereas cells expressing mobile Halotag PARC in the absence of surface immobilized antibodies did not enable a stable perturbation after photoactivation (**Figure 3.22**). This demonstrates the importance of the immobilization step to induce a stable perturbation of RhoGTPases.

Appendix

4.1 Antibody immobilization in mm-size spots for subcellular protein targeting

Under my supervision, another Bachelor student generated mm-size Cy7-labeled spots of immobilized anti-VSVG antibodies. Details about the protocol to fabricate those spots can be found in his thesis (**Jan Wolffgramm, 2015**). The idea behind fabricating those structures was that i) they are easier to make, as they do not require sophisticated lithography devices. ii) Cell polarization can be induced if cells attach at the border of those spots. Living Cos 7 cells expressing eDHFR-based Activator PARCs (VSVG-eDHFR PARC (CCL Citrine)), dominant active Rac fused to FKBP (mTurquoise-FKBP-RacQ61CAAX) and a Rac activity sensor (delCMV-phox^{p67}-mCherry) were plated on those structures. Selected cells growing at the spot interface displayed strong enrichment (average 1000%) of activatorPARC and those were subjected to chemically induced dimerization (**Figure 4.1g**). Addition of the small molecule dimerizer induced plasma membrane targeting of active Rac1 to one side of the cell (**Figure 4.1c**). Subsequent addition of the competitor reversed plasma membrane targeting. As expected, Rac sensor activity mirrored Rac targeting kinetics (**Figure 4.1e**). In the small set of 5 cells that were analyzed in those experiments, a small trend but no significant change in the plasma membrane targeting and sensor response were detected (**Figure 4.1h,i**). More robust results might be obtained after further optimization of the antibody immobilization protocol. This was not possible within this thesis due to time considerations.

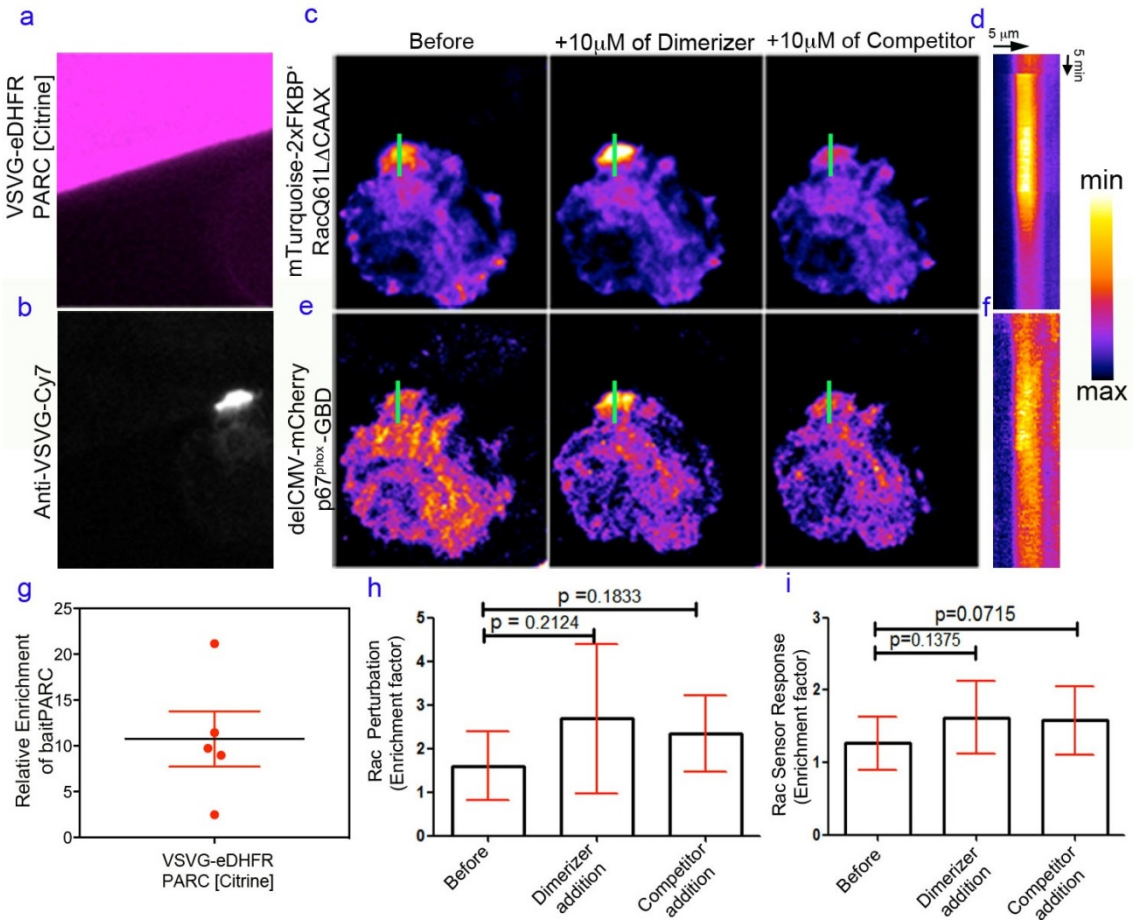

Figure 4.1: Antibody immobilization in mm-size spots for subcellular protein targeting **a.** Immobilized Anti-VSVG-Cy7 big spot on a glass surface **b.** COS7 cells plated on top of antibody arrays showed enrichment of eDHFR activatorPARCs **c, e.** Recruitment of active Rac mutant and Rac sensor during chemically induced dimerization **d, f.** Kymograph analysis of the perturbation and activity response kinetics **g.** Quantification of the relative enrichment (n= 5 cells from 1 independent experiment) **h,i.** Quantitative analysis of Rac Perturbation and Rac sensor response during perturbation (paired student-t-test; n>=5 cells)

4.2 Characterization of polymer pen printed micropatterns

Initially the arrays for studying multiple protein interactions were immobilized using Dip Pen Nanolithography. However, using this technology, the generation of 5x5 arrays' using a 12-pen silicon nitride cantilever tip was time consuming. To solve this problem, a custom-made, low-cost plotter device was developed by Prof Christof Niemeyer (KIT), Prof. Neyer (TU Dortmund) and co-workers. The 12-pen Silicon nitride tip was replaced with a 5184-polymer pen array and a micro fluidic device was developed to deliver DNA-based ink to the pen array (**Arrabito et al., 2014**). Dr.

Giuseppe Arrabito, a postdoctoral researcher in Prof. Niemeyer's lab used this polymer pen nanolithography device to fabricate immobilized EGF arrays. We used those arrays in collaboration with them to study how EGF affects EGF receptor activity. MCF-7 cells that stably express EGFR-EGFP were plated on immobilized EGF arrays and displayed local enrichment of EGF receptors. We also found that those receptors were phosphorylated via immunofluorescence staining using phospho-specific antibodies (**Figure 4.2**). We concluded that the arrays fabricated via Polymer Pen Nanolithography were of high quality and can be used to address cell biological questions for example concerning EGFR signaling **(Arrabito G et al., 2014)**.

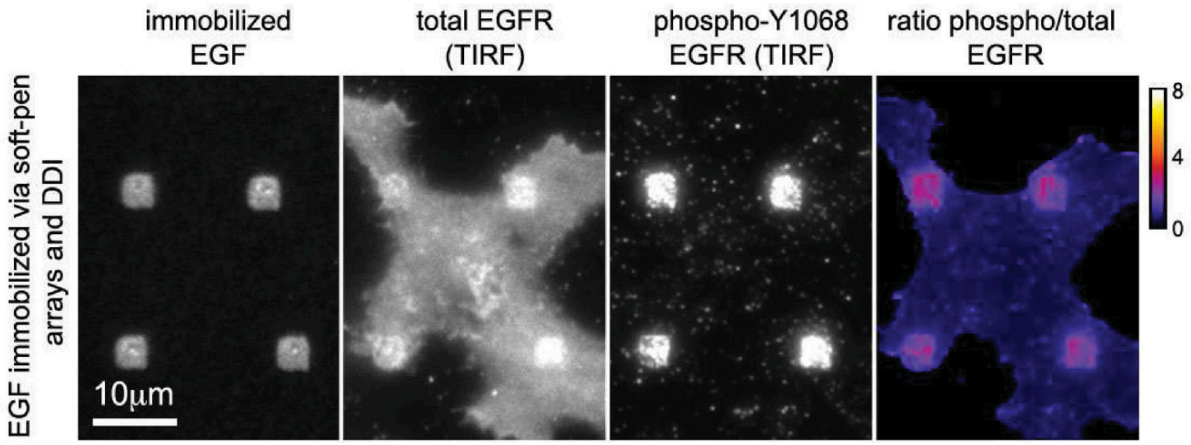

Figure 4.2: Activation of EGFR by surface immobilized EGF ligands. Our new plotter device was used to immobilize EGF ligands on glass substrates. DNA directed immobilization enabled the fabrication of the functionalized EGF arrays with single stranded DNA-streptavidin conjugates. Addition of biotinylated Cy7 dye facilitated the visualization of the EGF arrays. MCF-7 cells stably expressing EGFR-EGFP were plated onto functionalized EGF arrays were imaged in TIRF microscopy. Phospho-specific antibodies and alexa-conjugated antibodies in immunostaining revealed increased phosphorylation of EGFR at tyrosine residue 1068 within immobilized EGF spots. **Picture source: Arrabito G et al., 2014**

4.3 Molecular activity painting

We also developed a novel method for stable, light-induced, plasma membrane targeting of proteins on a surface that is homogenously coated with antibodies. We named this method “Activator-Painting”. This painting strategy is based on the photochemically induced dimerization concept that was already explained in **section 3.2.4**. Here, a homogenous surface is easily produced and thereby overcomes the requirement of the time-consuming lithography step. Basically, the activated surface is incubated with reactive single stranded DNA to immobilize antibodies homogenously on the whole surface (**Figure 4.3b;** see also **Section 2.2.2**) via a similar procedure, large spots in millimeter range can also be generated (**Figure 4.3c**), which can be used for cell polarization experiments. Antibody concentration measured via Cy7 intensity was compared between the homogenous and millimeter spot sample. Interestingly, the micrometer spots contained several fold lower antibody concentration compared to the homogeneous sample that was reflected in weaker Cy7 intensity (**Figure 4.3**)

Using those surfaces, we observed rapid, localized, stable targeting of GEF-H1 to the plasma membrane. Due to the homogenous immobilization of the antibody over the whole cell surface, uncaging can be performed in any geometrical shapes like spots or squares of distinct sizes, and even lines or symbols as shown in **Figure 4.3**. This method can be used to manipulate regulatory networks within sub-regions of the plasma membrane.

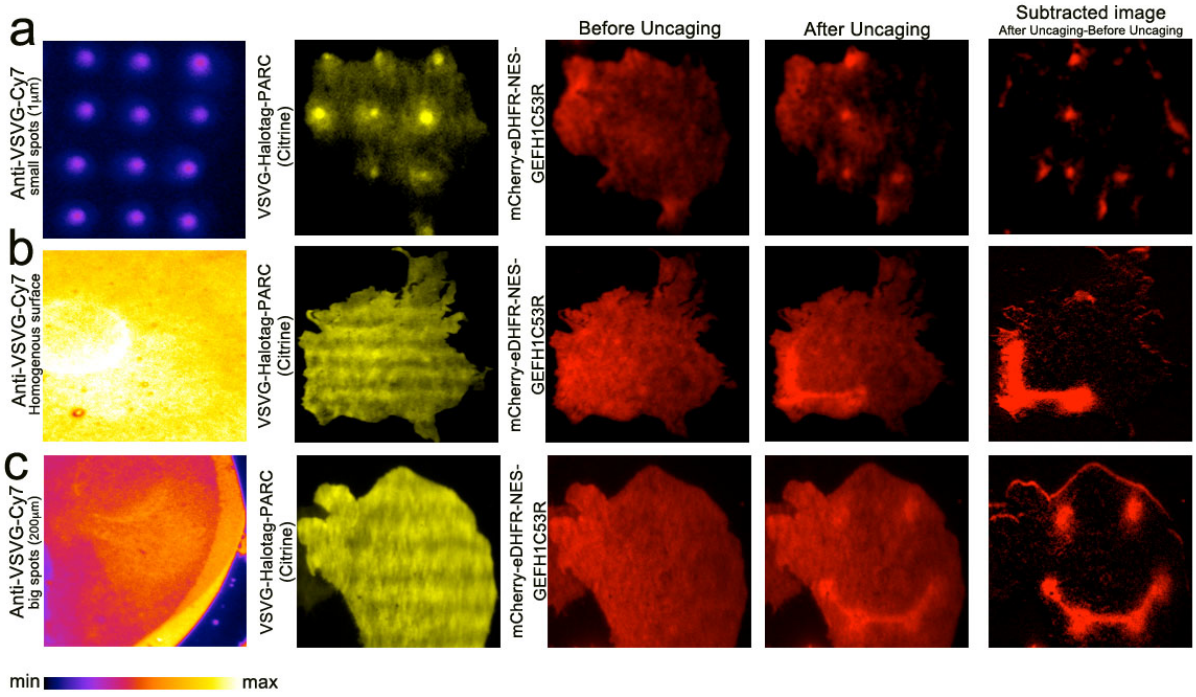

Figure 4.3: Molecular Activitiy Painting (MAP). **a.** Immobilization of Anti-VSVG in 1 μm size spots shows spatially controlled enrichment of HalotagPARCs and recruitment of GEF-H1 only in the region of photoactivation **b-c**. Homogenous immobilization of anti-VSVG antibodies and patterning of big spots (200 μm) faciliatated photouncaging and strong GEF-H1 recruitment in any defined shape.

5. DISCUSSION

5.1 Simultaneous monitoring of multiple protein reactions using intracellular protein interaction arrays

In this work, we demonstrate simultaneous monitoring of multiple protein interactions inside individual living cells. In particular, we analyzed the correlation among the interactions between the two regulatory subunits RI-α or RII-β and the catalytic subunit cat-α of the cAMP dependent protein kinase A. This analysis showed that cat-α binds preferentially to the regulatory subunit RII-β in living, unperturbed cells (**Figure 3.4**). Those measurements also pointed out cell-to-cell variance in the correlation between the response of RI-α or RII-β to pharmacological perturbation of β-adrenergic signaling (**Figure 3.4**). Other methods like surface plasmon resonance, mass spectrometry fail to address cell-to-cell variance as they are based on large ensembles of lysed cells.

An important prerequisite for successful measurements with this technique is an efficient enrichment of baitPARC at immobilized antibody patterns. This process was quantified using the relative enrichment, which is dependent on several experimental parameters, including i) the density of immobilized DNA, ii) the concentration of the antibody in the functionalization complex, iii) the affinity and accessibility of the epitope-antibody interaction at the cell surface/substrate interface, iv) the expression level of the baitPARC and v) the fraction of baitPARCs in the plasma membrane. In our proof of concept study (**Gandor et al, 2013**), RII-β based VSVG-baitPARCs were enriched by a factor of 289±125% . After optimization of the receptor design an enrichment of up to 908.2±77.89% was achieved for the VSVG-e-DHFR PARCs. The relative enrichment obtained for VSVG-eDHFR PARCs differed largely between

independent experiments that used DNA arrays from different batches. As all other factors are likely similar, we presume that the density of the immobilized DNA strongly affected the enrichment in these experiments. To directly evaluate this effect, simultaneous surface immobilization of an identical DNA strand tagged with a fluorophore can act as a reference to measure DNA density for individual experiments. We indirectly evaluated DNA immobilization by measuring fluorescence intensity of the Cy7-labeled functionalization complex and indeed observed that the amount of this complex is critical for efficient receptor enrichment. Also, the relationship between distinct epitopes and the respective relative enrichment of the corresponding receptors remains unknown. This is particularly difficult to address, as distinct antibody complexes and immobilized oligonucleotides cannot be easily compared based on fluorophore intensity. The optimal number of epitopes on receptors for maximal enrichment is also not known. Initial experiments suggested that three epitope repeats (3xVSVG) are advantageous compared to a single VSVG epitope (**Silke Gandor, PhD thesis**), but a quantitative measurement of the relative enrichment corresponding to those constructs was not yet performed.

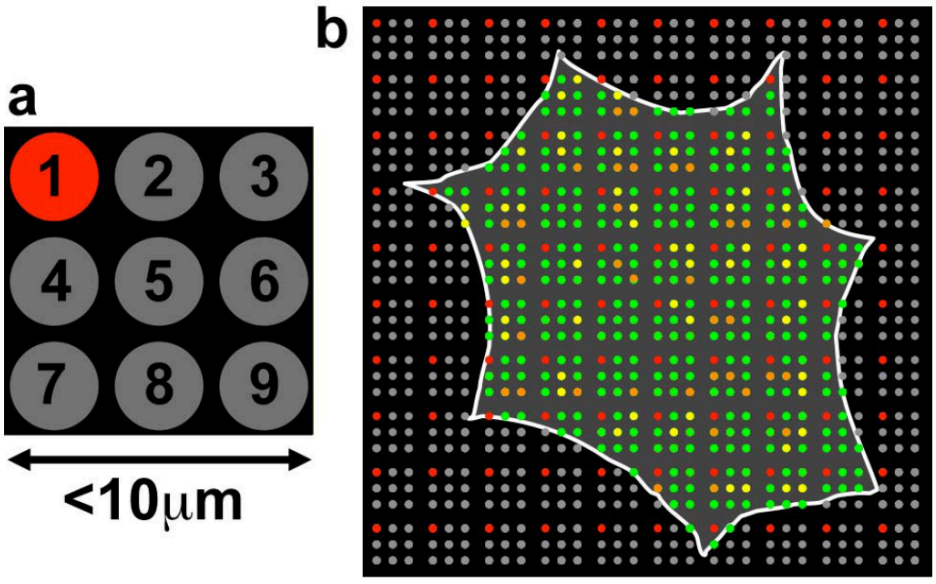

Figure 5.1: Extended multiplexing for studying protein interaction networks. a. A red spot in a 3x3 subarray acts as a reference spot for the remaining immobilized 8 spots (Scale bar: <10μm). b. A living cell plated on the array representing the baitPARC enrichment of distinct 3x3 checkerboard patterns.

An important limitation for multiplexing is the size and spacing of spot structures. A typical mammalian cell with a ~30 μm average diameter can roughly accommodate less than 10 spots with an average size of 4-5 μm, spaced within a distance of 10 μm. Theoretically, structures that are spaced apart by the diffraction limit can be distinguished by standard microscopy techniques. For the wavelengths used in this study (up to 600nm) this limit is close to 200nm for high aperture objectives, but the practical limit is closer to ~500nm. We were able to immobilize DNA spots with a diameter of about 500nm and a spot to spot distance of ~2-3 microns. With this spot distance more than 50 distinct spots could be present within the area of a single typical cell. Theoretically, this could be used to study more than 50 distinct protein interactions in a single cell. Alternatively, a smaller number of protein interactions could be observed repeatedly in 3x3 or 4x4 subarrays, enabling the analysis of the spatial organization of signal networks. It is to be noted that the first spot in each subarray should have a unique color or shape which can be used to assign the identity of bait proteins based on their position (**Figure 5.1**).

Extended multiplexing also requires multiple, distinct baitPARCs that specifically interact with their corresponding immobilized antibodies. In principle, the bait-PARC technology can be scaled up to study more proteins by generating distinct receptors that display distinct epitopes, such as the myc-tag, FLAG-tag and V5-tag. The need for multiple distinct epitopes in the baitPARCs can also be overcome by directed protein evolution **(Packer et al., 2015).** A particularly promising generic approach

could be based on replacing the epitope-antibody interaction with specific TALE-DNA or Zinc finger-DNA interaction pairs **(Mali et al., 2013)** (**Figure 5.2)**. TALE and Zinc finger proteins are known to interact with specific DNA sequences. Those domains could therefore replace epitopes on bait-PARCs, which could directly be recruited to surface immobilized oligonucleotides without the need for antibodies. Thus, the limited number of commercial epitope-specific antibodies could be overcome either by directed protein evolution or by replacing epitopes with specific oligonucleotide binding domains.

To be useful for studying signal networks in cells, neither the artificial receptors nor the immobilized antibodies should interfere with cellular function. This was achieved by designing artificial receptors based on protein domains that do not interact with endogenous signal pathways and by using antibodies directed against viral epitopes that are not present in uninfected cells **(Gandor et al., 2013).** In other words, the artificial receptors were designed to be bio-orthogonal with respect to endogenous cell functions and widely applicable to selected proteins of interest. During the course of the development of artificial receptors by Silke Gandor (**Gandor et al, 2013**), an Austrian research group developed a similar strategy (**Schwarzenbacher et al., 2008**). However, in that study, the interaction between the CD4 receptor and the associated regulator LCK was measured. Thus, this study did not use a bio-orthogonal, artificial receptor to pattern the protein interaction partners in cells and was therefore restricted to this particular biological question of CD4 receptor interactions. Furthermore, this study was also limited to study a single protein interaction inside a single living cell.

Another popular method to study protein interactions in living cells is fluorescence resonance energy transfer (FRET) **(Masi et al., 2010)**. However, FRET can only be used to study one to few protein interactions inside living cells due to the spectral limitations of available FRET fluorophore pairs. These limitations are overcome in our array technology, which can be used to study multiple protein interactions inside living cells with minimal perturbation of endogenous proteins.

The presented array technology also has its limitations: 1) Preparation of arrays is laborious, time-consuming and requires specific training for several specialized techniques, including the immobilization of DNA oligonucleotides using nanolithography, conjugation of streptavidin with the complementary DNA, DNA directed immobilization and special cell handling procedures for cell transfer to functionalized arrays. In principle, most of these laborious tasks can be automated for large-scale production, for example by combining the technology of polymer-pen nanolithography (**Arrabito et al., 2014)** with standardized surfaces and advanced, microscopy-based control mechanisms. 2) This method is limited to study protein-protein interactions that can occur near the plasma membrane and which therefore can be monitored with TIRF microscopy. 3) Cells prefer to spread on patterns of immobilized antibodies, which can constrain their dynamic behavior. This can limit studies of rapidly migrating cells like fibroblasts or neuronal precursors. 4) The generation of functionalized antibody arrays and the associated analysis of protein interactions involves sophisticated lithography methods and advanced microscopy techniques. Thus, the application of this method is relatively expensive. By demonstrating the assembly of a relatively low-cost plotter device (~15.000 Euro; **Arrabito et al., 2014**) we make this technology much more accessible, as TIRF

microscopy is already available in many modern imaging facilities. Furthermore, the lithography step can be bypassed by direct immobilization of biotin with a pipette tip (Section 4.1). Large antibody spots generated with this procedure can be used to induce polarization in one side of individual cells. However, this cost effective strategy is currently limited to analyze only one protein interaction per cell.

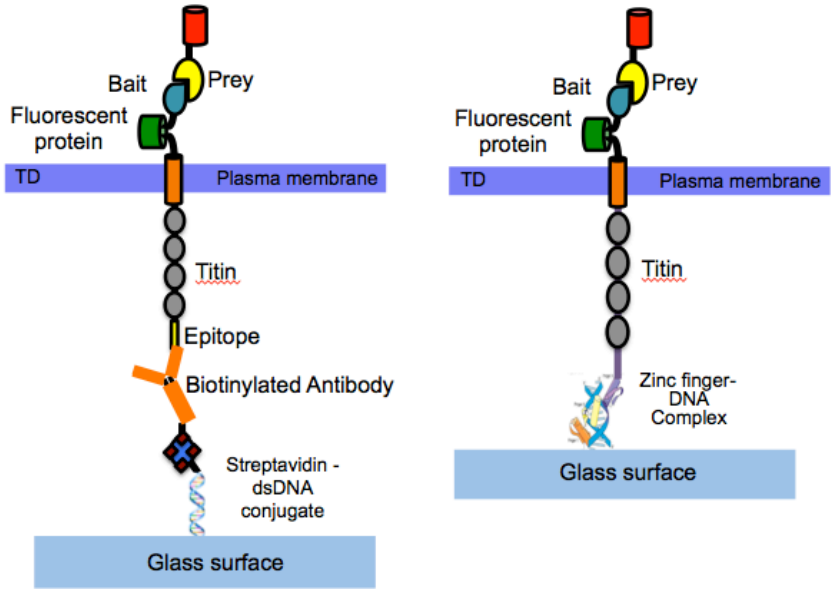

Figure 5.2: Comparsion of epitope-based and zinc-finger based baitPARCs. The limited number of commercially available biotinylated epitope-specific antibodies can be overcome by replacing the epitope-antibody interaction with the Zinc finger-DNA interaction.

5.2 Targeting and folding of baitPARCs in the secretory pathway

Just as any other transmembrane or secreted protein, bait PARCs are transported to the plasma membrane via the secretory pathway. For efficient plasma membrane targeting, BaitPARCs were designed to have a single transmembrane domain derived from platelet growth factor receptor (PDFR), and an N-terminal secretory signal sequence. During protein translation, this signal sequence of the nascent baitPARC polypeptide is recognized by the Signal Recognition Particle (SRP), which halts the

translation process. SRP bound polypeptide interacts with the ER bound SRP receptor and reinitiates the translation. This complex is then taken over by the Sec61 complex, which enables the translocation of the baitPARC transmembrane domain through the ER membrane and the removal of the signal sequence by signal peptidases **(Alberts B, 2002).**

In general, protein translation inside the cell occurs at the rate of ≈2–8 amino acid residues per second (**Alberts B, 2002**). Elongation of the nascent protein chain should not occur more rapidly than the folding capacity of the ER. If unfolded baitPARCs are present, a cascade of signaling events is triggered that indicates stress in the ER, which in turn leads to the activation of the unfolded protein response **(Anelli et al., 2008).** The folding kinetics of the baitPARCs are currently unknown. Presumably, the slowest folding rate of the baitPARC domains (titin, fluorescent protein and bait/activator) will be rate limiting for the folding of the overall structure of assembled baitPARCs.

During the optimization of baitPARCs, we frequently observed entrapment of receptors in the ER, presumably due to misfolding and blockage of entry into the secretory pathway. We solved this problem by generating constructs with functional linkers that directly or indirectly improved protein folding of individual domains. It should be noted that, fluorescent proteins isolated form cold-water organisms like jellyfish or corals exhibit improved folding when expressed at temperatures below the optimal growth of mammalian cells (26°C) (**Ward WW, 1998**). Indeed, our experiments suggest that fluorescent proteins contribute to folding problems in baitPARCs, which were improved by lower temperature expression. In principle, protein folding can also be improved via other strategies, such as the addition of

chemical chaperones (**Bandyopadhyay A et al., 2012**) or co-expression of protein-based Chaperones like BiP that shield the hydrophobic residues of baitPARC and protect cells from ER stress and allow continuous expression of mRNAs (**Morris et al., 1997**).

Replacing the conventional fluorescent proteins with Super folder GFP (SF-GFP) or FFTS-YFP could be used to further increase baitPARC folding and plasma membrane targeting. Those GFP variants show remarkable re-folding kinetics. For example, the yellow fluorescent protein variant FFTS-YFP folds 9 times faster than the original Venus variant (**Aliye, N. et al., 2014**). SF-GFP folds 3.5 times faster than the original GFP variant (**Pédelacq, J.D et al., 2006**).

The largest effect on plasma membrane targeting was observed for the bait- or activator protein inside artificial receptors. This is not surprising, as arbitrary proteins of interest might not fold well if they are fused to other domains or linkers. In contrast, the SNAPf and Halotag proteins are well-characterized protein domains that were found to fold in various contexts, including fusion proteins (**Stagge F et al 2013**). Indeed, replacing the regulatory subunit of PKA with those domains in activatorPARCs likely contributed to their excellent plasma membrane fraction levels (**Figure 3.9**)

5.3 Optimization of baitPARC folding

In order to improve the plasma membrane fraction of the baitPARCs, a glycosylation motif, an extended glycine linker, a coiled-coiled linker and a positively charged sequence were inserted between baitPARC domains. Those modifications significantly improved the plasma membrane fraction from -30% to -70%.

i) Introducing the flexible glycine linkers between the transmembrane domain and the fluorescent protein of the baitPARC might have improved the mobility of the connecting functional domains by providing them higher degree of freedom (**Chen et al., 2013**).

ii) A core oligosaccharide structure is added to the glycosylation motif (Asn-X-Ser/Thr residue) of the baitPARC chain by oligosaccharyl transferase. This initiates the process of N-glycosylation. Protein folding is enhanced by glycosylation in several ways. Based on **Schröder et al., 2005**, addition of a hydrophilic carbohydrate moiety to the baitPARC increases the solubility of this fusion protein. Presence of a glycosyl group in the baitPARC increases its hydration volume and shields it from the surrounding proteins. This post-translational modification stabilizes the conformation of baitPARC via an oligosaccharide-peptide backbone interaction. Finally, sugar residues in the glycosyl group are trimmed sequentially and this step is regulated by the lectin machinery of the CNX/CNT cycle. This cycle constantly monitors protein conformations and acts as protein quality control machinery in the ER to decide the destiny of the baitPARC (**Schröder et al., 2005**). As a result, the properly folded baitPARC is transported to the Golgi and follows the secretory pathway and the misfolded baitPARC is targeted to the lysosome for degradation via ERAD (**Anelli et al, 2008**).

iii) According to the positive inside rule, positively charged residues are predominantly found in the cytoplasmic side of membrane proteins (**Heijne G et al., 1988**). Addition of six lysine residues after the hydrophobic stretch of the transmembrane domain in baitPARCs significantly improved plasma membrane targeting. This is thought to be due to an increase in the membrane insertion efficiency and improved formation of

transmembrane helices by lowering the associated free energy (**Lerch-Bader M et al., 2008**).

iv) **Dill et al., 1990** described protein folding as a process to maximize the quantity of buried non-polar groups in the protein core. The amphipathic nature and non-polar/polar periodic properties of coiled-coiled linkers helps them to assemble within their hydrophobic areas, which can enhance folding of nearby proteins. Indeed, including a coiled-coiled linker at both ends of the fluorescent protein increased plasma membrane targeting.

In addition to those optimization steps, using a stronger secretory signal sequence could improve the interaction between the nascent baitPARC polypeptide and the SRP during translation at the ER. This step might thereby further increase the transport efficiency of baitPARCs along the secretory pathway. Furthermore, a blue fluorescent protein that was optimized for processing in the lumen of the ER, called SecBFP2, might be able to replace the current fluorescent proteins if it is localized to the N-terminal region of baitPARCs (**Costanini et al., 2015**).

5.4 Acute control of RhoGTPase activity by ligand induced dimerization

In the last decades, several chemical ligands that induce dimerization of two proteins were developed (**DeRose et al., 2013**). Among those, Rapamycin induced dimerization is best characterized. Rapamycin, a macrolide natural product, induces the interaction between the proteins FKBP and the FRB domain of the mTOR kinase when added to cells. This FKBP-FRB complex formation occurs within minutes, and it is driven by a low nanomolar affinity between the components (**Banaszynski L et al., 2006**). Even though it was widely applied, the interaction of Rapamycin with the

endogenous mTOR and FKBP proteins also leads to side effects (**Wehrens et al., 2008**). Another disadvantage of this system is its poor reversibility **(Peng Liu et al, 2013).**

In order to address these limitations, a novel bio-orthogonal, chemically induced dimerization (CID) strategy was developed. Here, addition of the small molecule SLF'-TMP enabled the hetero-dimerization of two proteins, eDHFR and FKBP' (**Liu P et al., 2014**). Unlike the Rapamycin system, the dimerizer does not interact with endogenous variants of those proteins in mammalian cells. Hence it is supposed to minimally perturb cellular function and therefore it is considered to be bio-orthogonal. Another attractive feature of this method is its reversible hetero-dimerization of eDHFR-FKBP' within minutes.

Using this CID approach, Abram Calderon induced plasma membrane targeting of fluorescent protein tagged active RhoGTPase mutants (Rac1Q61L and Cdc42Q61L) in N2a cells. Interestingly, he observed the formation of structures that are typical for the corresponding Rho GTPase, such as lamellopodia, filopodia and cell contraction.

Rho GTPase biosensors developed by Abram Calderon enabled direct activity measurement of Rac and Cdc42 RhoGTPase during plasma membrane targeting (**Abram Calderon, 2014**) (**Figure 3.11**). Unfortunately, Cos7 cells showed no significant phenotypic changes. This could be due the lack of spontaneous cell polarization in COS7 cells, which in turn could be due to missing signal activities that promote those phenotypic responses.

5.5 Integrating artificial receptors with CID for discovering feedback loops among RhoGTPases

In order to measure the crosstalk between RhoGTPases, we combined protein interaction arrays with the chemically induced dimerization system. Cos7 cells plated on anti-VSVG antibody arrays showed strong enrichment of VSVG-eDHFR PARCs. Addition of the chemical dimerizer induced plasma membrane targeting of constitutively active Rac and Cdc42 with high spatio-temporal precision (**Figure 3.13-3,14**). In principle, this method could be used to detect positive or negative feedback loops that might regulate Rho GTPases. Our preliminary analysis shows that differences in the perturbation and response kinetics can be measured independently on individual spots of an intracellular array. Such differences could hint to the presence of regulatory mechanisms, including feedback loops, which can then be further investigated by combined long-term perturbations via siRNA or the CRISPR-CAS system.

Due to time constraints, we were only able to perturb Rac and Cdc42 and monitor their corresponding sensor activity. Controlling a specific Rho GTPase (i.e. Cdc42) activity locally in the presence of sensors for distinct GTPases (i.e. Rac and/or Rho) could provide information about the crosstalk between individual RhoGTPases.

One key disadvantage with this combined array-CID system is the time required to achieve a stable perturbation. This kinetics was in the range of several minutes, which might be caused by slow diffusion of the dimerizer to enter the cell and slow encounter with the immobilized interaction partner. It should be noted that this slow CID plasma membrane targeting and de-targeting is much slower that many aspects of Rho GTPase signaling, which is thought to occur at the sub-second timescale (**Pertz O, 2009**).

5.6 A light based strategy induces rapid perturbation of RhoGTPases

In order to achieve rapid perturbation of RhoGTPases, we developed photochemically induced dimerization in collaboration with Dr. Xi Chen and his group leader Dr. Yaowen Wu. Although this method shares a similar principle with chemically induced dimerization, here two desired proteins (Halotag-eDHFR) are brought to close proximity only upon un-caging of the photoactivatable dimerizer (pTMP-Cl). This photocaged dimerizer is covalently linked to a membrane localized Halo-Tag. Unlike CID, activation kinetics in pCID are only limited by uncaging kinetics and intracellular diffusion of the dimerization domains and it does not dependent on the relatively slow diffusion of the dimerizer into the cell.

Photoactivation via a 405nm laser un-caged the dimerizer and targeted the protein (mCitrine-eDHFR-NES-Rac1Q61L) rapidly to the plasma membrane in Cos7, N2a, U2OS and Hela cells. Confined and focused spots of 405nm blue light enabled local perturbation of the desired protein.

The density of the dimerization domain in the plasma membrane and the exposure time determines the recruitment efficiency after photoactivation. However, laser power also needs to be optimized to maximize uncaging and to minimize side reactions, for example from phototoxicity. Even though the cell lines Cos7, Hela and U2OS showed strong and local plasma membrane targeting of the constitutively active Rac mutant to a CAAX membrane anchor, we did not observed lamellopodia or filopodia formation in those cells. On the other hand, in N2a cells, plasma membrane targeting of active Rac induces robust lamellipodia formation. A similar cell-type specific effect was also observed with CID (**Inoue T et al., 2005, Liu P et al., 2014**).

One key limitation of this pCID method was lateral diffusion of the CAAX box based plasma membrane anchor, leading to the loss of signal a few minutes after photo-activation (**Figure 3.18d**). Lateral diffusion is only partially overcome by applying multiple irradiation pulses of blue light, which resulted in the formation of localized membrane ruffling or cell protrusions.

5.7 Application of immobilized artificial receptors with pCID controls the spatio temporal activity of RhoGTPases

We solved the problem of lateral diffusion by replacing the CAAX box membrane anchor with immobilized Halotag-PARCs. Cos7 cells expressing Halotag-PARCs showed robust enrichment in antibody spot patterns and stable recruitment of active Rac mutant upon photo uncaging. Uncaging of the dimerizer on a CAAX box membrane anchor induced a 50-60% increase in recruitment of active Rac whereas recruitment to activatorPARC increased only by 30%. This is possibly due to the higher expression levels of the Halotag-CAAX construct in comparison to the Halotag-PARCs. On the other hand, Halotag-PARCs were enriched by a factor of 265.6-68.76%, which could have partially compensated for the reduced expression level. Local activation of active Rac showed significant activation within regions as small as 3.59±0.55 μm. As in the other methods, stable plasma membrane recruitment of active Rac showed minor or no traces of lamellopodia formation. A key limitation of this method is the need to synthesize the photocaged dimerizer and a relatively slow reversibility within minutes.

In conclusion, local, acute plasma membrane targeting of Rho GTPases or their regulators by this method enables the direct measurement of signal processing in

living cells, including the elucidation of Rho GTPase crosstalk and its spatio-temporal relation to effector signaling.

REFERENCES

Aagaard, L et al., (2007). RNAi therapeutics: Principles, prospects and challenges. *Advanced Drug Delivery Reviews, 59*(2-3), 75-86.

Abram Calderon (2014) Acute Perturbation and Activity Measurement of Rho GTPases in Living Cells (*PhD thesis*).

Aebersold, R. & Mann, M., 2003. Mass spectrometry-based proteomics. *Nature*, 422(6928), pp.198–207.

Albert, R., 2005. Scale-free networks in cell biology. *J Cell Sci*, 118(Pt 21), pp.4947–4957.

Alberts B, Johnson A, Lewis J, et al. Molecular Biology of the Cell, 4th Edition, New York: Garland Science; 2002.

Aliye, N. et al., 2014. Engineering color variants of green fluorescent protein (GFP) for thermostability, pH-sensitivity, and improved folding kinetics. *Applied Microbiology and Biotechnology*, 99(3), pp.1205–1216.

Anelli, T. & Sitia, R., 2008. Protein quality control in the early secretory pathway. *The EMBO journal*, 27(2), pp.315–27.

Arrabito, G., Reisewitz, S., Dehmelt, L., Bastiaens, P. I., Pignataro, B., Schroeder, H. and Niemeyer, C. M. (2013), Biochips for Cell Biology by Combined Dip-Pen Nanolithography and DNA-Directed Protein Immobilization. Small, 9: 4243–4249.

Arrabito, G. et al., 2014. Configurable low-cost plotter device for fabrication of multi-color sub-cellular scale microarrays. *Small*, 10(14), pp.2870–2876.

Arrabito, G et al., (2013). Biochips for Cell Biology by Combined Dip-Pen Nanolithography and DNA-Directed Protein Immobilization. *Small, 9*(24), 4243-4249.

Axelrod, D (2001). Total Internal Reflection Fluorescence Microscopy in Cell Biology. *Traffic, 2*(11), 764-774.

Ballister, E.R. et al., 2014. Localized light-induced protein dimerization in living cells using a photocaged dimerizer. *Nature communications*, 5, p.5475.

Banaszynski, L. A., Chen, L., Maynard-Smith, L. A., Ooi, A. G., & Wandless, T. J. (2006). A Rapid, Reversible, and Tunable Method to Regulate Protein Function in Living Cells Using Synthetic Small Molecules. *Cell, 126*(5), 995-1004.

Bandyopadhyay, A., Saxena, K., Kasturia, N., Dalal, V., Bhatt, N., Rajkumar,A., Chakraborty, K. (2012). Chemical chaperones assist intracellular folding to buffer mutational variations. *Nature Chemical Biology Nat Chem Biol, 8*(3), 238-245.

Barabási, A. & Oltvai, Z.N., 2004. Network biology: understanding the cell's functional organization. *Nature Reviews Genetics*, 5(2), pp.101–113.

Birkenfeld, J. et al., 2008. Cellular functions of GEF-H1, a microtubule-regulated Rho-GEF: is altered GEF-H1 activity a crucial determinant of disease pathogenesis? *Trends in Cell Biology*, 18(5), pp.210–219.

Bishop, A.L. & Hall, A., 2000. Rho GTPases and their effector proteins. *The Biochemical journal*, 348 Pt 2, pp.241–55.

Brazas, R., 2011. In Vitro and In Vivo Methods to Study Protein:Protein Interactions, p.62.

Brown, E. J., Albers, M. W., Shin, T. B., Ichikawa, K., Keith, C. T., Lane, W. S., &Schreiber, S. L. (1994). A mammalian protein targeted by G1-arresting rapamycin–receptor complex. *Nature, 369*(6483), 756-758.

Brückner, A. et al., 2009. Yeast two-hybrid, a powerful tool for systems biology. *International Journal of Molecular Sciences*, 10(6), pp.2763–2788.

Carmine Guirland et al., 2013 Direct cAMP Signaling through G-Protein-Coupled Receptors Mediates Growth Cone Attraction Induced by Pituitary Adenylate Cyclase-Activating Polypeptide J. Neurosci., 23(6):2274 –2283

Cherfils, J. & Zeghouf, M., 2013. Regulation of small GTPases by GEFs, GAPs, and GDIs. *Physiological reviews*, 93(1), pp.269–309.

Chesnut, J. D., Baytan, A. R., Russell, M., M.-P.Chang, Bernard, A., Maxwell, I. H., and Hoeffler, J. P. (1996). Selective Isolation of Transiently Transfected Cells from a Mammalian Cell Population with Vectors Expressing a Membrane Anchored Single-Chain Antibody. J. Imm. Methods 193, 17-27.

Chi, X. et al., 2013. Roles of Rho GTPases in intracellular transport and cellular transformation. *International Journal of Molecular Sciences*, 14(4), pp.7089–7108.

Costantini, L. M et al., (2015). A palette of fluorescent proteins optimized for diverse cellular environments. *Nature Communications Nat Comms, 6*, 7670.

Crivat, G. & Taraska, J.W., 2012. Imaging proteins inside cells with fluorescent tags. *Trends in Biotechnology*, 30(1), pp.8–16.

Darius Kaszta (2014) Optimierung der Plasmamembranlokalisation eines artifiziellen Rezeptors durch den Einbau eines Glyco-Tags (*Bachelor thesis*)

Derose, R., Miyamoto, T., & Inoue, T. (2013). Manipulating signaling at will: Chemically-inducible dimerization (CID) techniques resolve problems in cell biology. *Pflügers Archiv - European Journal of Physiology Pflugers Arch - Eur J Physiol, 465*(3), 409-417.

Dill, K. A (1990). Dominant forces in protein folding. *Biochemistry, 29*(31), 7133-7155.

Dovas, A. & Couchman, J.R., 2005. RhoGDI: multiple functions in the regulation of Rho family GTPase activities. *The Biochemical journal*, 390(Pt 1), pp.1–9.

Fan, E.K. et al., 2001. Intracellular Functions of N-Linked Glycans. *Science*, 291(March), pp.2364–2370.

Farhan, H. & Rabouille, C., 2011. Signalling to and from the secretory pathway. *Journal of cell science*, 124(Pt 2), pp.171–180.

Gaj, Thomas, Charles A. Gersbach, and Carlos F. Barbas. "ZFN, TALEN, And CRISPR/Cas-Based Methods For Genome Engineering". *Trends in Biotechnology* 31.7 (2013): 397-405.

Gandor, S. et al., 2013. A Protein-interaction array inside a living cell. *Angewandte Chemie - International Edition*, 52(18), pp.4790–4794.

Gautier, A. et al., 2014. How to control proteins with light in living systems. *Nature chemical biology*, 10(7), pp.533–41.

Gossen, M et al., (1992). Tight control of gene expression in mammalian cells by tetracycline-responsive promoters. *Proceedings of the National Academy of Sciences, 89*(12), 5547-5551.

Griesbeck, O. et al., 2001. Reducing the environmental sensitivity of yellow fluorescent protein. Mechanism and applications. *Journal of Biological Chemistry*, 276(31), pp.29188–29194.

Gronwald et al., (1988). Cloning and expression of a cDNA coding for the human platelet-derived growth factor receptor: Evidence for more than one receptor class. *Proceedings of the National Academy of Sciences, 85*(10), 3435-3439.

Guilluy, C., Garcia-Mata, R. & Burridge, K., 2011. Rho protein crosstalk: Another social network? *Trends in Cell Biology*, 21(12), pp.718–726.

Hall, A., 1998. Rho GTPases and the actin cytoskeleton. *Science (New York, N.Y.)*, 279(5350), pp.509–514. Available at:

Hanna, S et al., (2013). Signaling networks of Rho GTPases in cell motility. *Cellular Signalling, 25*(10), 1955-1961.

Harcum, S.W., 2006. Protein Glycosylation. , 3, pp.500–503.

Heasman, S.J. & Ridley, A.J., 2008. Mammalian Rho GTPases: new insights into their functions from in vivo studies. *Nature reviews. Molecular cell biology*, 9(9), pp.690–701.

Heijne G et al., 1988. C I R L Press Limited, Oxford, England. 16(14), p.8410058.

Herberg, F.W., Taylor, S.S. & Dostmann, W.R.G., 1996. Active site mutations define the pathway for the cooperative activation of cAMP-dependent protein kinase. *Biochemistry*, 35(9), pp.2934–2942.

Huo, F. et al., 2008. Polymer Pen Lithography. *Science*, 321(September), pp.1658–1660.

Inoue, T., Heo, W. D., Grimley, J. S., Wandless, T. J., & Meyer, T. (2005). An inducible translocation strategy to rapidly activate and inhibit small GTPase signaling pathways. *Nature Methods Nat Meth, 2*(6), 415-418.

Invitrogen, 2010. pDisplay ™ Vector.

J.A. Morris, A.J Dorner, C.A. Edwards, L.M. Hendershot, R.J. Kaufman Immunoglobulin binding protein (BiP) function is required to protect cells from endoplasmic reticulum stress but is not required for the secretion of selective proteins J. Biol. Chem., 272 (1997), pp. 4327–4334

Jaffe, A.B. & Hall, A., 2005. RHO GTPASES: Biochemistry and Biology. *Annual Review of Cell and Developmental Biology*, 21(1), pp.247–269.

Jan wolffgramm (2015) Optimierung von Antikörper-funktionalisierten Oberflächenstrukturen

zur Rekrutierung von *bait*-PARCs

Jordan, S.N. & Canman, J.C., 2012. Rho GTPases in animal cell cytokinesis: An occupation by the one percent. *Cytoskeleton*, 69(11), pp.919–930.

Karginov, A. V., Zou, Y., Shirvanyants, D., Kota, P., Dokholyan, N. V., Young, D. D, Deiters, A. (2011). Light Regulation of Protein Dimerization and Kinase Activity in Living Cells Using Photocaged Rapamycin and Engineered FKBP. *J. Am. Chem. Soc. Journal of the American Chemical Society, 133*(3), 420-423.

Karnoub, A.E. et al., 2004. Molecular basis for Rho GTPase signaling specificity. *Breast Cancer Research and Treatment*, 84(1), pp.61–71.

Katz, C. et al., 2011. Studying protein-protein interactions using peptide arrays. *Chemical Society reviews*, 40(5), pp.2131–2145.

Kennedy, M.J. et al., 2010. Rapid blue light induction of protein interaction in living cells. *Nature Methods*, 7(12), pp.973–975.

Kenworthy, A.K., 2001. Imaging protein-protein interactions using fluorescence resonance energy transfer microscopy. *Methods*, 24(3), pp.289–296. Available at:

Khalkhali, Z. et al., 1976. Glycosylation Invitro of an Asparagine Sequon Catalyzed By Preparations of Yeast-Cell Membranes. *Biochemical Journal*, 160(1), pp.37–41.

Klán, P et al., (2013). Photoremovable Protecting Groups in Chemistry and Biology: Reaction Mechanisms and Efficacy. *Chemical Reviews Chem. Rev., 113*(1), 119-191.

Krendel, M et al., (2002). Nucleotide exchange factor GEF-H1 mediates cross-talk between microtubules and the actin cytoskeleton. *Nature Cell Biology Nat. Cell Biol., 4*(4), 294-301.

Lerch-Bader, M. et al., 2008. Contribution of positively charged flanking residues to the insertion of transmembrane helices into the endoplasmic reticulum. *Proceedings of the National Academy of Sciences of the United States of America*, 105(11), pp.4127–4132.

Levskaya, A. et al., 2009. Spatiotemporal control of cell signalling using a light-switchable protein interaction. *Nature*, 461(7266), pp.997–1001.

Lin, Y.C. et al., 2013. The B7-1 Cytoplasmic Tail Enhances Intracellular Transport and Mammalian Cell Surface Display of Chimeric Proteins in the Absence of a Linear ER Export Motif. *PLoS ONE*, 8(9), pp.1–25.

Liu, P. et al., 2014. A bioorthogonal small-molecule-switch system for controlling protein function in live cells. *Angewandte Chemie - International Edition*, 53(38), pp.10049–10055.

Los, G. V et al., (2008). HaloTag: A Novel Protein Labeling Technology for Cell Imaging and Protein Analysis. *ACS Chem. Biol. ACS Chemical Biology, 3*(6), 373-382.

M. Wayne Davis, ApE-A plasmid Editor, 2013

Machacek, M. et al., 2009. Coordination of Rho GTPase activities during cell protrusion. *Nature*, 461(7260), pp.99–103.

Mali, P et al., (2013). Barcoding cells using cell-surface programmable DNA-binding Domains. *Nature Methods Nat Meth, 10*(5), 403-406.

Martin Kares Lucas (2014) Optimierung der Membranlokalisation eines künstlichen Rezeptors (*Bachelor thesis*)

Masi, A et al., (2010). Optical Methods in the Study of Protein-Protein Interactions. *Advances in Experimental Medicine and Biology Integrins and Ion Channels,* 33-42.

Mattila, P.K. & Lappalainen, P., 2008. Filopodia: molecular architecture and Cellular functions. *Nature reviews. Molecular cell biology*, 9(6), pp.446–454.

Melanie Grässl., 2015. Dynamic regulation of Rho GTPase networks and correlation with effector pathways Universität Duisburg-Essen aus Essen November 2015. , (November).

Meyer, R. et al., 2014. Advances in DNA-directed immobilization. *Current Opinion in Chemical Biology*, 18(1), pp.8–15.

Michael Örlich (2013) Optimierung von Antikörper-funktionalisierten Oberflächenstrukturen zur Rekrutierung von bait -PARCs (*Bachelor thesis*).

Miller, L.W. et al., 2005. In vivo protein labeling with trimethoprim conjugates: a flexible chemical tag. *Nature methods*, 2(4), pp.255–257.

Milstein, S., Nguyen, M., Meyers, R., and de Fougerolles, A. (2013). Measuring RNAi knockdown using qPCR. Methods Enzymol. 533, 57–77.

Moharir, A. et al., 2013. The Role of N-Glycosylation in Folding, Trafficking, and Functionality of Lysosomal Protein CLN5. *PLoS ONE*, 8(9).

Niemeyer, C.M. et al., 1994. Oligonucleotide-directed self-assembly of proteins: semisynthetic DNA--streptavidin hybrid molecules as connectors for the generation of macroscopic arrays and the construction of supramolecular bioconjugates. *Nucleic Acids Research*, 22(25), pp.5530–5539.

Niemeyer, C.M. et al., 1999. DNA-Directed Immobilization: Efficient, Reversible, and Site-Selective Surface Binding of Proteins by Means of Covalent DNA–Streptavidin Conjugates. *Analytical Biochemistry*, 268(1), pp.54–63.

Niethammer, P. et al., 2007. Discrete states of a protein interaction network govern interphase and mitotic microtubule dynamics. *PLoS Biology*, 5(2), pp.0190–0202.

Nufer, O. et al., 2002. Role of cytoplasmic C-terminal amino acids of membrane proteins in ER export. *Journal of cell science*, 115(Pt 3), pp.619–628.

Packer, M. S et al., (2015). Methods for the directed evolution of proteins. *Nat Rev Genet Nature Reviews Genetics, 16*(7), 379-394.

Padrick, S.B. & Rosen, M.K., 2010. Physical mechanisms of signal integration by WASP family proteins. *Annual review of biochemistry*, 79, pp.707–35.

Parri, M. & Chiarugi, P., 2010. Rac and Rho GTPases in cancer cell motility control. *Cell communication and signaling : CCS*, 8, p.23.

Pédelacq, J.D. et al., 2006. Engineering and characterization of a superfolder green fluorescent protein. *Nature biotechnology*, 24(1), pp.79–88.

Pertz, O., 2010. Spatio-temporal Rho GTPase signaling - where are we now? *Journal of cell science*, 123(Pt 11), pp.1841–1850.

Pertz, O. et al., 2006. Spatiotemporal dynamics of RhoA activity in migrating cells. *Nature*, 440(7087), pp.1069–72.

Piehler, J., 2005. New methodologies for measuring protein interactions in vivo and in vitro. *Current Opinion in Structural Biology*, 15(1 SPEC. ISS.), pp.4–14.

Pollard, Thomas D. "Regulation Of Actin Filament Assembly By Arp2/3 Complex And Formins". *Annual Review of Biophysics and Biomolecular Structure* 36.1 (2007): 451-477.

Prydz, K. et al., 2013. Arrivals and departures at the plasma membrane: Direct and indirect transport routes. *Cell and Tissue Research*, 352(1), pp.5–20.

Raftopoulou, M. & Hall, A., 2004. Cell migration: Rho GTPases lead the way. *Developmental Biology*, 265(1), pp.23–32.

Rakhit, R., Navarro, R. & Wandless, T.J., 2014. Chemical biology strategies for posttranslational control of protein function. *Chemistry and Biology*, 21(9), pp.1238–1252.

Reisewitz, S et al., 2010). Capture and Culturing of Living Cells on Microstructured DNA Substrates. *Small, 6*(19), 2162-2168.

Riederer, M.A. & Hinnen, A., 1991. Removal of N-glycosylation sites of the yeast acid phosphatase severely affects protein folding. *Journal of Bacteriology*, 173(11), pp.3539–3546.

Schlessinger, J., 2002. Ligand-induced, receptor-mediated dimerization and activation of EGF receptor. *Cell*, 110(6), pp.669–672.

Schröder, M. & Kaufman, R.J., 2005. the Mammalian Unfolded Protein Response. *Annual Review of Biochemistry*, 74(1), pp.739–789.

Schwarzenbacher, M. et al., 2008. Micropatterning for quantitative analysis of protein-protein interactions in living cells. *Nature Methods*, 5(12), pp.1053–1060.

Shental-Bechor, D. & Levy, Y., 2008. Effect of glycosylation on protein folding: a close look at thermodynamic stabilization. *Proceedings of the National Academy of Sciences of the United States of America*, 105(24), pp.8256–61.

Sit, S.T. & Manser, E., 2011. Rho GTPases and their role in organizing the actin cytoskeleton. *Journal of cell science*, 124(Pt 5), pp.679–683.

Socher, E. & Imperiali, B., 2013. FRET-Capture: A Sensitive Method for the Detection of Dynamic Protein Interactions. *ChemBioChem*, 14(1), pp.53–57.

Spiering, D. & Hodgson, L., 2011. Dynamics of the rho-family small GTPases in actin regulation and motility. *Cell Adhesion and Migration*, 5(2), pp.170–180.

Stagge, F. et al., 2013. Snap-, CLIP- and Halo-Tag Labelling of Budding Yeast Cells. *PLoS ONE*, 8(10), pp.1–9.

Stephanie Reisewitz (2013) Entwicklung mikrostrukturierter Oberflächen zur Analyse von Protein-Protein Interaktionen in lebenden Zellen (*PhD thesis*).

Strickland, D., Lin, Y., Wagner, E., Hope, C. M., Zayner, J., Antoniou, C.,Glotzer, M (2012). TULIPs: Tunable, light-controlled interacting protein tags for cell biology. *Nature Methods Nat Meth, 9*(4), 379-384.

Tischer, D. & Weiner, O.D., 2014. Illuminating cell signalling with optogenetic tools. *Nature reviews. Molecular cell biology*, 15(8), pp.551–8.

Tnimov, Z. et al., 2012. Quantitative analysis of prenylated RhoA interaction with its chaperone, RhoGDI. *Journal of Biological Chemistry*, 287(32), pp.26549–26562.

Toettcher, J.E. et al., 2011. Light-based feedback for controlling intracellular signaling dynamics. *Nature Methods*, 8(10), pp.837–839.

Toettcher, J.E., Weiner, O.D. & Lim, W.A., 2013. Using optogenetics to interrogate the dynamic control of signal transmission by the Ras/Erk module. *Cell*, 155(6), pp.1422–1434.

Trache, A. & Meininger, G.A., 2008. Total Internal Reflection Fluorescence (TIRF) microscopy. *Current Protocols in Microbiology*, (SUPPL. 10), pp.1–22.

Uzman, A., 2001. Molecular Cell Biology (4th edition) Harvey Lodish, Arnold Berk, S. Lawrence Zipursky, Paul Matsudaira, David Baltimore and James Darnell; Freeman & Co., New York, NY, 2000, 1084 pp., *Biochemistry and Molecular Biology Education*, 29(3), pp.126–128.

Van Aelst, L. & D'Souza-Schorey, C., 1997. Rho GTPases and signaling networks. *Genes & development*, 11(18), pp.2295–2322.

van Bergeijk, P. et al., 2015. Optogenetic control of organelle transport and positioning. *Nature*, 518(7537), pp.111–4.

Vandamme, J., Castermans, D. & Thevelein, J.M., 2012. Molecular mechanisms of feedback inhibition of protein kinase A on intracellular cAMP accumulation. *Cellular Signalling*, 24(8), pp.1610–1618.

Vicente-Manzanares, M., Webb, D.J. & Horwitz, a R., 2005. Cell migration at a glance. *Journal of cell science*, 118(Pt 21), pp.4917–4919.

Walther, K. a et al., 2011. Precise measurement of protein interacting fractions with fluorescence lifetime imaging microscopy. *Molecular bioSystems*, 7(2), pp.322–336.

Ward, W.W. Biochemical and Physical Properties of Green Fluorescent Protein in *Green Fluorescent Protein: Properties, Applications, and Protocols* (eds. Chalfie, M. & Kain, S.) 45–75 (Wiley-Liss, New York, 1998).

Wang, Y. et al., 2013. Rho GTPases orient directional sensing in chemotaxis. *Proceedings of the National Academy of Sciences of the United States of America*, 110(49), pp.E4723–32.

Wehrens, X. H., et al. (2005). Intracellular Calcium Release And Cardiac Disease. *Annual Review of Physiology Annu. Rev. Physiol., 67*(1), 69-98.

Weston, L., Coutts, a. S. & La Thangue, N.B., 2012. Actin nucleators in the nucleus: an emerging theme. *Journal of Cell Science*, 125(15), pp.3519–3527.

Wiebke Obermann (2015) Bachelorarbeit Lokale Stimulation von Signalnetzwerken durch künstliche Rezeptorkonstrukte (*Bachelor thesis*)

Yazawa, M. et al., 2009. Induction of protein-protein interactions in live cells using light. *Nature biotechnology*, 27(10), pp.941–945.

Yoshizumi, A. et al., 2011. Designed coiled coils promote folding of a recombinant bacterial collagen. *Journal of Biological Chemistry*, 286(20), pp.17512–17520.

Zheng, Z. et al., 2009. Multiplexed protein arrays enabled by polymer pen lithography: Addressing the inking challenge. *Angewandte Chemie - International Edition*, 48(41), pp.7626–7629.

Zhu, J. et al., 2013. Protein interaction discovery using parallel analysis of translated ORFs (PLATO). *Nature biotechnology*, 31(4), pp.331–4.

Zimmermann, M. et al., 2014. Cell-permeant and photocleavable chemical inducer of dimerization. *Angewandte Chemie - International Edition*, 53(18), pp.4717–4720.

ACKNOWLEDGEMENTS

Leif**,** I'm really glad I did my PhD under your supervision. I will end up writing a bachelor thesis if I have to mention the skillsets I acquired from you and all the life lessons I learnt because of you. Your down to earth nature, sincerity in teaching, dedication in making presentations, brilliant powerpoint schemes & talks, scientific knowledge & intelligence, sense of humor, humbleness, constant appreciation and motivation to move forward, patience to handle every student, one to one teaching, transparency and straightforward nature made me always admire you. I'm really lucky and happy to share the office with you during the past four and half years and I look forward to work with you again. *Vielen Dank!*

Prof Philippe Bastiaens**,** Your systems biology lectures were brilliantly given and I often find your tone inspiring and motivational. Amidst having busy schedules, having you in my presentation always opened the door for crazy ideas. Your word of appreciation '*This is fascinating/great/interesting'*, '*learn to play the violin*', '*your thesis is like your baby*' etc constantly pushed me out of my comfort zone and made me work hard with my projects. Those meditation lessons, ringberg trips cheerful smiles and 'hello' gestures, warmed my heart every single time. Thank you for all your guidance and support. *Dank je!*

Prof. Jan G. Hengstler, I'm quite happy to have you in the thesis committee as my 'Second Gutachter' to review my thesis. Thank you very much for assessing my work on a short notice. *Vielen Dank!*

Abram**,** There were times I really missed you and there were times I'm glad you left our lab. Actually, your departure made me stand alone and strong. You were that ideal student all the professors crave for. Your epitome of perfection and kind attitude often left me jaw dropping and I'm glad I inculcated some of your habits to make myself professionally better. The way you did your experiments, maintained labnotes, tutoring your students, gave lot of insights and helped me to mold myself. I'm happy that we shared some fun times during our Euro trips, movie nights and gossiping. Thank you for being a wonderful friend and a lovely brother. *Gracias y el amor!*

Tomas**,** Thank you very much for all those brilliant image scripts, road trips and movie nights Your cheerful smile and always happy to help attitude is one hell of good sign to start a day. *Děkuji!*

Thuy, Thank you for your Vietnamese stories, patience and tolerance in answering my questions, sharing lab space without complaining and being a good friend. *cảm ơn bạn!*

Dominic**,** for sitting on the beads experiment jokes, for all the *Mr. Tom* we shared, for all the swearing, for all the Game of Thrones, Breaking Bad stories and the university gossip, and for being such a brilliant student and good friend. *Vielen Dank!* Some of my wisdom quotes

'Hello dear,

No fear,

Muthu is here'

'Don't cry, let us try, Domi',

'You know nothing'

Michael, Darius, Martin, Jan, Wiebke, Philip, Vanessa, *I* really enjoyed teaching you bits and pieces of cloning and microscopy. I realized at the end of the thesis, I learned several concepts, principles and philosophy during the process. I hope you had good time in our lab.. Thank you for being my aerial roots and supporting my work. *Dziękuję Ci and Vielen Dank!*

Giuseppe, Kathrin, Stephanie for being kind, patient and friendly to share your knowledge about polymer pen lithography and DNA directed immobilization in a one to one fashion. Gracie and Vielen Dank!

Ola, for sharing plasmids, being kind and sharing a smile, always. Say flower. شكرا

I would like to thank different members of *Department II, Max Planck Institute for Molecular Physiology* for providing feedback during my presentations (***Aneta, Antonios, Malte Márton, Wayne***), for being a wonderful colleague and friend (***Amit, Marija, Sarah***), constantly maintaining microscopes in good shape (***Sven***), sharing reagents & troubleshooting the problems I encountered in cloning (***Annette, Lisaweta, Hendrike, Reichl and Jutta***) Organizing my progress report talks and conference trips (***Astrid and Tanja***). Vielen dank!

Johannes, Jana, Melanie, Rutu and Peri*,* thank you for being sweet with your gestures, sharing ideas & reagents and organizing lovely Christmas parties. teşekkür ederim & Vielen dank!

Yaowen Wu and Xi Chen, for colloborating with our group and supporting me constantly with ideas and dimerizers. It is a pleasure to work together as a team. 谢谢

Akim, Bharathy, Cristina, Gopal, Jayakumar, Rajkumar, Santhosh, Saranya, Sowmya and Thawfeek**,** *for being open minded, for sharing space, for pouring your heart out, for trusting me completely,* for giving me hope and courage during tough times, for all the personal advices, for all the unforgettable Euro-trips *and (most importantly) cooking mouth watering spicy indian and western food.* நன்றி

Swasti**,** Thank you for all those sweet memories, online chats, local trips in berlin & bonn, indian food, popcorns and being a wonderful friend.

I would like to thank my indian friends and their family (***Amit, Amrita, Anweshan, Babu, Dinesh, Divya, Eshwar, Mamta-di, Mani, Murali, Sarah, Siva, Shankar, Shweta, Suba and Suresh***) who made my stay in dortmund pleasant and memorable. Thank you for all the sweets and memories.

Vishnu**,** for being my lovely brother; ***Dhakshitha*** for all the needed compassion and affection, you are a life saver; ***Kanaga*** for all the inspiration. நன்றி

*'**Any logical reasons can be found only in the mysterious equations of love**'*.

This work will not be possible without the sacrifices and the personal support from my dear parents and cheerful sisters. Thank you for the emotional attachment, affection, care and love.